REVIEW

A Review of the Structure and Dynamics of Upper-Level Frontal Zones

DANIEL KEYSER

Laboratory for Atmospheres, NASA/Goddard Space Flight Center, Greenbelt, MD 20771

M. A. SHAPIRO

NOAA/ERL/Wave Propagation Laboratory, Boulder, CO 80303

(Manuscript received 28 March 1985, in final form 3 September 1985)

ABSTRACT

This article presents a review of upper-level fronts with the intent of synthesizing observational and modeling studies into a conceptual and dynamical description of these fronts and their evolution relative to the life cycle of midlatitude baroclinic waves. The discussion begins by tracing present-day concepts concerning the structure of upper-level frontal systems, which are based on composite analyses of radiosonde and aircraft data, from their origins in the pioneering analyses of upper-air data in the 1930s. Perspectives from scales both smaller and larger than upper-level frontal systems are provided respectively by considering the effects of turbulent processes on frontal structure and dynamics and by relating variations in frontal structure to the evolution of the baroclinic waves that provide the dynamical environment for upper-level frontogenesis.

The dynamics of upper-level fronts are shown to comprise the interactions between the primary (geostrophic) and secondary (ageostrophic) circulations. To elucidate the mechanisms and feedbacks contributing to the evolution of upper-level fronts in relation to their setting within baroclinic waves, the two-dimensional theory of forced secondary circulations in the cross-front plane developed by Sawyer and Eliassen is presented and interpreted, and theoretical and numerical examples of the formation of upper-level fronts in idealized two-dimensional flows are reviewed. In the three-dimensional case, the presence of along-front ageostrophic circulations superimposed upon the cross-front ageostrophic circulations treated by the two-dimensional theory is discussed in terms of the gradient wind. The relative contribution of the along-front ageostrophic circulation to upper-level frontogenesis is considered in the context of the results from three-dimensional β-plane channel models of baroclinic wave growth.

Directions for future observational, diagnostic and theoretical investigation are identified, including the scale interactions between upper-level fronts, their environmental baroclinic waves and related low-level cyclones, and between upper-level fronts and mesoscale convective systems. The review concludes with a discussion of the potential role of recent innovations in remote-sensing technology and trends in numerical weather prediction using mesoscale models in motivating continuing interest and future advances in frontal research.

CONTENTS

1. Introduction

A fundamental property of baroclinic wave disturbances is the tendency for synoptic-scale variations in the thermal and wind fields to become concentrated into narrow transition zones referred to as fronts. Fronts are characterized by large horizontal temperature gradients, static stability, absolute vorticity and vertical wind shear. When viewed on surfaces of constant pressure or height, fronts appear as long, narrow features with the along-front scale typically an order

of magnitude larger than the cross-front scale (1000–2000 km compared with 100–200 km). Because of this geometrical configuration, horizontal variations in the thermal and wind fields tend to be much greater in the cross-front than in the along-front direction. When depicted in vertical cross section, fronts appear as sloping zones with a vertical thickness typically on the order of 1 to 2 km. Although fronts have been identified at all levels in the troposphere and lower stratosphere, their formation is favored by the presence of the naturally imposed quasi-horizontal boundaries consisting of the Earth's surface and the tropopause. Since fronts generated by processes based at the surface and at the tropopause exhibit differences in structure, are generated by distinct dynamical processes, and may occur independently of each other, the respective designations of "surface" or "low-level" and "upper-tropospheric" or "upper-level" serve as a convenient classification for frontal phenomena and processes.

Fronts owe their existence in a kinematic sense (Petterssen, 1936, 1956; Miller, 1948) to spatially differential advection of the thermal and wind patterns resulting from sheared horizontal and vertical velocity fields associated with baroclinic waves. For example, in the absence of diabatic processes, horizontal potential temperature gradients are modified following parcel trajectories by horizontal confluence and convergence along with tilting of vertical gradients of potential temperature (static stability) into the horizontal plane according to

$$\frac{d}{dt}\left(\frac{\partial\theta}{\partial n}\right) = -\frac{\partial v_n}{\partial n}\frac{\partial\theta}{\partial n} - \frac{\partial\omega}{\partial n}\frac{\partial\theta}{\partial p}. \tag{1.1}$$

In this equation, θ is potential temperature, n is a horizontal coordinate oriented normal to the isentropes depicted on a constant pressure surface (positive toward colder air), v_n is the component of velocity in the n direction, and ω is the vertical velocity in the pressure (p) coordinate system (symbols and acronyms appearing in this paper are listed in the Appendix). In the absence of frictional processes, absolute vorticity measured on pressure surfaces is generated along parcel trajectories by horizontal convergence and the tilting of vertical wind shears into the horizontal plane according to

$$\frac{d(\zeta+f)}{dt} = -(\zeta+f)\nabla_p\cdot\mathbf{V} - \mathbf{k}\cdot\left(\nabla_p\omega\times\frac{\partial\mathbf{V}}{\partial p}\right). \tag{1.2}$$

In (1.2), ζ is the relative vorticity evaluated on surfaces of constant pressure and f is the Coriolis parameter. The horizontal wind velocity is denoted by $\mathbf{V}$, and the horizontal gradient operator for surfaces of constant pressure by ∇_p.

Spatially differential advection is responsible not only for generating frontal properties consisting of horizontal and vertical gradients of the thermal and wind fields, but also for the long, narrow geometrical configuration of frontal zones. Shears in the three-dimensional velocity field are associated with deformation in horizontal and vertical planes, which has the property of stretching and constricting broad regions of a fluid into narrow zones. A classic demonstration of this "scale-contraction process" is given by Welander (1955) in numerical simulations with a barotropic model of the evolution of a passive tracer in a flow field typical of those observed in the midtroposphere within midlatitudes. Further evidence for the frontogenetical role of deformation is found in the appearance of impressively realistic front-like features in the laboratory experiments of Fultz (1952) and Faller (1956), in which baroclinic eddies resembling midlatitude cyclones develop in a differentially heated, rotating fluid. The dynamics of frontogenesis, which account for the mutual interactions among the thermal and wind fields, are strongly influenced by the Earth's rotation through the Coriolis force. The significant role of rotation in fronts distinguishes them from a number of related phenomena in which divergence is dominant, such as internal gravity waves, gravity or density currents and squall lines. Furthermore, lineal phenomena generated primarily through localized surface-based differential heating rather than synoptic-scale deformation (e.g., sea-breeze fronts) usually are excluded from dynamical considerations of fronts. The time scale in which fronts form from "smooth" synoptic-scale variations in the thermal and wind fields is on the order of several days, although rapid intensification may be focused into shorter, mesoscale periods of 6 to 12 h.

The meteorological significance of both surface and upper-level fronts stems from their relationship to the structure and evolution of midlatitude baroclinic waves and cyclones. Although fronts occupy only a relatively small fraction of the atmospheric volume affected by baroclinic waves, they contribute a substantial fraction of the dynamical forcing for the irrotational part of the ageostrophic circulation, which contains the divergence and vertical motion fields. The divergence patterns associated with upper-level frontal systems and their accompanying jet streaks[1] play an active part in midlatitude cyclogenesis by contributing to low-level geopotential height (mass) changes. The vertical circulations associated with upper-level and surface frontal zones also are a component in the development and organization of midlatitude cloud and precipitation systems, which assume a diversity of forms ranging from areas of widespread slant convection, organized systems of upright convection, and individual convective storms. Upper-level fronts are of further interest because they are preferred regions of small-scale mixing by a variety of phenomena including gravity waves,

[1] Palmén and Newton (1969, p. 199, pp. 206–212) use the term "jet streak" to describe a wind speed maximum situated along the axis of a jet stream at the level of maximum wind.

Kelvin-Helmholtz billows and patchy turbulent eddy motions, all of which are labeled generically as clear-air turbulence (CAT). The location and intensity of upper-level fronts and jets are of considerable relevance to aircraft operations not only for avoiding regions of CAT and its potential safety hazards, but also for economical flight routing in terms of fuel consumption. Finally, upper-level fronts are regions of significant mass exchange between the stratosphere and troposphere, including radioactive debris and chemical trace constituents.

This review is intended to document the present level of knowledge and understanding of upper-level fronts, with an emphasis on their relationship to the structure and life cycle of midlatitude baroclinic waves.[2] An examination of low-level fronts is considered beyond the scope of this review, as this topic is of sufficient extent and depth to be treated separately.[3] The motivation for a review of upper-level fronts derives from the contention that observational research, which in the past has been based substantially on operationally available radiosonde data and in recent times supplemented by research aircraft measurements, has matured to a point of diminishing returns. Nevertheless, emerging remote-sensing technologies such as ground-based wind profiling systems and satellite-derived soundings of temperature, moisture and ozone offer the possibility of filling some of the gaps in spatial coverage, temporal resolution and data uncertainty characteristic of radiosonde instrumentation. Parallel advances in computing technology are leading to limited-area mesoscale models with sufficiently fine horizontal and vertical resolution to resolve upper-level frontal systems explicitly for the first time. By providing temporally continuous, high-resolution, dynamically consistent datasets, numerical models offer the potential of conducting realistic diagnostic investigations and of testing hypotheses through systematic, controlled experimentation. It is tempting to speculate that research on upper-level fronts is on the threshold of major advances comparable with those realized in the past from radiosonde and aircraft observations. Consequently, an objective of this review not only is to place current knowledge and thinking into perspective by tracing its evolution from previous concepts, but also to identify unresolved problems and controversies in order to establish contexts and directions for future research.

Section 2 documents the evolution of structural models of upper-level frontal systems, beginning with early applications of upper-air data in the 1930s and concluding with present concepts based on analyses combining radiosonde and aircraft observations. Perspectives from scales smaller and larger than fronts themselves are provided respectively by considering the effects of turbulent processes on frontal structure and dynamics and by relating variations in frontal structure to the stages of development of the baroclinic waves that provide the frontogenetical environment during their life cycle. Section 3 presents the two-dimensional theory for determining the ageostrophic, vertical circulations associated with frontal zones that was introduced by Sawyer (1956) and extended by Eliassen (1962). In Section 4, theoretical and numerical evidence is presented for dynamical processes involved in the formation of upper-level fronts in idealized two-dimensional flows and in three-dimensional baroclinic waves. Unresolved issues and problems awaiting future research are identified and discussed in Section 5, and the review is concluded in Section 6.

2. Observations of upper-level frontal structure

The first descriptions of the three-dimensional thermal structure associated with midlatitude baroclinic waves and cyclones resulted from analyses of observations taken over northern Europe with lightweight, retrievable, balloon-borne meteorographs that recorded temperature and pressure. These instruments were constructed during the late 1920s by Jaumotte in Uccle, Belgium (Bjerknes and Palmén, 1937), and set the stage for the introduction of the radiosonde and systematic upper-air observations in the 1930s. The early investigations revealed narrow zones of concentrated thermal contrast extending through the middle and upper troposphere, resulting in the generalization of previous frontal concepts based on surface observations alone. The modification and evolution of structural models and interpretations pertaining to upper-level fronts and the tropopause are discussed in this section. The discussion begins with the schematic in Fig. 1 from Reed and Danielsen (1959) illustrating several models for analyzing upper-level fronts and tropopauses.

a. Historical overview

A representative example of the investigations of the structure of upper-level fronts and the tropopause based on meteorograph ascents is that of Bjerknes and Palmén (1937).[4] Figure 2 consists of vertical cross sections of temperature and potential temperature extending northeastward across Europe from Spain to Sweden. Prominent features include the familiar vertical lapse of temperature in the troposphere and the overlying

[2] This review is restricted to upper-level frontal systems found within midlatitude baroclinic waves. The structure of upper-level frontal systems associated with the subtropical jet stream is reviewed by Palmén and Newton (1969, pp. 212–227). Recent examples of upper-level frontal systems observed in arctic regions are provided by Shapiro et al. (1984b) and Shapiro (1985).

[3] Readers interested in recent reviews of surface fronts from an observational perspective may consult Palmén and Newton (1969, pp. 259–263), Shapiro (1983) and Keyser (1986); theoretical aspects are covered by Hoskins (1982) and Bluestein (1986).

[4] Additional references are cited and summarized by Palmén and Newton (1969, pp. 131–133).

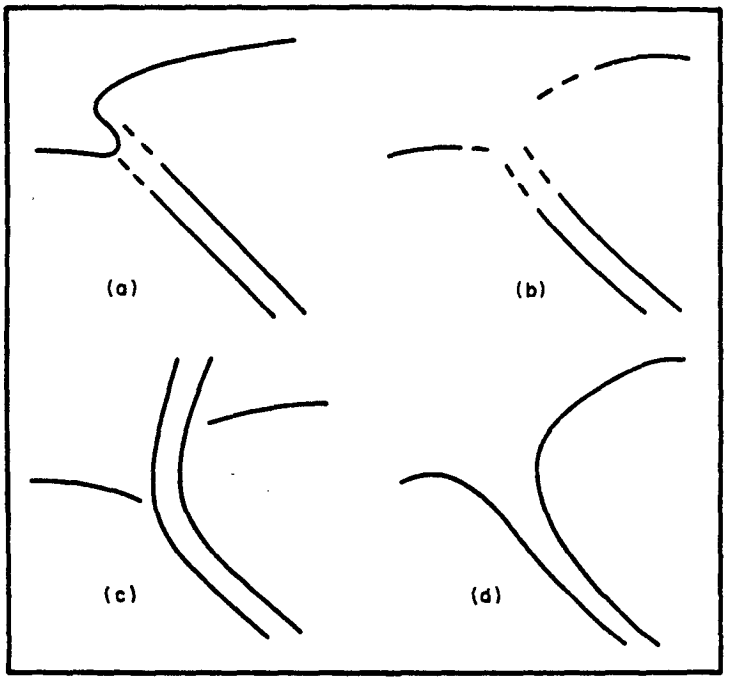

FIG. 1. Schematic diagrams of models used in the past for analyzing upper-level fronts and tropopauses: (a) Bjerknes and Palmén (1937); (b) Palmén and Nagler (1949); (c) Berggren (1952); (d) Reed and Danielsen (1959). See section 2a for detailed discussion. From Reed and Danielsen (1959).

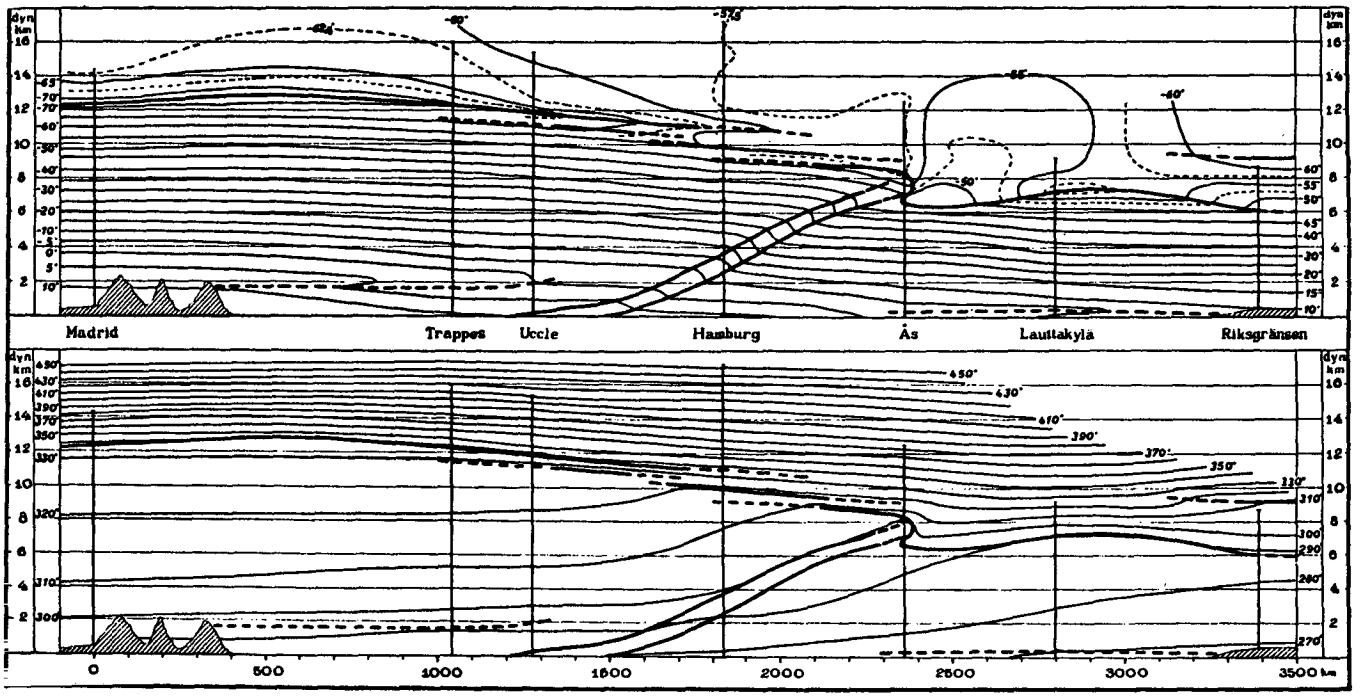

FIG. 2. Cross sections from Spain to Sweden of temperature (°C, top) and potential temperature (K, bottom) for the evening of 15 February 1935, depicting the structure of the tropopause and an upper-level frontal zone analyzed to extend to near the Earth's surface. Thin solid lines denote isotherms or isentropes, thick solid lines depict frontal and tropopause boundaries, and thick dashed lines represent bases of temperature inversions. From Bjerknes and Palmén (1937).

nearly isothermal stratosphere, which slopes downward toward the north. A deep frontal layer, characterized by enhanced static stability and horizontal gradients of temperature, extends from the surface to the upper troposphere. This type of frontal zone was envisioned to separate polar from tropical air at all altitudes, and can be considered a vertical extension of the polar front identified by the Bergen School in Norway in their classic conceptual model of the structure and evolution of midlatitude cyclones (Bjerknes, 1919; Bjerknes and Solberg, 1921, 1922).

At the upper extent of the frontal zone in Fig. 2, where the horizontal temperature gradient becomes diffuse, the tropopause is folded into a characteristic "S" shape (Fig. 1a). The analysis of the fold is derived from soundings in the vicinity of upper fronts that contain an upper-tropospheric layer of pronounced static stability with potential temperatures at its base similar to those along the adjoining northern tropopause surface. The separation between the upper extension of the front and the folded tropopause inhibits the exchange of mass between the stratosphere and troposphere in the region of the fold. Nevertheless, quasi-horizontal transport between the stratosphere and troposphere is permitted in regions such as that south of the frontal zone where the tropopause rises discontinuously in a series of steps consisting of overlapping leaves. The analysis of the tropopause in Figs. 1a and 2 is compatible with the then-current thinking concerning stratospheric–tropospheric exchange, which held that the tropopause insulates the troposphere from the stratosphere except for slow leakage through the breaks in the tropopause and diffusion across the tropopause itself.

According to Palmén and Newton (1969, pp. 181–182), the structural model in Fig. 1a eventually fell into disuse because of limited observational evidence, and was replaced by that illustrated schematically in Fig. 1b and applied in a cross-section analysis based on radiosonde data in Fig. 3 (Palmén and Nagler, 1949). In this model, the folded tropopause is replaced by a "break region" separating the tropospheric frontal layer and the tropopauses overlying the polar and tropical air masses. As in the analysis of Bjerknes and Palmén, the tropospheric frontal zone is considered to separate polar from tropical air and is discontinued in the upper troposphere where the horizontal temperature gradient diminishes. The tropospheric frontal layer is also a zone of concentrated cyclonic and vertical shear of the component of the geostrophic wind normal to the cross section, which is computed from thermal wind considerations. Although the front is not analyzed above the tropopause break, the cyclonic shear is extended into the lower stratosphere within a broader zone than in the troposphere. Finally, the geostrophic wind analysis contains a jet core at the level of the tropical tropopause situated above the position of the frontal layer in the midtroposphere. The extremely

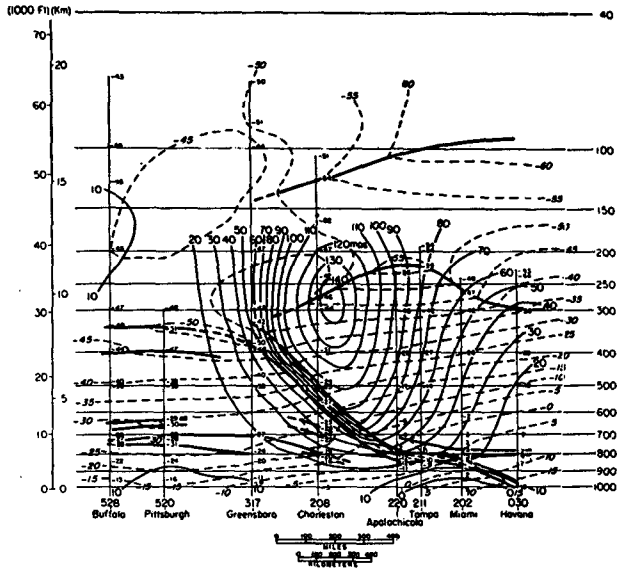

FIG. 3. North–south cross section from Buffalo, New York, to Havana, Cuba, oriented normal to an upper-level frontal zone embedded within a deep upper trough for 1500 GMT 5 February 1947. Thin solid lines are the component of the geostrophic wind normal to the cross section (m s^{-1}), dashed lines are isotherms (°C) and the thick solid lines are tropopauses or frontal boundaries (drawn dashed when relatively indistinct). From Palmén and Nagler (1949).

large geostrophic wind speeds in the jet core reflect the orientation of the cross section through a well-developed trough characterized by cyclonic curvature.

Berggren (1952) proposed an alternative structural model of upper-level fronts and the tropopause, which is shown in Figs. 1c and 4. This model differs from that used by Palmén and Nagler in that the tropospheric frontal layer is continued upward through the region of the tropopause break into the stratosphere. Within the tropopause break in the vicinity of the level of maximum wind (LMW) and in the lower stratosphere, where the horizontal temperature gradient becomes negligible and reverses in sign from that in the troposphere, the frontal zone is defined by strong cyclonic wind shear. The extension of the frontal zone high into the stratosphere could not be confirmed observationally and was discontinued in a later application of this model by Palmén (1958). As noted by Shapiro (1976), direct evidence for the narrow (~100 km) cross-front scale in the vicinity of the LMW was provided by the European sounding network, characterized by 100 km station spacing and a 6 h sampling frequency.

The greater spatial and temporal resolution afforded by the European radiosonde network in comparison with that of North America (400 km station spacing, 12 h sampling interval) probably contributed to the differences between the analyses of the cyclonic shear zone in the vicinity of the LMW and in the lower stratosphere by Berggren and by Palmén and Nagler, the latter of which is broader and more diffuse (compare

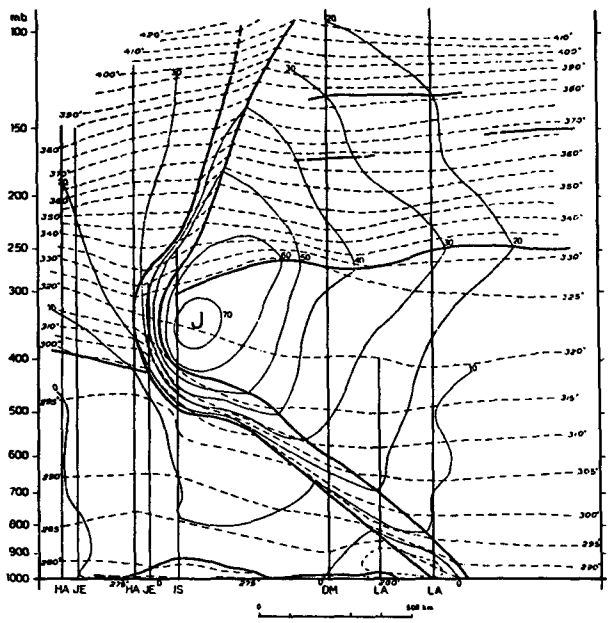

FIG. 4. Cross section oriented east–west across northern Europe from Hannover, West Germany, to Valentia, Ireland, of potential temperature (K, thin dashed lines) and observed wind speed (m s^{-1}, thin solid lines) for 0300 GMT 9 November 1949. Thick solid lines denote frontal boundaries, tropopauses and inversions; thin vertical lines give location and vertical extent of wind soundings. From Berggren (1952).

Figs. 3 and 4). The spatial resolution of the radiosonde network is less of an issue for the tropospheric part of the frontal zone than for the region of the tropopause break and lower stratosphere. The tropospheric portions of upper-level frontal zones contain significant vertical wind shear and static stability by virtue of their slope. Consequently, the cross-front horizontal scale can be determined from the detailed vertical resolution inherent within sounding data and knowledge of the frontal slope from adjacent soundings passing through the frontal layer. Spatial resolution becomes a significant factor where the frontal zone assumes a nearly vertical orientation, which occurs in the region of the LMW and lower stratosphere.

Contemporary with Berggren's approach for analyzing upper-level fronts was that introduced by a number of investigators including Newton (1954) and Reed (1955) and advocated by Reed and Danielsen (1959). In this approach (Figs. 1d and 5), the polar and tropical tropopauses are respectively joined with the lower (cold) and upper (warm) boundaries of the tropospheric frontal layer. In contrast to Berggren's model, the cyclonic shear zone in the stratosphere occupies a scale of hundreds of kilometers (Fig. 5a), a likely consequence of the limitations in North American radiosonde data referred to before. The Reed-Danielsen model explicitly accounts for stratospheric–tropospheric exchange through the hypothesis that upper-level frontal systems result from a process known as tropopause folding (Reed and Sanders, 1953; Reed, 1955), in which upper- and midtropospheric subsidence transports lower stratospheric air downward into the troposphere, occasionally reaching 700 to 800 mb in particularly intense cases. This hypothesis was based on the use of potential vorticity,[5]

$$P = -(\zeta_\theta + f)\frac{\partial \theta}{\partial p}, \tag{2.1}$$

where $\zeta_\theta + f$ is the absolute vorticity measured on isentropic surfaces, as a dynamical tracer for distinguishing between stratospheric and tropospheric air, which is valid to the extent that adiabatic, inviscid conditions prevail along parcel trajectories. The composite cross section in Fig. 5b shows the frontal boundaries separating potential vorticity values in the stratosphere of at least an order of magnitude greater than those in the troposphere, which is evidence of air of recent stratospheric origin within the tropospheric part of the frontal zone. The decrease of potential vorticity with decreasing altitude within the frontal layer is suggestive of turbulent-scale mixing of tropospheric and stratospheric air across the frontal boundaries.

The Reed-Danielsen frontal model represented a break from previous thinking in several respects. Based on earlier work by Reed and Sanders (1953) and Reed (1955), this model no longer required upper-level fronts to separate polar from tropical air. Rather than forming as a result of confluence between polar and tropical air currents through a deep tropospheric layer, upper-level fronts were hypothesized to develop primarily through the effects of tilting [in the prognostic equations for the horizontal potential temperature gradient (1.1) and vorticity (1.2)] due to differential subsidence associated with tropopause folding. According to this view, upper-level fronts were considered to separate stratospheric from tropospheric air rather than polar from tropical air. Furthermore, upper-level fronts were not required to extend to the surface, but could arise independently of low-level fronts and frontogenetical processes, a point emphasized by Sanders (1955) in connection with surface fronts. As referred to earlier, the tropopause folding process provided for the transport of stratospheric air toward the middle and lower troposphere, where it could mix with tropospheric air and eventually reach the Earth's surface. Interest in this particular exchange process in the 1950s and 1960s stemmed from the concern that stratospheric radioactivity generated by the atmospheric testing of nuclear weapons could reach the surface, exposing the biological risks of such a practice.

[5] An extensive review of meteorological applications of potential vorticity from observational and theoretical perspectives, including historical developments, is presented by Hoskins et al. (1985).

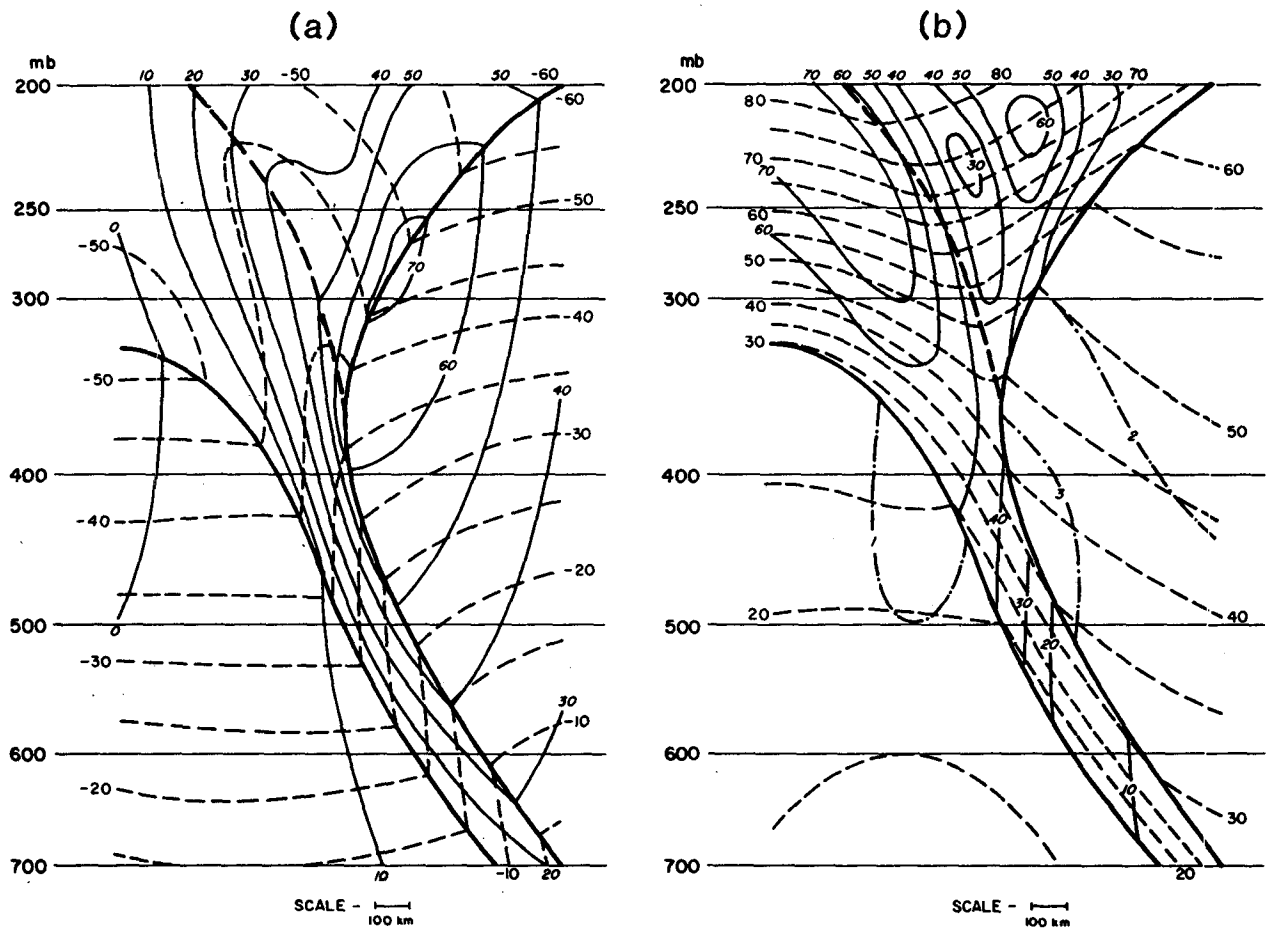

FIG. 5. Composite cross sections of upper-level frontal and tropopause structure. Frontal boundaries and the tropopause are indicated by heavy solid lines; axis of warm air in lower stratosphere is denoted by a heavy dashed line: (a) isotachs of the component of geostrophic wind normal to cross section (m s^{-1}, light solid lines) and isotherms (°C, light dashed lines); (b) isopleths of potential vorticity (10^{-6} K mb^{-1} s^{-1}, light solid and dash–dot lines) and isentropes (°C, light dashed lines). From Reed and Danielsen (1959).

Perhaps as a result of their novelty, coupled with the limitations of radiosonde data, the interpretations concerning upper-level frontogenesis derived from the Reed-Danielsen model remained controversial until additional independent observational evidence could be produced. Aircraft measurements of tracers such as water vapor, ozone and radioactivity (e.g., Briggs and Roach, 1963; Danielsen, 1964, 1968) confirmed the presence of stratospheric air within tropopause folds. Extensive diagnostic studies based on radiosonde data such as those of Staley (1960), Bosart (1970) and Shapiro (1970) demonstrated the importance of tilting effects due to differential subsidence in generating cyclonic vorticity and horizontal potential temperature contrasts characterizing upper-tropospheric fronts. The use of meteorologically instrumented aircraft to observe upper-level frontal systems directly in conjunction with conventional radiosonde data was to result in observational and conceptual advances culminating in the present-day structural model of upper-level fronts, which forms the subject of the following subsection.

b. The contemporary structural model of upper-level frontal systems

The direct probing of upper-level fronts with instrumented aircraft has resulted in refinements and extensions of concepts based on radiosonde data. In the first of a series of studies of upper-level frontal structure using aircraft measurements to supplement conventional radiosonde observations, Shapiro (1974) pointed out that earlier aircraft studies in the 1960s were limited by uncertainties in extracting horizontal winds using Doppler navigation techniques. The introduction of inertial navigation systems provided a degree of precision in the winds sufficient for sensing horizontal and vertical air motions within frontal zones down to the spatial and temporal scales of turbulent motions. Major results from the application of aircraft measurements to frontal research include the direct documentation of the ~100 km cross-front scale at the LMW as proposed by Berggren (1952), and a clearer appreciation of the nature and effects of CAT on the structure of upper-level fronts.

In reexamining upper-level fronts with mesoscale data from the European upper-air network, Shapiro (1976) reproduced Berggren's finding that the cyclonic shear in the lower stratosphere is confined to a scale on the order of 100 km rather than spread across a larger distance on the order of 500 km characterizing the Reed-Danielsen model (Fig. 5a). Direct wind measurements taken during horizontal traverses across the cyclonic shear zone in the vicinity of the LMW provided further confirmation of the mesoscale structure of upper-level fronts at the LMW and in the lower stratosphere. Figure 6 is a schematic illustration of the structural model derived from the results of aircraft flights combined with conventional radiosonde data, an example of which is shown in Fig. 7a. The schematic contains elements from both the Berggren and Reed-Danielsen models. As in the Berggren model (Fig. 1c), the frontal zone extends into the lower stratosphere where it slopes in the opposite sense as it does in the troposphere. Unlike the Berggren model, the tropopauses overlying the cold and warm tropospheric air masses do not break at the front, but are connected respectively with the lower and upper boundaries of the upper-tropospheric portion of the frontal zone, as in the Reed-Danielsen model (Fig. 1d).

The dynamical quantity absolute momentum,

$$m = u_g - fy, \tag{2.2}$$

introduced by Eliassen (1962), can be used to define upper-level frontal zones. In (2.2), u_g is the along-front (x) component of the geostrophic wind,

$$\mathbf{V}_g = \frac{1}{f}\mathbf{k} \times \nabla_p\phi = \left(-\frac{1}{f}\frac{\partial\phi}{\partial y}\right)\mathbf{i} + \left(\frac{1}{f}\frac{\partial\phi}{\partial x}\right)\mathbf{j}, \tag{2.3}$$

f is the Coriolis parameter, which is taken to be constant, and y is the cross-front coordinate, positive toward colder air. In (2.3), ϕ is the geopotential of a pressure surface. The quantity m is termed absolute momentum since it is the Cartesian (tangent-plane) analogy to absolute angular momentum for the rotating Earth. A property of m is that it describes the absolute geostrophic vector vorticity in the cross-front plane according to the relationship

$$\zeta_{g2} = -\mathbf{i} \times \nabla_2 m = -\frac{\partial m}{\partial p}\mathbf{j} - \frac{\partial m}{\partial y}\mathbf{k}, \tag{2.4}$$

where $\nabla_2 \equiv \partial/\partial y\ \mathbf{j} - \partial/\partial p\ \mathbf{k}$ is the two-dimensional gradient operator in the cross-front (y, p) plane.[6] The validity of (2.4) requires the frontal zone to be sufficiently straight and along-front variations to be sufficiently small to be considered two-dimensional ($|\partial v_g/\partial x| \ll |\partial u_g/\partial y|$). According to (2.4), the absolute geostrophic vector vorticity lies along lines of constant m.

Application of the thermal wind relationship

$$\frac{\partial \mathbf{V}_g}{\partial p} = -\gamma\mathbf{k} \times \nabla_p\theta = \left(\gamma\frac{\partial\theta}{\partial y}\right)\mathbf{i} + \left(-\gamma\frac{\partial\theta}{\partial x}\right)\mathbf{j} \tag{2.5}$$

allows the vertical gradient of m to be expressed in terms of the cross-front gradient of potential temperature; i.e.,

$$\frac{\partial m}{\partial p} = \gamma\frac{\partial\theta}{\partial y}. \tag{2.6}$$

Equations (2.5) and (2.6) are based on (2.3) and the hydrostatic equation in the form

$$\frac{\partial\phi}{\partial p} = -f\gamma\theta, \tag{2.7}$$

where

$$\gamma = \frac{R}{fp_0}\left(\frac{p_0}{p}\right)^{c_v/c_p} \tag{2.8}$$

is a function of pressure alone (for the assumption of constant f), p_0 is a reference pressure (1000 mb), R is the ideal gas constant for dry air, and c_v and c_p are the specific heats for dry air at constant volume and pressure, respectively. Inspection of (2.2) and (2.6) shows that the vertical component of absolute vorticity and the degree of baroclinicity characterizing a frontal zone are described respectively by the cross-front and vertical gradients of m. The vertical cross section in Fig. 8a displays the m field for the frontal zone in Fig. 7a. It

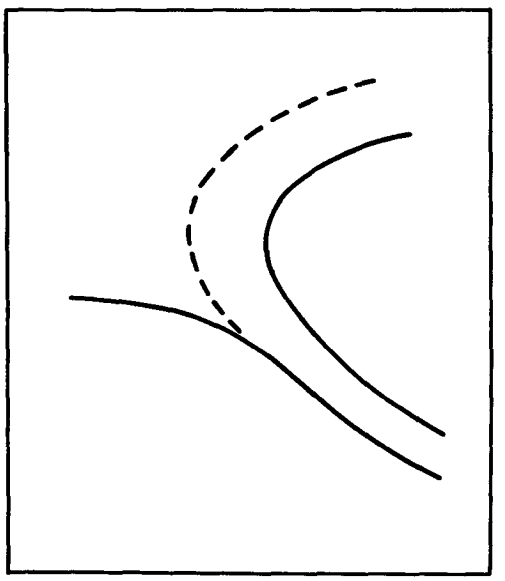

FIG. 6. Schematic diagram of the present-day model for analyzing upper-level fronts and tropopauses. Solid lines denote frontal and tropopause boundaries; dashed line depicts the boundary of cyclonic shear zone in the lower stratosphere.

[6] Defining the gradient operator in terms of $-\partial/\partial p$ allows the use of pressure as the vertical coordinate while preserving the familiar properties of a righthanded Cartesian coordinate system. Consistent with this definition of the gradient operator, the three-dimensional vector velocity is defined as $u\mathbf{i} + v\mathbf{j} - \omega\mathbf{k}$. This approach is equivalent to utilizing $-p$ as the vertical coordinate, as in Bluestein (1986).

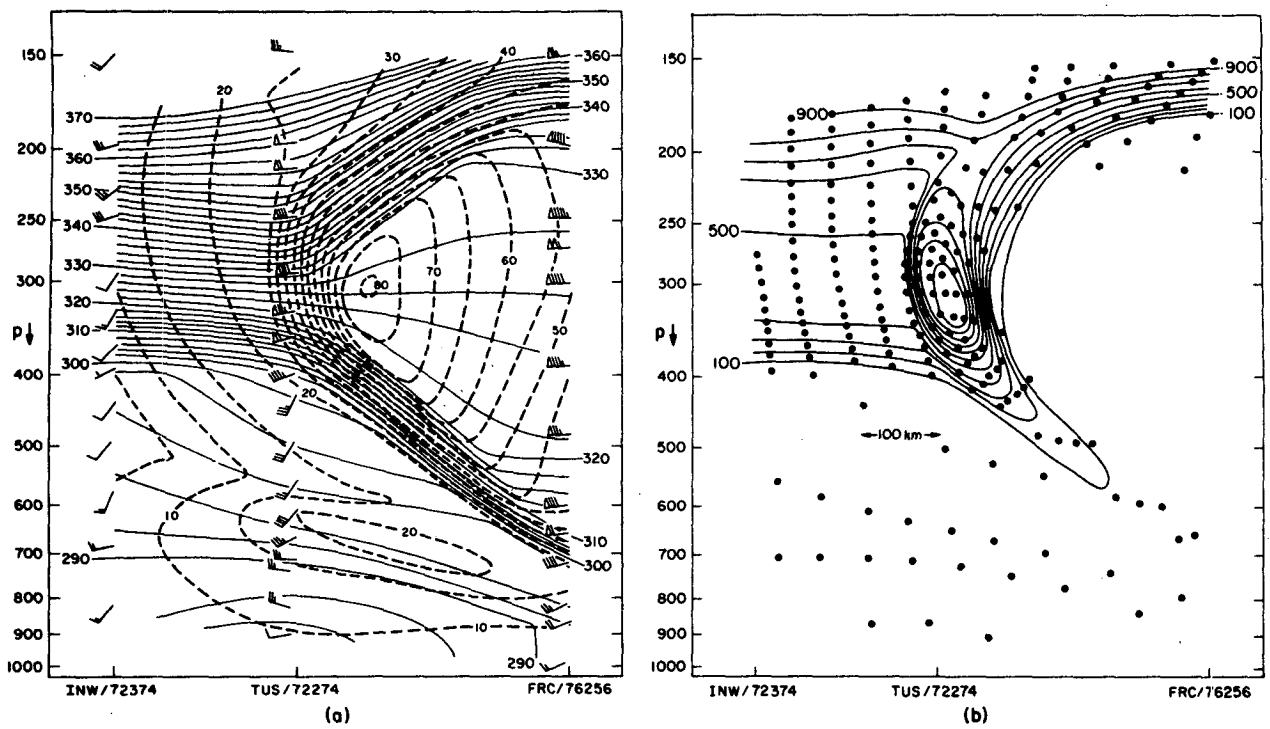

FIG. 7. Cross sections for 0000 GMT 17 April 1976 based on radiosonde observations at Winslow, Arizona (INW), Tucson, Arizona (TUS), and Fraccionamiento, Mexico (FRC), supplemented with NCAR Sabreliner aircraft data in the layer between 250 and 300 mb: (a) Potential temperature (K, solid lines) and wind speed (m s^{-1}, dashed lines). Winds are plotted with respect to north at the top of the figure; flags, full barbs and half barbs respectively indicate speeds of 25, 5 and 2.5 m s^{-1}. (b) Potential vorticity (10^{-7} K mb^{-1} s^{-1}, solid lines) and array of dots formed by the intersection of (m, θ) coordinates displayed in Fig. 8b. From Shapiro (1981).

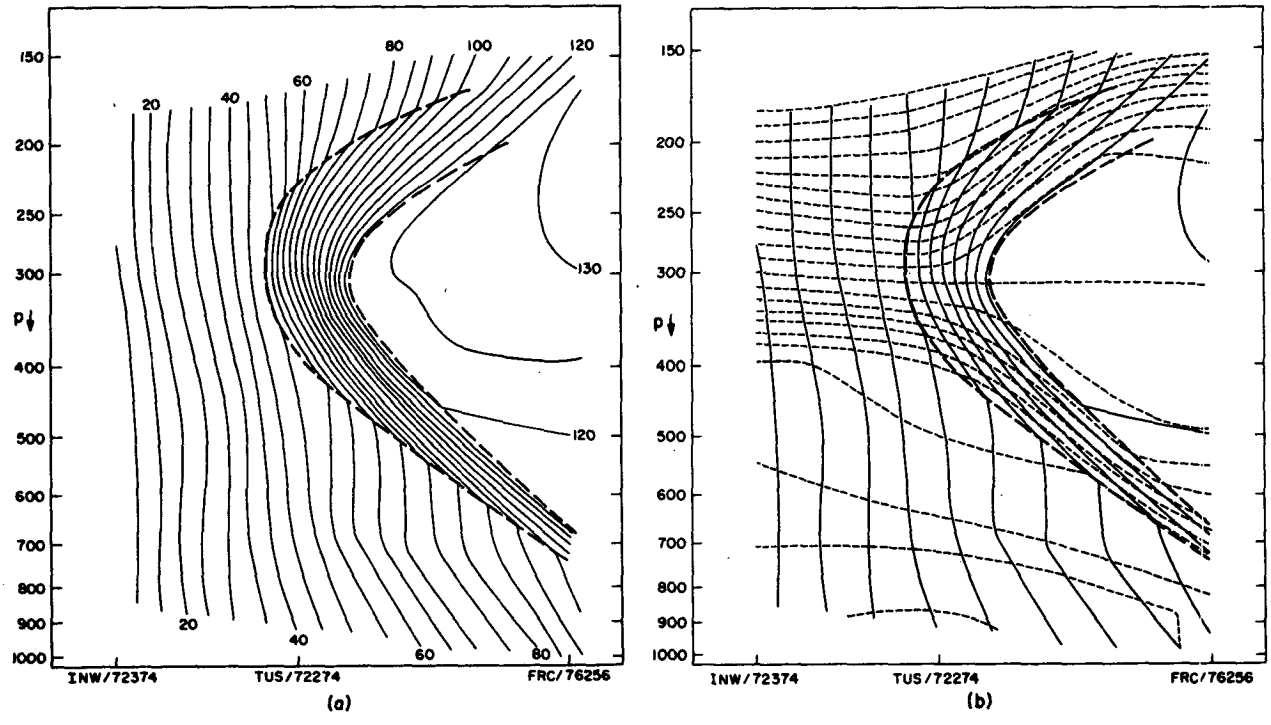

FIG. 8. Cross sections as in Fig. 7, except for (a) absolute momentum, $m = u_g - fy$, (m s^{-1}, solid lines) with $y = 0$ at left side of figure, decreasing toward the right; (b) (m, θ) coordinate grid from patterns in Figs. 7a and 8a, with contour intervals of 10 m s^{-1} and 4 K. Heavy dashed lines in (a) and (b) indicate first-order discontinuities in m. From Shapiro (1981).

is readily apparent that (i) the entire frontal zone is described by the region of large gradients of m in the (y, p) plane, (ii) the frontal zone is characterized by large magnitudes of the absolute geostrophic vector vorticity (2.4), and (iii) the frontal boundaries can be represented as discontinuities in the gradient of m. Thus, absolute momentum is a single parameter capable of describing two-dimensional frontal zones provided that the along-front component of the wind is approximately geostrophic.

For those situations where frontal zones satisfy the conditions for two-dimensionality alluded to following (2.4) and the along-front component of the wind is approximately geostrophic, the potential vorticity (2.1) can be expressed entirely in terms of the variation of quantities in the cross-front plane (denoted by subscript 2). Replacing $\zeta_\theta + f$ with $-\partial m/\partial y_\theta$ and transforming to pressure coordinates yields the expression

$$P_2 = J_{yp}(m, \theta), \tag{2.9}$$

where

$$J_{yp}(m, \theta) = -\mathbf{i} \cdot (\nabla_2 m \times \nabla_2 \theta) = \frac{\partial m}{\partial y_p}\frac{\partial \theta}{\partial p} - \frac{\partial m}{\partial p}\frac{\partial \theta}{\partial y_p}. \tag{2.10}$$

The Jacobian form of P_2 dictates that its magnitude is directly proportional to the areal density of intersections between contours of m and θ, or inversely proportional to the size of the solenoids formed by the intersections of adjacent pairs of m and θ contours. These interpretations are illustrated respectively in Figs. 7b and 8b. [In these figures the areal proportionality does not hold exactly because the vertical axes of the cross sections are drawn with respect to $\ln(p)$]. Potential vorticity is largest in the zone of stratospheric cyclonic shear, where the m lines and isentropes are concentrated and oriented nearly perpendicular to each other. This configuration may be contrasted to the tropospheric portion of the frontal layer where m lines and isentropes are closely spaced but nearly parallel to each other.

The structure of the cyclonic shear zone in the lower stratosphere turned out to have a significant implication concerning the effect of turbulent mixing on upper-level frontal structure. As cited earlier, the Reed-Danielsen model assumed more-or-less uniform distributions of stratospheric and tropospheric potential vorticity, which are discontinuous at the tropopause-frontal boundaries. The ~500 km horizontal scale of the cyclonic shear zone is consistent with the assumption of nearly uniform potential vorticity within the stratosphere and the upper-tropospheric portion of the frontal layer. In particular, reference to (2.1) and Fig. 5 reveals that large values of potential vorticity in the tropospheric part of the frontal zone are associated primarily with large static stability. Absolute vorticities are relatively moderate because isotachs coincide approximately with sloping isentropic surfaces. In the region of the LMW and lower stratosphere, the static stability is similar to that in the tropospheric part of the front, but the isentropes have a much smaller slope. Consequently, the isotachs must spread apart and occupy a larger cross-front scale to maintain values of potential vorticity comparable with those in the tropospheric part of the frontal zone.

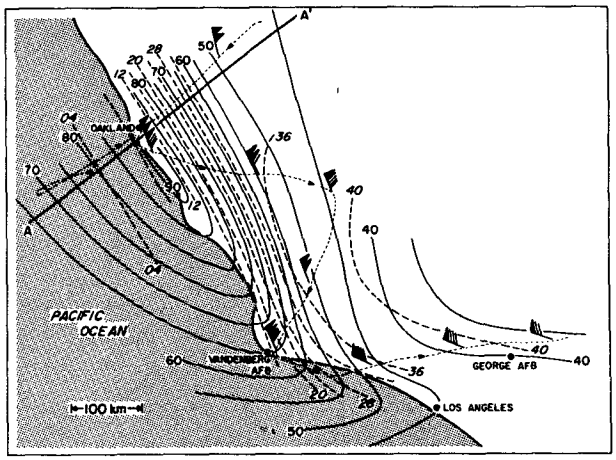

FIG. 9. Analyses of wind speed at 287 mb (m s^{-1}, solid) and ozone concentration (pphm vol^{-1}, heavy dashed lines) derived from Sabreliner data taken between 0615 and 0700 GMT 16 April 1976. Flight tracks are indicated by light dashed and dot–dashed lines. Line AA' is the projection for the cross section in Fig. 10. From Shapiro (1978).

In the case of the Berggren model, the ~100 km scale of the stratospheric cyclonic shear in the vicinity of the LMW implies much greater values of absolute vorticity on isentropic surfaces compared with the upper-tropospheric portion of the frontal layer and the stratospheric portion sloping over the jet core (Fig. 8b). Therefore, the potential vorticity at the LMW must be anomalously large relative to background stratospheric values rather than slowly varying, as evident from comparing Figs. 5b and 7b. The question that immediately arises concerns the source of the anomalous potential vorticity maximum in the LMW. If potential vorticity were conserved, this maximum would not be anticipated. Consideration of the hypothesis that potential vorticity is generated locally at the LMW led Shapiro (1976, 1978) to examine the roles of diabatic and frictional processes associated with turbulent mixing in upper-level frontal zones.[7]

c. *The effects of turbulent processes on upper-level frontal systems*

Figures 9 and 10 respectively display horizontal and cross-sectional subjective analyses of an upper-level jet

[7] A comprehensive summary of the results of earlier investigations of turbulent processes in upper-level frontal zones is given by Reiter (1969, pp. 191–220).

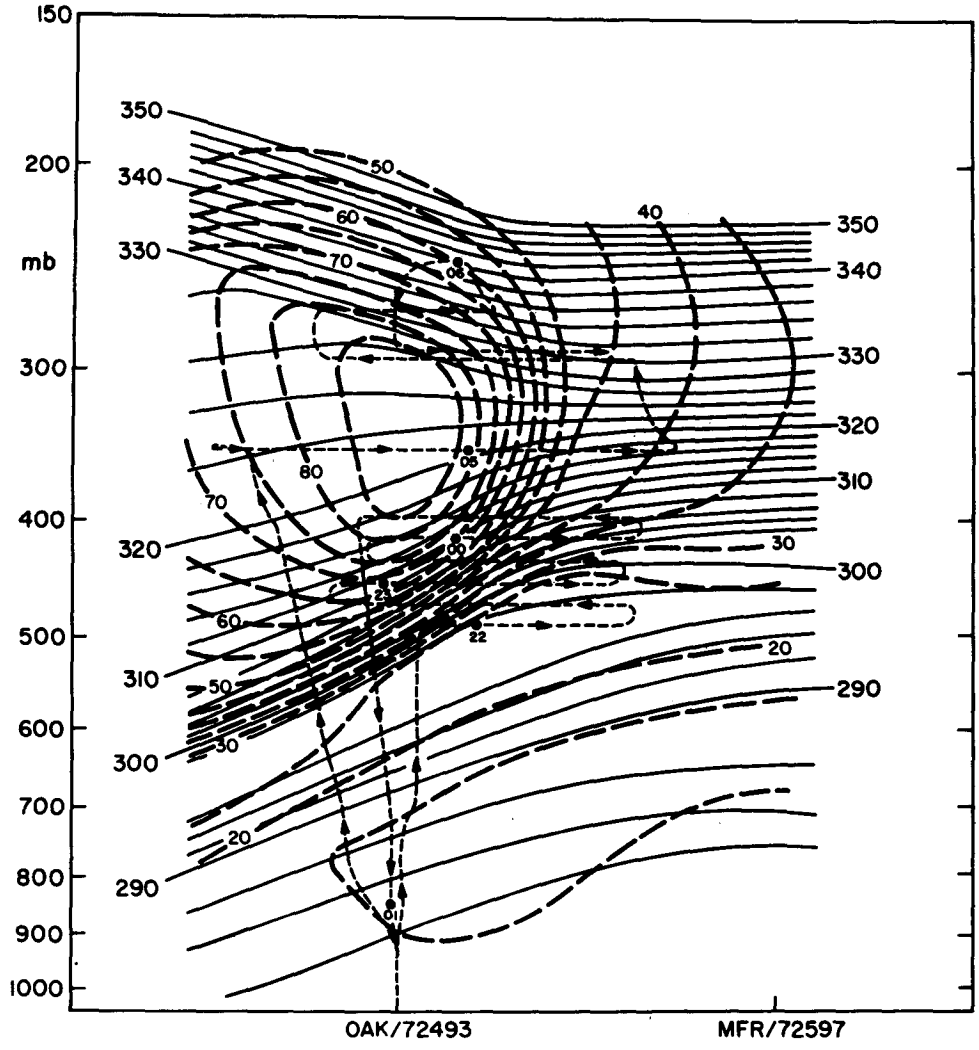

FIG. 10. Composite cross-section analysis based on aircraft and radiosonde data for 0000 GMT 16 April 1976 along line AA′ in Fig. 9. Heavy dashed lines indicate wind speed (m s^{-1}); solid lines are potential temperature (K). Flight path is denoted by light dashed lines; solid circles are times (GMT). Horizontal distance between OAK and MFR is about 500 km. From Shapiro (1978).

streak and its associated frontal zone, based on radiosonde data and supplemented by aircraft data. The aircraft traverses confirm the upward extension of the ~100 km scale cyclonic shear zone into the lower stratosphere. The cross-sectional distributions of potential vorticity and ozone (Figs. 11a and 11b), the latter of which can be considered a conservative quantity over the time scale of the generation of an upper-level front, suggest that potential vorticity is produced locally. If potential vorticity were conservative, its distribution would be expected to match that of the ozone much more closely. The lack of potential vorticity conservation, proposed previously by Eliassen and Kleinschmidt (1957) and Staley (1960), should not be taken as contradictory of earlier inferences on tropopause folding and upper-level frontogenesis by Reed (1955) and Reed and Danielsen (1959), which are confirmed by the downward-directed tongue in the ozone pattern.

The development of the potential vorticity maximum in the vicinity of the LMW evident in Figs. 7b and 11a can be discussed quantitatively in terms of the prognostic equation for the potential vorticity [as defined in (2.1)], which is

$$\frac{dP}{dt} = -(\zeta_\theta + f)\frac{\partial \dot{\theta}}{\partial p} + \frac{\partial \theta}{\partial p}\left[\mathbf{k}\cdot\left(\nabla_\theta \dot{\theta} \times \frac{\partial \mathbf{V}}{\partial \theta}\right)\right] - \frac{\partial \theta}{\partial p}[\mathbf{k}\cdot(\nabla_\theta \times \mathbf{F})]. \quad (2.11)$$

In the above expression, ∇_θ is the horizontal gradient operator for isentropic surfaces, and $\mathbf{F}$ and $\dot{\theta}$ are the

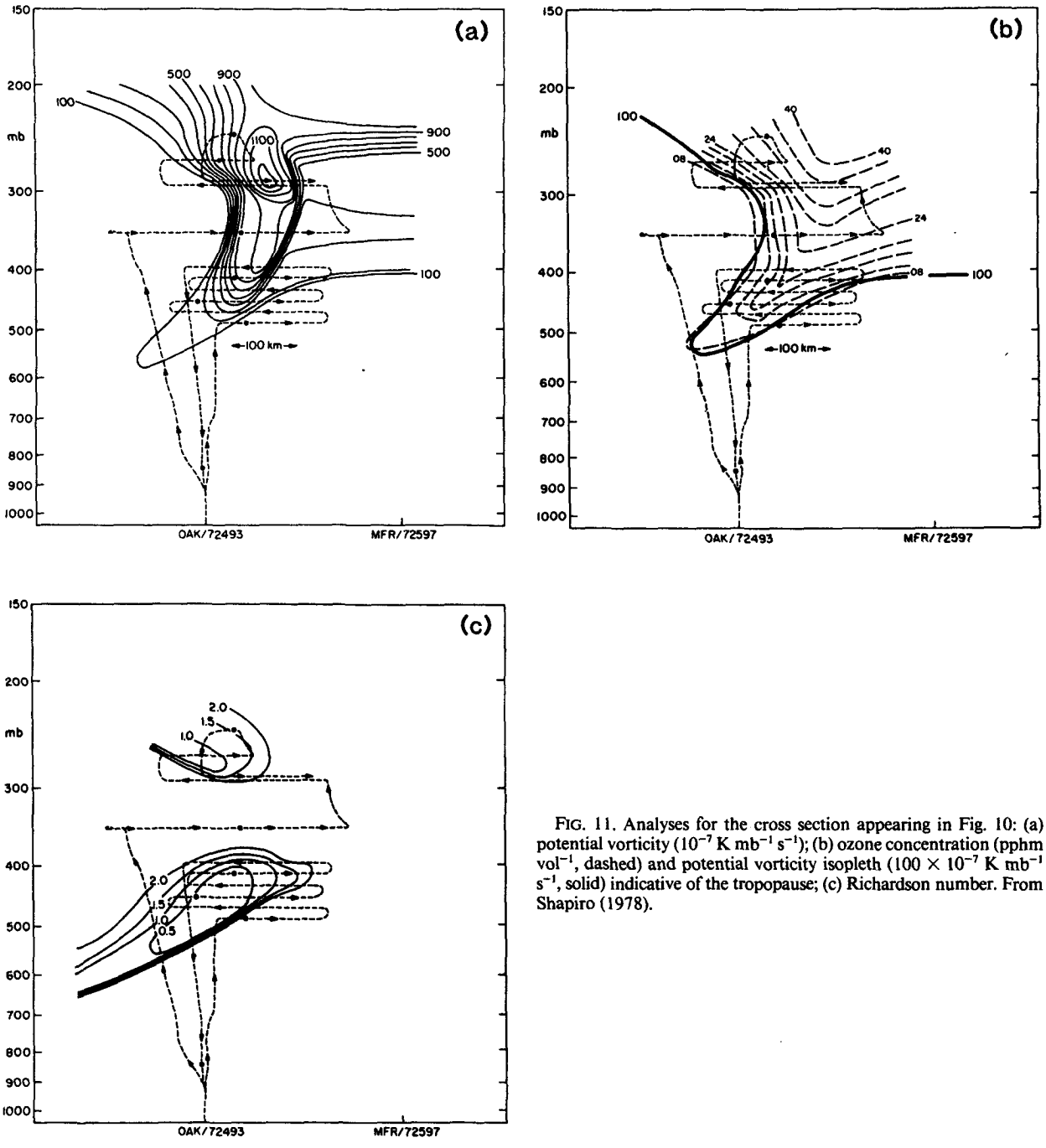

FIG. 11. Analyses for the cross section appearing in Fig. 10: (a) potential vorticity (10^{-7} K mb^{-1} s^{-1}); (b) ozone concentration (pphm vol^{-1}, dashed) and potential vorticity isopleth (100×10^{-7} K mb^{-1} s^{-1}, solid) indicative of the tropopause; (c) Richardson number. From Shapiro (1978).

frictional and diabatic contributions to the prognostic equations for the horizontal vector wind and potential temperature. Detailed discussion of (2.11) can be found in Staley (1960) and Gidel and Shapiro (1979). Shapiro (1976) applied (2.11) at the LMW in the stratospheric zone of cyclonic shear (approximately 355 mb in Figs. 10 and 11), which removed the middle term on the right from consideration. On the basis of the results of a scale analysis, Shapiro further neglected frictional processes and focused on the first term, describing the effect of the vertical distribution of diabatic heating due to vertical mixing by CAT. The diabatic heating rate may be expressed as

$$\dot{\theta} = g \frac{\partial}{\partial p} (\rho \overline{w'\theta'}), \tag{2.12}$$

where g is gravity, ρ is the density of dry air, w is the vertical velocity in terms of height, z, primed quantities

denote turbulent eddy motions and the overbar indicates an ensemble average. With the above assumptions, (2.11) reduces to

$$\frac{dP}{dt} = g(\zeta_\theta + f)\frac{\partial^2}{\partial p^2}(-\rho\overline{w'\theta'}). \qquad (2.13)$$

The vertical eddy flux of potential temperature, $\overline{w'\theta'}$, is expected to be large and negative (downward) in regions of CAT, which is favored by small values of Richardson number,

$$\mathrm{Ri} = \frac{g}{\theta}\frac{\partial\theta}{\partial z}\Big/\left|\frac{\partial \mathbf{V}}{\partial z}\right|^2. \qquad (2.14)$$

The cross-sectional distribution of Ri is shown in Fig. 11c for the frontal zone in Fig. 10. As evident from these figures and the schematic illustration in Fig. 12, Ri is minimized in kidney-shaped patches of large vertical wind shear situated above and below the jet core, implying maximum positive values of $-\overline{w'\theta'}$ in these regions. The postulated vertical profile of $-\overline{w'\theta'}$ in Fig. 13, applicable to the cyclonic shear side of the jet core, reflects the vertical distribution of the Richardson number described above, and indicates static stabilization and potential vorticity generation at the LMW, where the curvature of the $-\overline{w'\theta'}$ profile is maximized. This inference is based on the approximated form of the potential vorticity equation (2.13). The overall effect of CAT is to produce warming (cooling) in the ~1 km thick layer above (below) the LMW through a convergence (divergence) of the vertical eddy flux of potential temperature [$\dot{\theta} \approx -\partial(\overline{w'\theta'})/\partial z$]. The vertical distribution of diabatic heating due to CAT acts to inhibit the vertical spreading of the isentropes at the LMW that would be required if potential vorticity were conserved during the frontogenetical scale contraction of the cyclonic shear zone to ~100 km. Direct measurements of the eddy flux of potential temperature using research aircraft indicate that the described mechanism is sufficiently intense to account for an exponential "doubling" time of about 10 h for the potential vorticity (Shapiro, 1978).

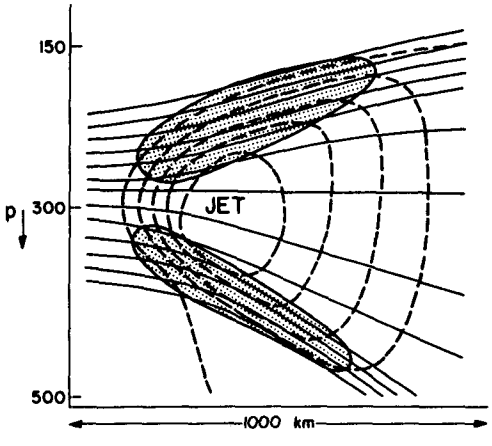

FIG. 12. Schematic illustration of regions of clear-air turbulence (stippled) in the vicinity of an upper-level jet core and frontal zone. Solid and dashed lines respectively indicate potential temperature and wind speed. From Shapiro (1976).

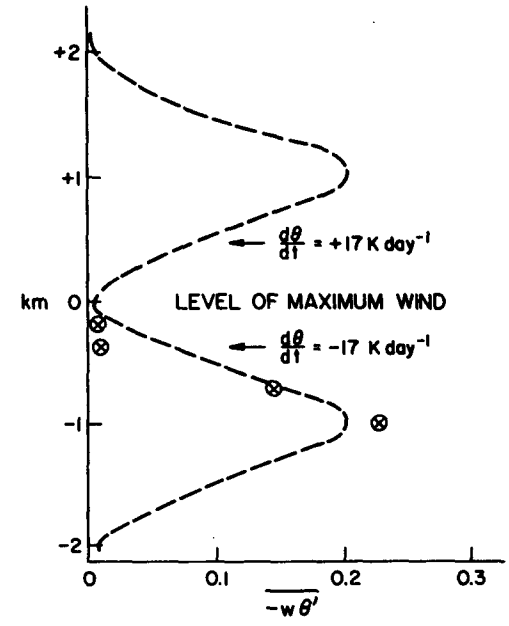

FIG. 13. Vertical profile of the downward eddy flux of potential temperature ($-\overline{w'\theta'}$ in m s^{-1} K) expected on the cyclonic shear side of an upper-level jet. Circles enclosing x's indicate observed fluxes from Kennedy and Shapiro (1975). From Shapiro (1976).

The mechanism responsible for enhancing the static stability within the LMW can also be shown to diminish the static stability within the frontal shear layers, as apparent from the curvature of the $-\overline{w'\theta'}$ profile 1 km above and below the LMW in Fig. 13. Browning and Watkins (1970) and Browning (1971) documented the occurrence of such a decrease in static stability in an upper-tropospheric frontal layer as a result of an episode of Kelvin-Helmholtz billows, which were detected by radar. Time–height sections illustrating the wind speed along with its vertical shear and the static stability are respectively shown in Figs. 14a and 14b. The statically stable layer marking the upper-tropospheric frontal zone is shown to split as a consequence of vertical mixing during the billow event. The profiles of vertical wind shear, Richardson number and static stability immediately before and after the billow event (Fig. 15) indicate an overall decrease in the wind shear and increase in the Richardson number. The static stability is diminished within the shear layer and enhanced at its top and bottom, as would be expected from considering a vertical profile of $-\overline{w'\theta'}$ similar to that in Fig. 13 below the LMW.

The bulk effect of CAT is to limit the horizontal and vertical scale contractions of sloping upper-tropo-

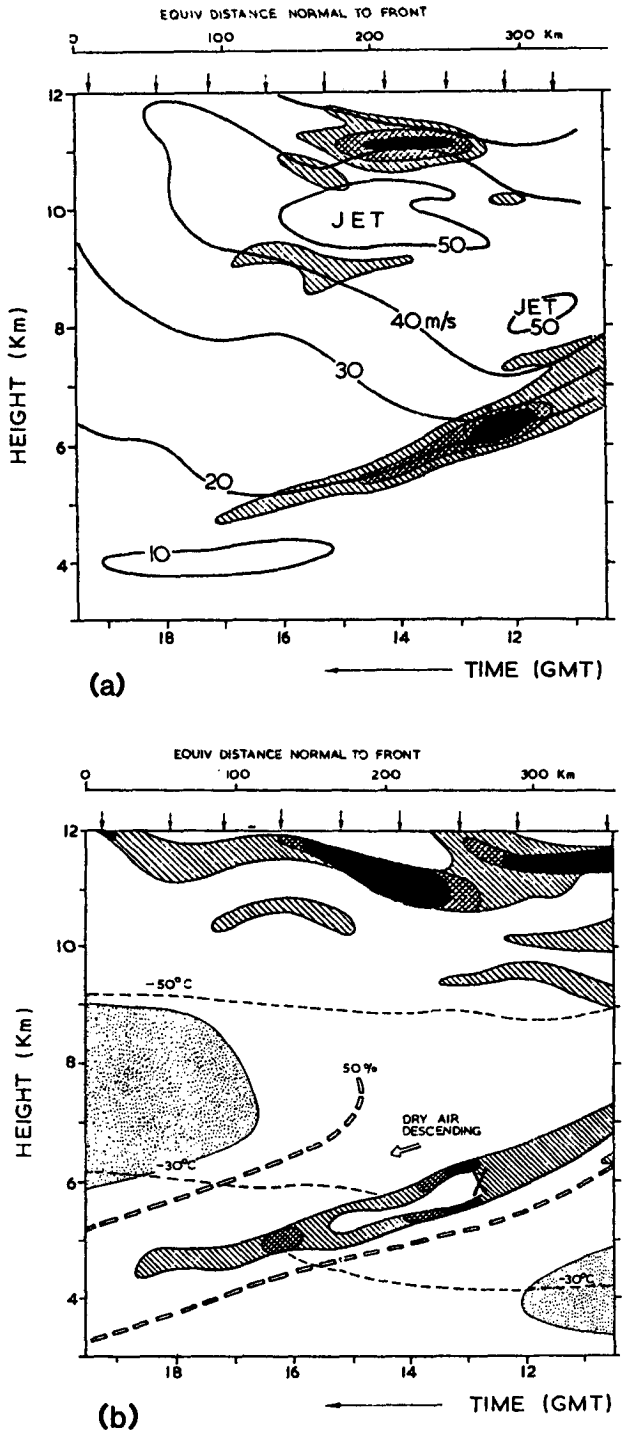

FIG. 14. (a) Time–height cross section of wind speed and the magnitude of the vertical wind shear for an upper-level jet on 6 February 1970, derived from balloon-borne targets tracked by radar at the times indicated by vertical arrows. Solid lines are isotachs (contour interval 10 m s^{-1}); hatched, cross-hatched and solid shading respectively indicate shears of 8–12, 12–16 and >16 m s^{-1} over 400 m. (b) Time–height cross section of the vertical gradient of potential temperature determined from radiosonde ascents at the times indicated by vertical arrows. Hatched, cross-hatched and solid shading respectively correspond to $\partial\theta/\partial z > 1.5$, 2 and 2.5°C (100 m)$^{-1}$. Thin dashed lines indicate isotherms (°C). The thick dashed contours reveal the boundaries of dry air (relative humidity of 50% with respect to ice). Stippling denotes region of cirrus. The large X indicates the time and location of a Kelvin-Helmholtz billow event, which is followed by the splitting of the stable frontal layer. From Browning (1971).

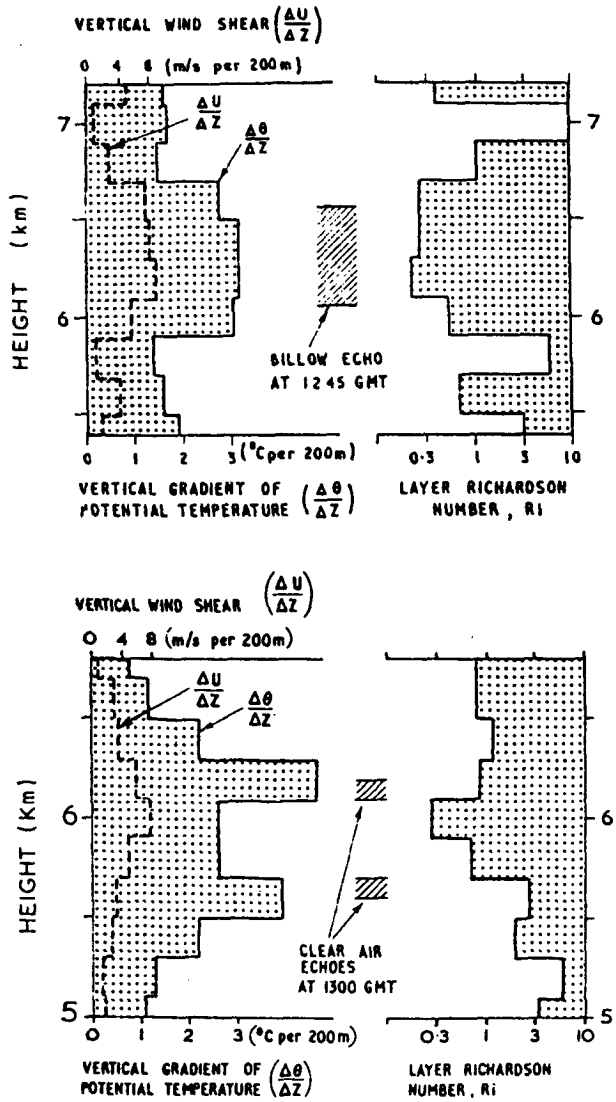

FIG. 15. Vertical profiles of static stability, vertical wind shear and Richardson number derived from radiosonde ascents on 6 February 1970 immediately before (top, 1207 GMT) and after (bottom, 1309 GMT) a large-amplitude billow event. All of the above quantities are evaluated over a 200 m height increment. The clear-air radar echoes correspond to the vertical extent of the Kelvin-Helmholtz billows at 1245 GMT (top) and to the two-layer structure in the static stability profile at 1300 GMT (bottom). From Browning and Watkins (1970).

spheric frontal layers to the observed minimum values of approximately 100 km and 1.5 km (100 mb) (Browning et al., 1970; Roach, 1970). The limiting horizontal scale can be related to the Richardson number according to the expression

$$\delta y = \left(\frac{\gamma \mu_\theta \delta\theta}{f}\right) \mathrm{Ri}, \qquad (2.15)$$

where δy is the cross-frontal scale, μ_θ is the slope of isentropes ($\delta p/\delta y_\theta$) within the frontal zone and $\delta\theta$ is the potential temperature difference across the front. Equation (2.15) is derived from the expression for Ri in pressure coordinates with the assumption that $\partial V/\partial p$ can be replaced by the vertical shear of the along-front component of the geostrophic wind, $\partial u_g/\partial p$. Taking values typical of the 500 mb level in midlatitudes ($\gamma = 4.71 \times 10^3$ m^2 s^{-1} K^{-1} mb^{-1}, μ_θ = (100 mb) (100 km)$^{-1}$, $\delta\theta = 10$ K, $f = 1 \times 10^{-4}$ s^{-1}) and Ri between 0.25 and 0.3, which is compatible with the measurements in Fig. 15, yields δy between 120 and 140 km. This estimate of the cross-frontal scale is comparable with observed values.

An implication of the nonconservation of potential vorticity is that the folded tropopause associated with a well-developed upper-level frontal zone is not a material surface, but is a region of active systematic transport of air between the stratosphere and troposphere. In particular, the generation of potential vorticity at the LMW provides a mechanism by which trajectories following the mean motion may enter the stratosphere from the troposphere. Further discussion of the stratospheric–tropospheric exchange process with respect to upper-level frontal zones appears in papers by Shapiro (1978, 1980). At the time of their publication, there existed widespread interest among the scientific community in identifying processes by which chlorofluoromethanes could enter the stratosphere from the troposphere and participate in the chemical consumption of ozone, which is required to filter the ultraviolet portion of the spectrum of incoming solar radiation. This focus may be contrasted with the emphasis 20 years earlier on the transport of radioactivity from the stratosphere to troposphere. A more general perspective on the stratospheric–tropospheric exchange problem is provided in the review by Reiter (1975).

d. *The relationship of upper-level frontal systems to baroclinic wave structure*

Although a rather complete description of the structural characteristics of well-developed upper-level frontal systems has emerged over the past 50 years, progress has been limited in describing and understanding the temporal evolution of upper-level fronts in the context of structural changes of baroclinic waves through their life cycles. The slow rate of progress can be attributed primarily to restrictions in spatial coverage, temporal resolution and accuracy of radiosonde data. A consequence of limited coverage and temporal resolution is that upper-level frontal zones cannot be tracked continuously throughout their entire life histories. Significant structural changes often occur over data-sparse regions or between upper-air observing times (typically separated by 12 h). As a result, observational documentation of the initial development of upper-level fronts, as well as details of the frontogenesis process, has been virtually nonexistent or at best fragmentary. Restrictions in horizontal resolution have not been as much of a problem as temporal resolution, because the detailed vertical resolution in radiosonde observations can be converted into horizontal resolution finer than that anticipated from the station spacing in regions of sloping tropospheric frontal layers, as alluded to in Section 2a and discussed by Shapiro (1970), Shapiro and Hastings (1973) and Petersen (1986).

Observational uncertainties in radiosonde data have been emphasized regarding winds, especially within and above the upper troposphere under strong-wind conditions, where balloon elevation angles become small and errors in differences in balloon position become magnified. As a result, direct measurement of jet-stream winds is not always possible and estimates of ageostrophic winds are subject to uncertainty. Consequently, the results of observational studies of dynamical interactions between the primary (geostrophic) and secondary (ageostrophic) circulations in upper-level frontal systems often have been controversial. Finally, the role of aircraft data has been to augment the spatial resolution of radiosonde observations and also to reduce uncertainties in radiosonde-derived winds. Investigation of upper-level frontal systems with aircraft observations has been limited, however, to documenting the structure of upper-level fronts over short time intervals; it has not been feasible to deploy aircraft to monitor upper-level fronts continuously through a segment of (let alone all of) their life histories.

A case study of the evolution of a baroclinic wave over North America during a 48 h period by Newton (1958) contains many of the salient aspects known concerning the relationship of upper-level frontal systems to the synoptic-scale baroclinic waves in which they are embedded. In Fig. 16, depicting the development of an upper-level trough at a relatively early stage, the upper-level frontal zone and jet are clearly defined in the northwesterly flow upstream of the trough axis. Downstream of the trough axis, frontal structure is most apparent at the surface, whereas it is diffuse aloft. One day later (Fig. 17), the upper trough has amplified and the surface cyclone has intensified, while the frontal structure has become more-or-less symmetric relative to the trough axis. At the final time shown (Fig. 18), the frontal system on the downstream side of the trough axis is more distinct in comparison with that on the upstream side, so that the asymmetry is essentially reversed from its configuration two days earlier. A similar chain of events is described by Palmén and Newton (1969, pp. 335–338). Questions concerning the interpretation of the sequence of events in Figs. 16–18 center on the details of the process by which the upper-level frontal system becomes established on the downstream side of the trough between Figs. 16 and 17. Data lim-

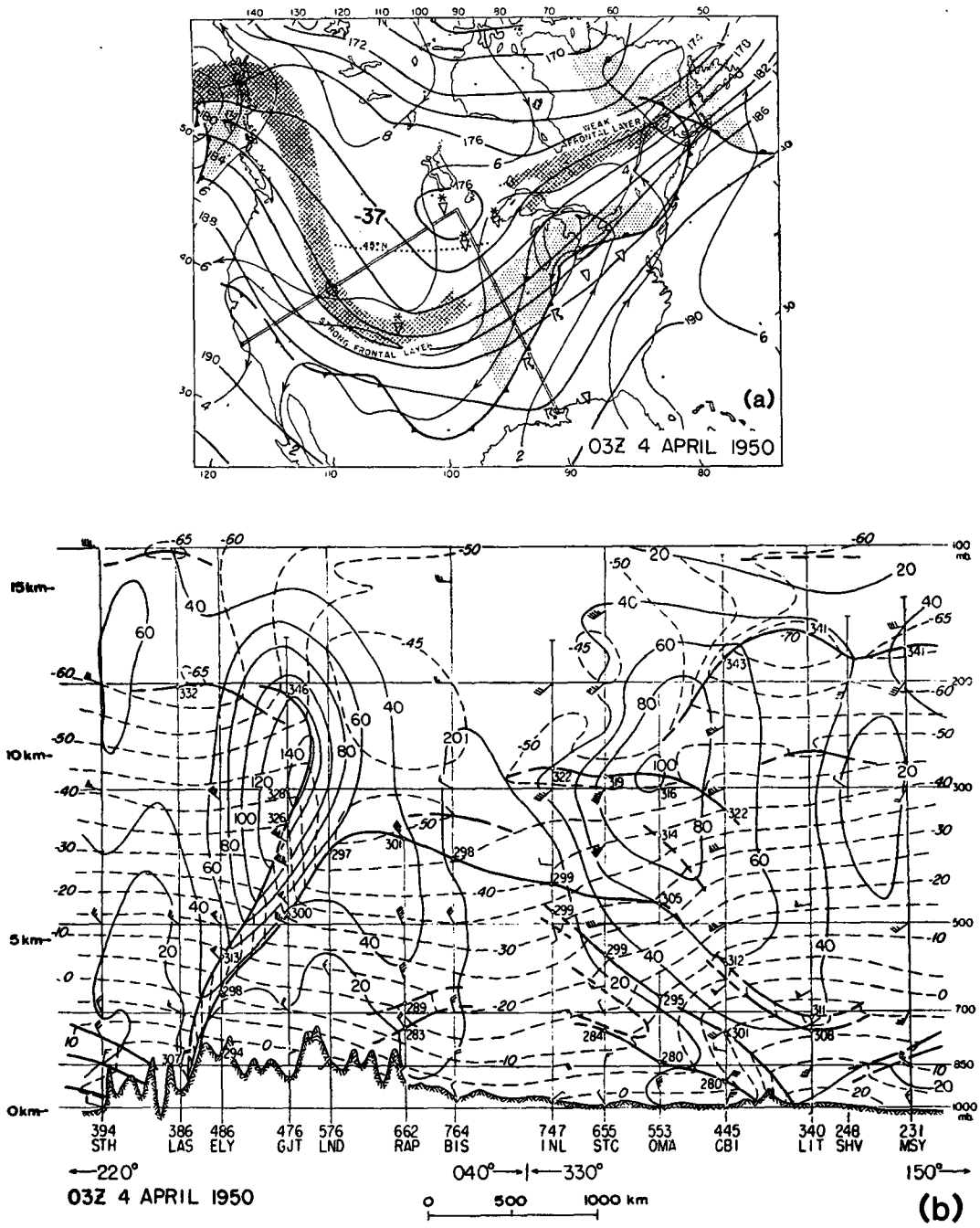

FIG. 16. Synoptic analyses over North America for 0300 GMT 4 April 1950. (a) Surface fronts, 1000 mb height contours (thin lines, contour interval 200 ft) and 500 mb height contours (thicker lines, contour interval 200 ft). Stippling indicates continuous precipitation; cross hatching represents well-defined frontal zones at 500 mb. (b) Cross section along thin double lines in (a). Heavy lines denote tropopauses and boundaries of frontal and stable layers. Total wind speed (kt) is depicted by thin solid lines, temperature (°C) by dashed lines. Selected winds are plotted with respect to north at the top of the figure; flags, full barbs and half barbs respectively indicate 50, 10 and 5 kt. Three-digit numbers are potential temperature (K). From Newton (1958).

itations of the type referred to above prevent establishing the degree to which the frontal structure is advected in from the west relative to being generated locally, and the extent to which the upper-level and surface systems merge as indicated relative to remaining structurally independent.

Various investigators have examined the structure of upper-level fronts during particular stages of the se-

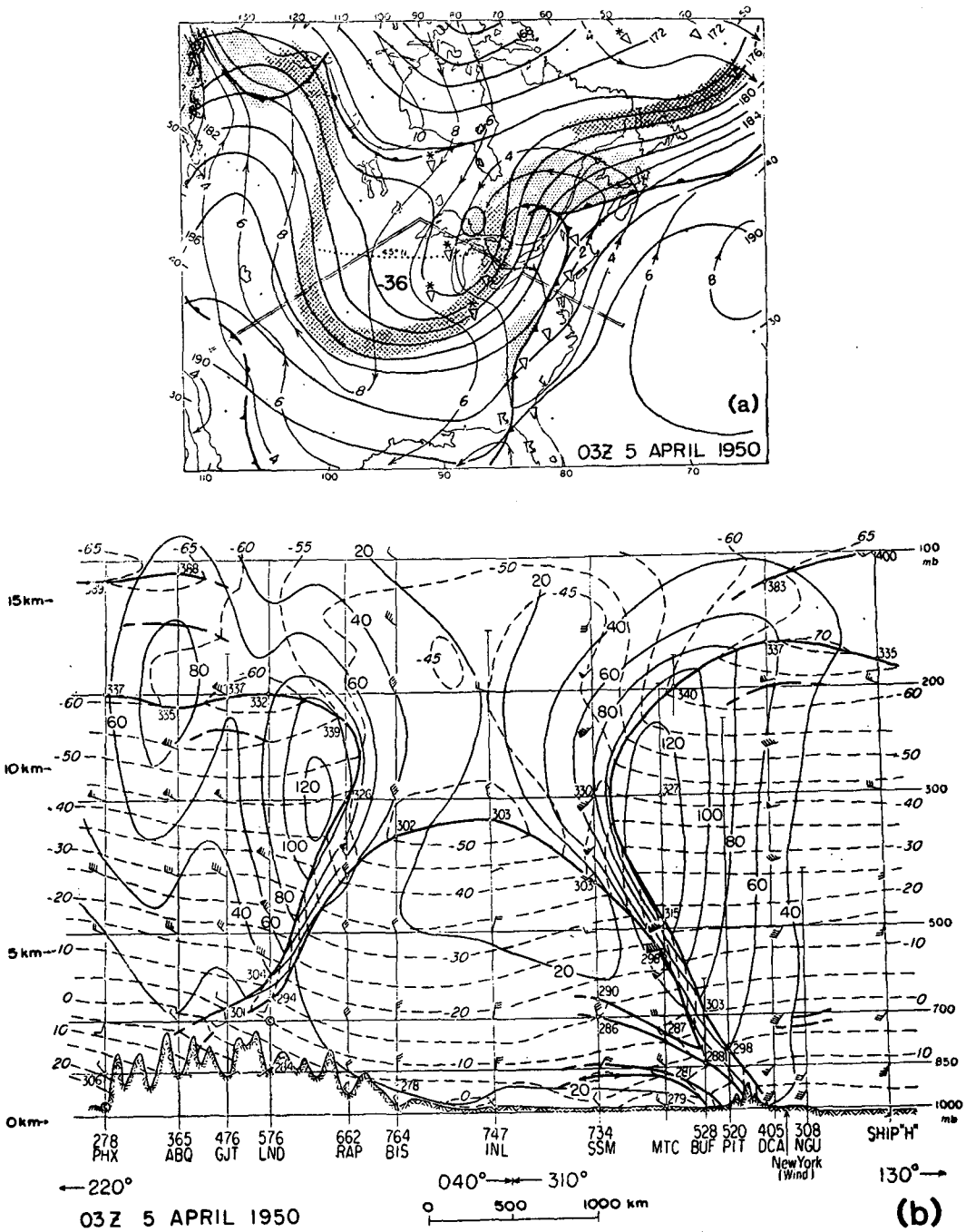

FIG. 17. As in Fig. 16, except for 0300 GMT 5 April 1950.

quence of events illustrated in Figs. 16–18. The majority of case studies have focused on the stage in Fig. 16, where an upper-level front is embedded in the northwesterly flow upstream of a trough axis, including those of Reed and Sanders (1953), Newton (1954), Staley (1960), Shapiro (1970) and Uccellini et al. (1985). A consistent outcome of these studies is the dominance of tilting, due to a cross-stream gradient of vertical motion such that subsidence is maximized on the warm side of the frontal zone, in generating the cross-frontal potential temperature gradient (1.1) and cyclonic vorticity (1.2). A more general case study by Reed (1955) describing the development of a major trough over North America also documents the importance of differential subsidence in producing upper-level frontogenesis and associated tropopause folding

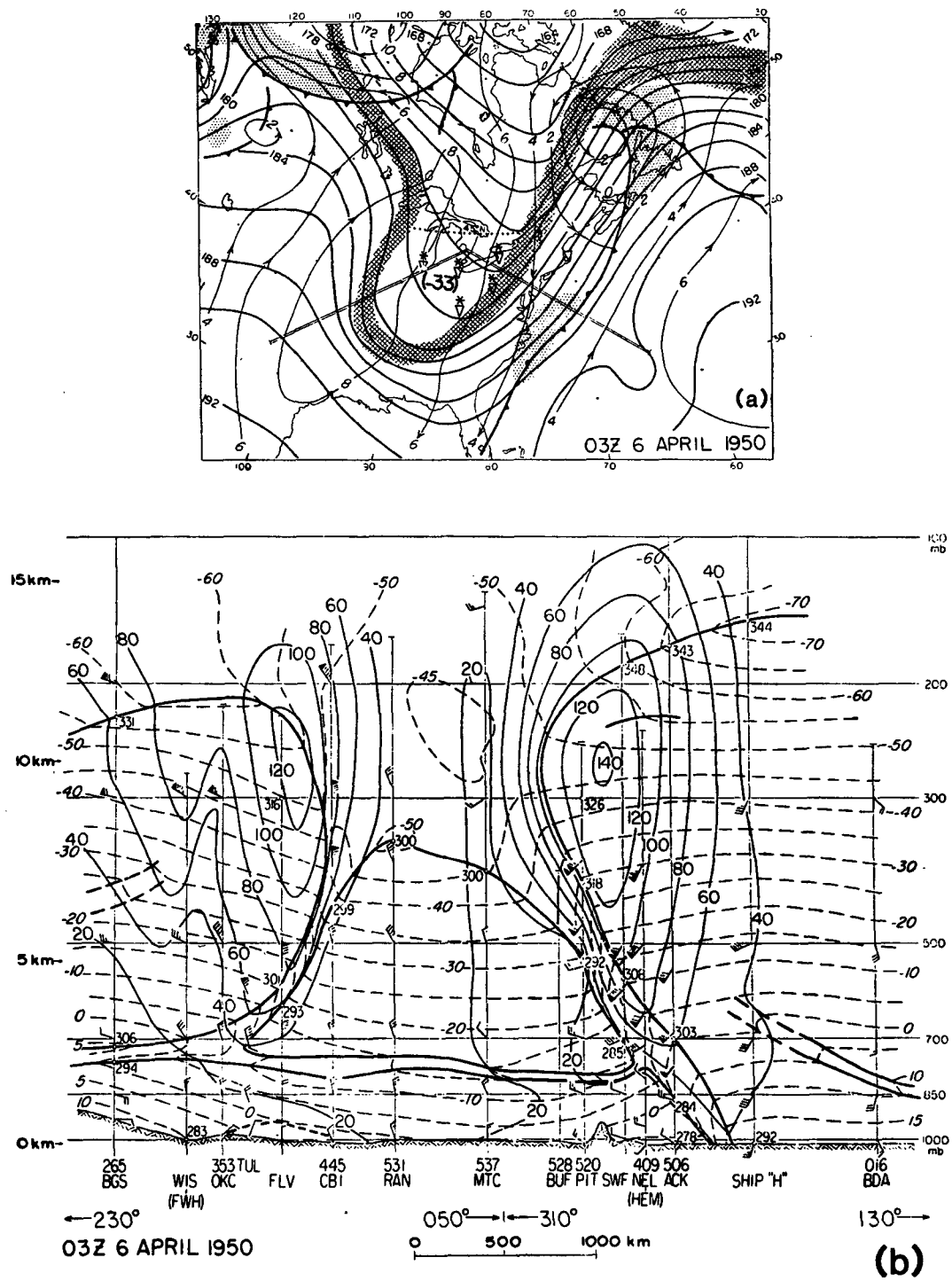

FIG. 18. As in Fig. 16, except for 0300 GMT 6 April 1950.

in the northwesterly flow upstream of the trough axis. In Reed's case, the upper-level frontal system eventually attained its greatest intensity and the tropopause fold reached its maximum downward penetration in the confluent southwesterly flow downstream of the trough axis. The outcome of this study suggests that the upper-level front was generated in the northwesterly flow upstream of the trough axis by tilting processes, and was

subsequently transported around the base of the trough into the southwesterly flow where its intensity was maintained or augmented by horizontal confluence.

A progression of events similar to that in Reed's case study is evident in the case examined by Bosart (1970), who considered upper-level frontogenesis in terms of the migration of a short-wave trough comprising the frontal zone through a major long-wave trough. Temporal resolution of 3 h was available through a special radiosonde network situated over the southeastern United States. The upper-level front intensified initially as a result of tilting in the northwesterly flow upstream of the axis of the long-wave trough. The frontal zone then reached its maximum strength in the southwesterly flow downstream of the axis of the long-wave trough as a result of horizontal confluence. At this stage, tilting effects were found to be frontolytical, with the reversal in sign having occurred as the upper-level front propagated around the base of the long-wave trough.

Shapiro (1983) synthesized the preceding observational evidence into a hypothetical schematic depicting the migration of an upper-tropospheric jet-front system[8] through a synoptic-scale baroclinic wave situated over North America (Fig. 19). The stages represented in this schematic correspond closely with those identified by Riehl et al. (1952, Fig. 15), Riehl et al. (1954, Fig. 2.7) and Krishnamurti (1968) for the passage of a short-wave trough through a long-wave trough. The progression of events begins over western Canada with the confluence between a polar trough and a midlatitude ridge (Fig. 19a), a flow configuration hypothesized by Namias and Clapp (1949) to be conducive to the formation and intensification of upper-level fronts and jets. Roughly a day later (Fig. 19b), the jet and front have progressed to the inflection in the northwesterly flow upstream of a diffluent trough exhibiting a northwest–southeast tilt. The thermal wave lags the height wave by one-quarter wavelength, which places the front in a region of cold advection. The tilt in the height field is a sign of barotropic amplification provided that the background (zonally averaged) zonal wind becomes increasingly westerly with latitude in the vicinity of the developing short-wave disturbance (Haltiner and Williams, 1980, pp. 72–75), while the separation between the thermal and height waves is optimal for baroclinic amplification (Holton, 1979, pp. 134–135, 223–227). The flow configuration in Fig. 19b reflects the sense of the asymmetrical trough structure in the early stages of development identified by Newton (1958) in Fig. 16, and is consistent with previous descriptions of upper-level frontogenesis due to differential subsidence occurring in the northwesterly flow inflection.

At the following time (Fig. 19c), the jet-front system has reached the base of the long-wave trough and assumed a curved orientation. The absence of asymmetries in terms of the disappearance of the latitudinal tilt and phase separation between the thermal and height fields indicates the cessation of barotropic and baroclinic amplification. At the final time (Fig. 19d), the jet and front have migrated to the inflection in the southwesterly flow downstream of the long-wave trough, which has taken on a confluent configuration. The southwest–northeast tilt of the trough axis and the thermal wave leading the height wave respectively signal barotropic and baroclinic damping. The sense of the asymmetry is reversed from that in Fig. 19b, and corresponds to the stage of upper-trough development illustrated in Fig. 18 and the observational descriptions of upper-level fronts maintained by confluence in the southwesterly flow downstream of a long-wave trough axis.

The preceding discussion underscores the relationship between upper-level frontal evolution and the environmental baroclinic wave. The synoptic-scale wave structure provides the dynamical setting in which processes involving the interplay between primary and secondary circulations lead to scale contractions resulting in and maintaining fronts. The following section will introduce and interpret a theoretical approach for diagnosing the vertical (secondary) circulations, given the geostrophic (primary) flow field, that is applicable to idealized, two-dimensional flow configurations. This diagnostic approach will establish a quantitative basis for examining upper-level frontogenesis in Section 4 in relation to the conceptual description provided by Fig. 19.

3. Diagnosis of transverse ageostrophic circulations in upper-level frontal zones

The results of scale analyses of the adiabatic, inviscid meteorological equations (Eliassen, 1962; Shapiro, 1970; Hoskins and Bretherton, 1972; Emanuel, 1985) indicate that provided a frontal zone is sufficiently straight[9] and along-front variations are sufficiently small, the along-front component of the wind can be approximated by its geostrophic value. As a conse-

[8] The schematic depictions of upper-tropospheric jet-front systems in Fig. 19, as well as in Figs. 21 and 23, apply at a level that is sufficiently low for the horizontal temperature gradient to be well-defined and sufficiently high for the jet structure in the wind field to be apparent. The choice of such a "compromise level" (~400 mb) is dictated by the observed structure of upper-level jet-front systems (see Fig. 7a), in which horizontal temperature gradients are best defined in the midtroposphere, while the jet pattern is most distinct in the vicinity of the tropopause (LMW), a level at which the horizontal temperature pattern is typically diffuse.

[9] The condition that a frontal zone is straight does not necessarily require that the isentropes are oriented parallel to the zone ($\partial\theta/\partial x = 0$). A frontal zone consists of a region in which the horizontal potential temperature gradient is maximized, and is not necessarily bounded by isentropes. The schematics in Figs. 19b, 19d and 21b provide examples of along-front potential temperature variation.

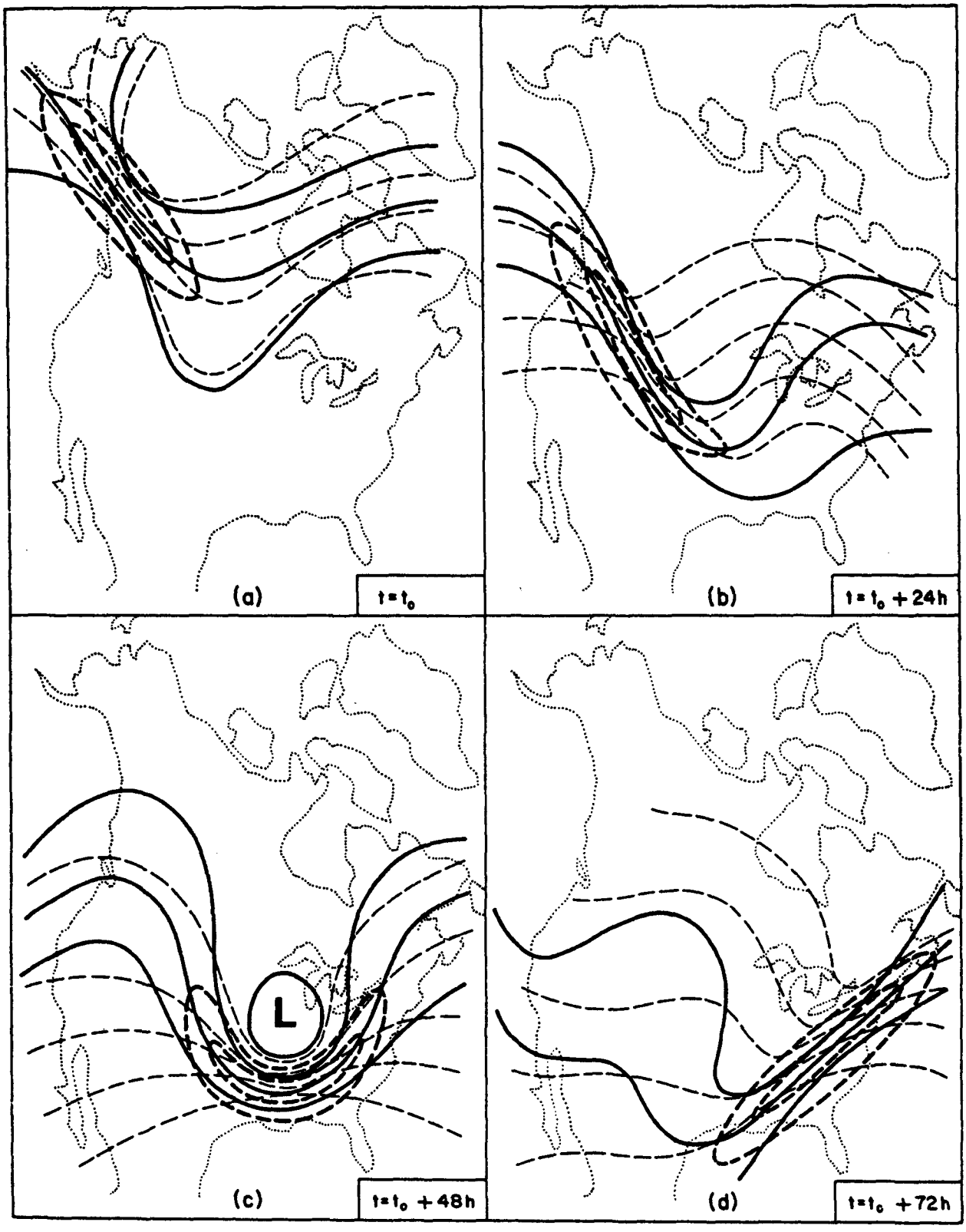

FIG. 19. Idealized schematic depiction on a constant pressure surface of the propagation of an upper-tropospheric jet-front system through a midlatitude baroclinic wave over a 72 h period: (a) formation of jet-front in the confluence between mid- and high-latitude currents; (b) jet-front situated in the northwesterly flow inflection of amplifying wave; (c) jet-front at the base of the trough of fully developed wave; (d) jet-front situated in the southwesterly flow inflection of damping wave. Geopotential height contours, thick solid lines; isotachs, thick dashed lines; isentropes or isotherms, thin dashed lines. From Shapiro (1983).

quence of this approximation, the ageostrophic circulation is confined to the cross-front (transverse) plane. This approximation is often referred to as "cross-front geostrophy," which describes the near balance of the Coriolis and pressure gradient forces in the cross-front direction, and is a special case of the geostrophic momentum approximation ($|d\mathbf{V}_{ag}/dt| \ll |d\mathbf{V}_g/dt|$), leading to the semigeostrophic equations (Hoskins, 1975). The two-dimensionality of the ageostrophic circulations in straight frontal zones provides a considerable conceptual simplification in understanding the dynamical processes producing vertical circulations.

a. *Dynamical equations for absolute momentum and potential temperature*

For a straight frontal zone oriented in the east–west direction, the approximation of cross-front geostrophy implies

$$|u_{ag}| \ll |u_g|, \tag{3.1a}$$

$$\left|\frac{du_{ag}}{dt}\right| \ll \left|\frac{du_g}{dt}\right|, \tag{3.1b}$$

$$\left|\frac{\partial u_{ag}}{\partial x}\right| \ll \left|\frac{\partial v_{ag}}{\partial y}\right| \approx \left|\frac{\partial \omega}{\partial p}\right|. \tag{3.1c}$$

These relations are a consequence of the geometrical properties of fronts, i.e., that the cross-front length scale is much less than the along-front scale and that the cross-front component of velocity is much less than the along-front component. As a consequence of (3.1), the prognostic equations for m (2.2) and θ are

$$\frac{dm}{dt} = -\frac{\partial \phi}{\partial x} + F_x, \tag{3.2}$$

$$\frac{d\theta}{dt} = \dot{\theta}, \tag{3.3}$$

where

$$\frac{d}{dt} = \frac{\partial}{\partial t} + u_g\frac{\partial}{\partial x} + (v_g + v_{ag})\frac{\partial}{\partial y} + \omega\frac{\partial}{\partial p}. \tag{3.4}$$

In the above equations, F_x is the along-front component of the friction term in the equation of motion, $\mathbf{F}$, and the subscript ag denotes ageostrophic. In (3.2) and (3.3), it is implicitly assumed that F_x and $\dot{\theta}$ are sufficiently small in magnitude so as not to invalidate the approximation of cross-front geostrophic balance.

As a consequence of (3.1c) and the assumption of constant Coriolis parameter, the mass continuity equation reduces to

$$\frac{\partial v_{ag}}{\partial y} + \frac{\partial \omega}{\partial p} = 0. \tag{3.5}$$

This form of the continuity equation permits definition of an ageostrophic streamfunction, ψ, such that[10]

$$\mathbf{V}_{ag2} = -\mathbf{i} \times \nabla_2\psi = -\frac{\partial \psi}{\partial p}\mathbf{j} - \frac{\partial \psi}{\partial y}\mathbf{k}, \tag{3.6}$$

where $\mathbf{V}_{ag2} = v_{ag}\mathbf{j} - \omega\mathbf{k}$ and ∇_2 is as defined in Section 2b. As defined in (3.6), when facing toward the positive x direction, the ageostrophic circulation is clockwise (counterclockwise) around maxima (minima) in ψ (Fig. 20). Additional equations to be used with (3.2)–(3.6) are the components of the geostrophic wind (2.3) and the thermal wind (2.5).

Prognostic equations may be developed for the cross-front and vertical gradients of m and θ, which describe absolute vorticity ($\partial m/\partial y$), the components of cross-front thermal wind balance ($\partial m/\partial p = \gamma\partial\theta/\partial y$) and static stability ($\partial\theta/\partial p$). Taking $\partial/\partial y$ and $\partial/\partial p$ of (3.2) and (3.3) results in

$$\frac{d}{dt}\left(\frac{\partial m}{\partial y}\right) = J_{yp}(m, \omega) + \frac{\partial F_x}{\partial y}, \tag{3.7}$$

$$\frac{d}{dt}\left(\frac{\partial m}{\partial p}\right) = -J_{yp}(u_g, v_g) - J_{yp}(m, v_{ag}) + \frac{\partial F_x}{\partial p}, \tag{3.8}$$

$$\frac{d}{dt}\left(\gamma\frac{\partial \theta}{\partial y}\right) = J_{yp}(u_g, v_g) + \gamma J_{yp}(\theta, \omega) + \left(\frac{\partial m}{\partial p}\frac{d\ln\gamma}{dp}\right)\omega + \gamma\frac{\partial \dot{\theta}}{\partial y}, \tag{3.9}$$

$$\frac{d}{dt}\left(\frac{\partial \theta}{\partial p}\right) = -J_{yp}(\theta, v_{ag}) + \frac{\partial \dot{\theta}}{\partial p}. \tag{3.10}$$

The Jacobian operator is that defined in (2.10). In (3.9), the term involving $d\ln\gamma/dp$ [$= -(c_v/c_p)/p$] is usually neglected, which is a form of the Boussinesq approximation for the pressure coordinate system.

Equations (3.7) and (3.10) reveal that the vorticity and static stability changes involving the motion field depend only on the ageostrophic circulation. On the

[10] Use of $\mathbf{V}_{ag2}$ in (3.6) to denote the transverse ageostrophic circulation should be distinguished from the more conventional notation, $\mathbf{V}_{ag}$, which refers to the horizontal ageostrophic wind ($u_{ag}\mathbf{i} + v_{ag}\mathbf{j}$). The latter usage is intended, for example, in the inequality describing the condition for the geostrophic momentum approximation, appearing at the beginning of this section.

other hand, (3.8) and (3.9) indicate that in the absence of frictional and diabatic processes temporal changes in the components of cross-front thermal wind balance depend on both geostrophic and ageostrophic processes, which are partitioned among the first and second Jacobian terms [aside from the "non-Boussinesq" term in (3.9)]. The geostrophic Jacobian term common to (3.8) and (3.9) shows that geostrophic motions contribute to temporal changes of $\partial m/\partial p$ and $\gamma\partial\theta/\partial y$ along parcel trajectories at rates that are equal in magnitude but opposite in sign. Therefore, ageostrophic circulations are required to preserve thermal wind balance [$d(\partial m/\partial p)/dt$ and $d(\gamma\partial\theta/\partial y)/dt$ must be everywhere equivalent], which cannot be maintained by geostrophic motions alone, a paradox noted by Hoskins et al. (1978). The principle of preserving thermal wind balance leads to the formulation of a diagnostic equation for the transverse ageostrophic circulation (v_{ag}, ω) from (3.8) and (3.9). In this equation, the transverse ageostrophic circulation will be viewed as a response to frontogenetical processes, with respect to $\partial m/\partial p$ and $\gamma\partial\theta/\partial y$, involving the geostrophic flow along with frictional and diabatic processes.

b. *The Sawyer-Eliassen equation for the transverse ageostrophic circulation*

Since the left sides of (3.8) and (3.9) are assumed to remain equal, a diagnostic equation for (v_{ag}, ω) can be formed by subtracting the two equations, yielding

$$J_{yp}(m, v_{ag}) + \gamma J_{yp}(\theta, \omega) + \left(\frac{\partial m}{\partial p}\frac{d\ln\gamma}{dp}\right)\omega = -2J_{yp}(u_g, v_g) + \frac{\partial F_x}{\partial p} - \gamma\frac{\partial\dot{\theta}}{\partial y}. \quad (3.11)$$

The definition of ψ (3.6) allows the transverse ageostrophic circulation to be expressed in terms of a single variable at the expense of obtaining a higher-order equation. Separating the Jacobians into their individual components and using (3.6) leads to a linear, second-order partial differential equation in ψ with variable coefficients:

$$\left(-\gamma\frac{\partial\theta}{\partial p}\right)\frac{\partial^2\psi}{\partial y^2} + \left(2\frac{\partial m}{\partial p}\right)\frac{\partial^2\psi}{\partial y\partial p} + \left(-\frac{\partial m}{\partial y}\right)\frac{\partial^2\psi}{\partial p^2} + \left(\frac{\partial m}{\partial p}\frac{d\ln\gamma}{dp}\right)\frac{\partial\psi}{\partial y} = -2J_{yp}(u_g, v_g) + \frac{\partial F_x}{\partial p} - \gamma\frac{\partial\dot{\theta}}{\partial y}. \quad (3.12)$$

Equation (3.12) was formulated originally by Sawyer (1956) for the special case of the absence of along-front variations in potential temperature [$J_{yp}(u_g, v_g)$ reduces to $-(\partial u_g/\partial p)(\partial v_g/\partial y)$], which were subsequently included by Eliassen (1962).

The coefficients of the second-order terms on the left of (3.12) respectively quantify the static stability, baroclinicity and inertial stability. The distributions of m and θ as well as the right side of (3.12) (the forcing) are assumed known, so that ψ (the response) can be determined uniquely provided that boundary conditions are specified and an ellipticity condition,

$$\gamma\frac{\partial m}{\partial y}\frac{\partial\theta}{\partial p} - \left(\frac{\partial m}{\partial p}\right)^2 = \gamma P_2 > 0, \quad (3.13)$$

is satisfied everywhere in the (y, p) domain. The equality within (3.13) can be verified by referring to (2.9) and (2.10) along with (2.6). The condition of positive potential vorticity ensures that transverse ageostrophic circulations will arise only in response to the forcing terms on the right of (3.12), rather than to self-exciting instabilities of the zonal current containing the frontal zone. In particular, symmetric baroclinic instability [detailed descriptions and references are given by Hoskins (1974), Orlanski and Ross (1977) and Emanuel (1979)] is possible in regions of negative potential vorticity. This instability can lead to significant magnitudes of du_{ag}/dt, which are not considered in the formulation of (3.12). Under such circumstances, a more general formulation for ψ must be developed that incorporates the time history of ψ through terms involving its temporal derivatives and specified initial conditions. The theories of forced frontal circulations and symmetric baroclinic instability may be considered complementary in the sense that frontal circulations are treated in the absence of symmetric baroclinic instability through the constraint of positive potential vorticity, while symmetric baroclinic instability occurs in the absence of frontal circulations through the assumption of a straight zonal current in which v_g is constant (typically zero), eliminating the geostrophic forcing term in (3.12).

Since the Sawyer-Eliassen equation (3.12) is second-order and the coefficients of the $\partial^2/\partial y^2$ and $\partial^2/\partial p^2$ terms are typically positive, positive (negative) values of the forcing correspond to relative minima (maxima) in ψ (Fig. 20). According to the previous discussion of the definition of ψ (3.6) and with the y axis pointing toward colder air, relative minima (maxima) in ψ are associated with thermodynamically direct (indirect) circulations. For a thermodynamically direct circulation (Fig. 20a), cold air is sinking and warm air is rising, which contributes to decreasing the cross-front thermal contrast. At the same time, westerly and easterly momentum are created respectively at upper and lower levels [through the inviscid u_g momentum equation, $du_g/dt = fv_{ag}$, obtainable from (3.2)], which contributes to increasing the vertical shear of the along-front wind component. Conversely, for a thermodynamically indirect circulation (Fig. 20b), the cross-frontal thermal contrast is enhanced and the vertical shear of the along-front wind component is diminished.

In addition to estimating the sense of the transverse ageostrophic circulation from the sign of the forcing,

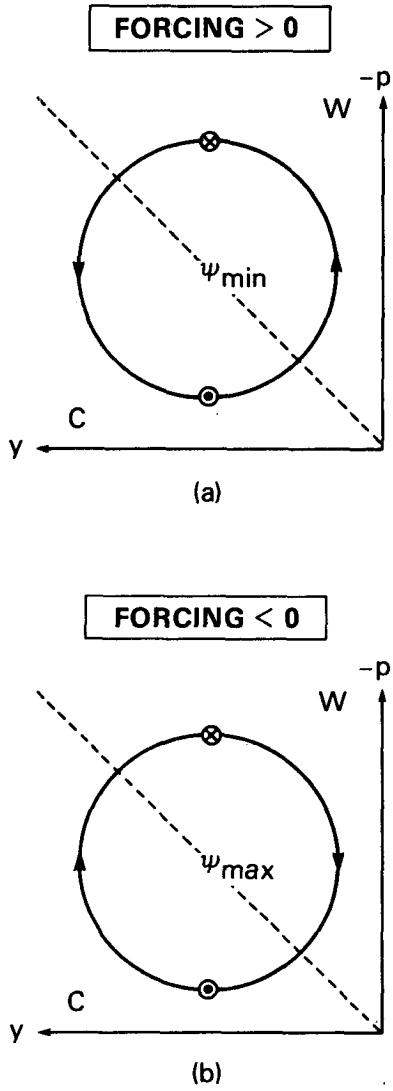

FIG. 20. Schematic illustration of sign of forcing and sense of transverse ageostrophic circulation from diagnostic Sawyer-Eliassen equation. Ageostrophic circulation is denoted by solid lines; dashed lines depict an isentrope separating potentially colder from warmer air. Small circles enclosing x and dot respectively indicate along-front wind into and out of the cross section. Transverse ageostrophic circulation is thermodynamically direct in (a) and indirect in (b).

it is possible to infer qualitatively the shape of the circulation, which for a given forcing depends on the relative magnitudes and distributions of the coefficients on the left side of (3.12). Such inferences can be determined from the properties of the Green's function for (3.12), which physically describes the response (ψ) to forcing consisting of a point source (δ-function) for a given choice of lateral boundary conditions. The results of such an analysis (Eliassen, 1962) indicate the following: (i) large potential vorticity and small inertial stability inhibit vertical motions and favor horizontal ageostrophic motions, resulting in an elliptical circulation with a relatively small aspect ratio; (ii) small potential vorticity and large inertial stability favor vertical motions and inhibit horizontal ageostrophic motions, resulting in an elliptical circulation with a relatively large aspect ratio; (iii) the baroclinicity determines the tilt of the circulation from the vertical; (iv) for a given forcing, the amplitude of ψ varies inversely with the inertial stability.

Interpretation of the Sawyer-Eliassen equation is facilitated by considering its quasi-geostrophic counterpart. The justification for such an approach is that the semigeostrophic equations, which include the same assumptions as those used in deriving (3.12), predict a distortion of solutions determined from the quasi-geostrophic equations, rather than leading to entirely different solutions (Hoskins, 1975). This behavior is understandable in that the dominant terms in the semigeostrophic equations are those constituting the quasi-geostrophic equations. The quasi-geostrophic counterpart to (3.4) is

$$\frac{d}{dt} = \frac{\partial}{\partial t} + u_g \frac{\partial}{\partial x} + v_g \frac{\partial}{\partial y}. \tag{3.14}$$

Comparison with (3.4) shows that the transverse ageostrophic circulation is neglected in determining parcel trajectories. The effect of vertical motions is included in the thermodynamic equation (3.3), however, by accounting for adiabatic warming and cooling through the term, $-\omega d\Theta/dp$, where $\Theta(p)$ is a reference distribution of potential temperature. The quasi-geostrophic counterparts to (3.7)–(3.10) are

$$\frac{d}{dt}\left(\frac{\partial m}{\partial y}\right) = -f\frac{\partial \omega}{\partial p} + \frac{\partial F_x}{\partial y}, \tag{3.15}$$

$$\frac{d}{dt}\left(\frac{\partial m}{\partial p}\right) = -J_{yp}(u_g, v_g) + f\frac{\partial v_{ag}}{\partial p} + \frac{\partial F_x}{\partial p}, \tag{3.16}$$

$$\frac{d}{dt}\left(\gamma\frac{\partial \theta}{\partial y}\right) = J_{yp}(u_g, v_g) - \gamma\frac{d\Theta}{dp}\frac{\partial \omega}{\partial y} + \gamma\frac{\partial \dot{\theta}}{\partial y}, \tag{3.17}$$

$$\frac{d}{dt}\left(\frac{\partial \theta}{\partial p}\right) = -\frac{d\Theta}{dp}\frac{\partial \omega}{\partial p} + \frac{\partial \dot{\theta}}{\partial p}. \tag{3.18}$$

It can be confirmed that (3.15)–(3.18) can be determined from (3.7)–(3.10) by approximating m by $-fy$ and θ by Θ in all terms involving the ageostrophic circulation.

The quasi-geostrophic form of (3.12) is

$$\left(-\gamma\frac{d\Theta}{dp}\right)\frac{\partial^2 \psi}{\partial y^2} + f\frac{\partial^2 \psi}{\partial p^2} = -2J_{yp}(u_g, v_g) + \frac{\partial F_x}{\partial p} - \gamma\frac{\partial \dot{\theta}}{\partial y}. \tag{3.19}$$

The discrepancies between the ageostrophic circulations resulting from (3.12) and (3.19) are due entirely to differences in response, since the forcing is identical

in both equations. A corresponding analysis of the properties of the Green's function would show that for a given latitude only variations in static stability can affect the aspect ratio of the elliptical circulation, and that the circulation cannot tilt from the vertical, since the mixed-derivative term on the left of (3.12) does not appear in (3.19). The ellipticity condition for (3.19), which is the quasi-geostrophic counterpart of (3.13), is that the static stability is positive, i.e.,

$$-f\gamma \frac{d\Theta}{dp} > 0. \tag{3.20}$$

The dynamical forcing to the Sawyer-Eliassen equation (3.12) and its quasi-geostrophic counterpart (3.19) can be expressed in four equivalent forms. The first is

$$-2J_{yp}(u_g, v_g) = 2\mathbf{i}\cdot(\nabla_2 u_g \times \nabla_2 v_g)$$
$$= -2\left(\frac{\partial u_g}{\partial y}\frac{\partial v_g}{\partial p} - \frac{\partial u_g}{\partial p}\frac{\partial v_g}{\partial y}\right), \tag{3.21a}$$

which can be verified from the definition of the Jacobian operator in (2.10). This form is convenient for visually evaluating the forcing from the solenoids formed by the intersections of u_g and v_g isotachs on a (y, p) cross section. Use of the thermal wind (2.5) and the nondivergence of the geostrophic wind on an f-plane ($\partial u_g/\partial x = -\partial v_g/\partial y$) in (3.21a) results in

$$-2\gamma J_{xy}(u_g, \theta) = -2\gamma\mathbf{k}\cdot(\nabla_p u_g \times \nabla_p \theta)$$
$$= -2\gamma\left(\frac{\partial u_g}{\partial x}\frac{\partial \theta}{\partial y} - \frac{\partial u_g}{\partial y}\frac{\partial \theta}{\partial x}\right). \tag{3.22a}$$

This form is useful for estimating the forcing of the cross-front ageostrophic circulation from constant pressure charts of u_g and θ. In natural coordinates (3.22a) becomes $2\gamma|\partial\theta/\partial n|\partial u_g/\partial s$, where n points toward colder air and s is oriented along isentropes 90° to the right of n.

Two additional forms of the dynamical forcing can be obtained by substituting the expression for the nondivergence of the geostrophic wind into (3.21a) and (3.22a):

$$-2J_{yp}(u_g, v_g) = -2\left(\frac{\partial u_g}{\partial p}\frac{\partial u_g}{\partial x} + \frac{\partial u_g}{\partial y}\frac{\partial v_g}{\partial p}\right), \tag{3.21b}$$

$$-2\gamma J_{xy}(u_g, \theta) = 2\gamma\left(\frac{\partial v_g}{\partial y}\frac{\partial \theta}{\partial y} + \frac{\partial u_g}{\partial y}\frac{\partial \theta}{\partial x}\right). \tag{3.22b}$$

These expressions respectively correspond to the geostrophic contributions to $d(\partial m/\partial p)/dt$ and $d(-\gamma\partial\theta/\partial y)/dt$, and will be used to demonstrate how the geostrophic wind differentially advects u_g and θ to disturb thermal wind balance in (3.8)–(3.9) and (3.16)–(3.17).

The schematic patterns of u_g and θ in Fig. 21 allow the interpretation of the dynamical forcing for the transverse ageostrophic circulation in terms of modifications to the cross-front potential temperature gradient through (3.22a) and (3.22b). Figure 21a shows a straight upper-tropospheric jet maximum with isentropes parallel to its axis, which eliminates the second terms in (3.22a) and (3.22b) from consideration. The first terms in the expressions for the forcing are positive and negative respectively in the confluent entrance and diffluent exit regions of the jet, implying direct and indirect circulations about the jet-front system in the entrance and exit regions (Fig. 20). These transverse circulation patterns are consistent with the four-quadrant pattern of upper-level convergence and divergence implied from considering temporal changes of along-front momentum ($du_g/dt = fv_{ag}$) or vorticity [see (3.15)] for parcels migrating through the jet more-or-less parallel to the geopotential streamlines (e.g., Riehl et al., 1952, 1954; Cahir, 1971; Uccellini and Johnson, 1979).[11] Figure 21b illustrates the complementary sit-

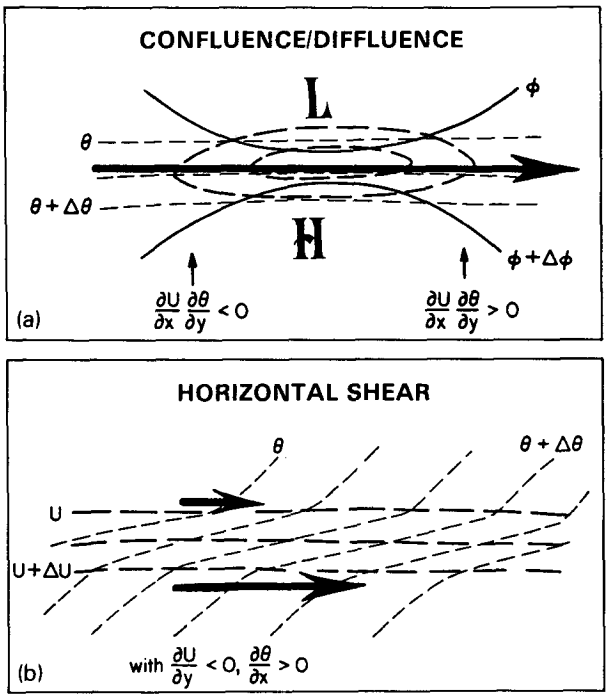

FIG. 21. Schematic depictions on a constant pressure surface of straight upper-tropospheric frontal zones characterized by (a) confluence and diffluence associated with a jet maximum and (b) horizontal shear in the presence of a positive along-front thermal gradient. Geopotential height contours, thick solid lines; isotachs of the along-front geostrophic wind component (u_g, denoted by U), thick dashed lines; isentropes, thin dashed lines. Heavy arrows indicate the jet axis in (a) and the sense of cross-front shear of the along-front wind component in (b). Adapted from Shapiro (1983).

[11] The cross-front ageostrophic wind component and horizontal divergence associated respectively with the temporal rates of change of along-front momentum and vorticity following parcel trajectories tend to reach a maximum at the LMW in upper-level jet-front systems, since the along-jet relative flow and gradients of the along-front wind component and vorticity are largest at this level. On the other hand, the magnitude of the geostrophic forcing (3.22a) of the Sawyer-Elias-

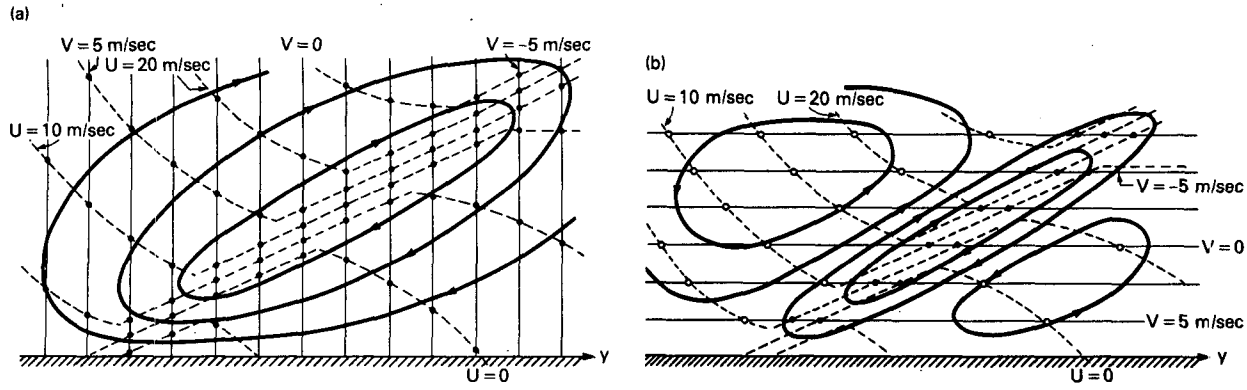

FIG. 22. Transverse ageostrophic circulations for an idealized frontal zone characterized by (a) confluence ($\partial v_g/\partial y < 0$, $\partial v_g/\partial p = 0$) and (b) horizontal shear ($\partial v_g/\partial y = 0$, $\partial v_g/\partial p > 0$). Dashed lines, isotachs of u_g (denoted by U); thin solid lines, isotachs of v_g (denoted by V); thick solid lines, streamlines of ageostrophic circulation. Adapted from Eliassen (1962).

uation in which the effects of confluence and diffluence are eliminated by assuming u_g is uniform in the along-front direction. The second terms in (3.22a) and (3.22b) are negative, implying an indirect circulation (Fig. 20b) for this case of cold advection (potential temperature increasing downstream) in the presence of cyclonic shear ($\partial u_g/\partial y < 0$). This part of the geostrophic forcing is referred to as the horizontal shear effect. Finally, the natural-coordinate form of the geostrophic forcing, introduced following (3.22a), can be used to determine the sense of the ageostrophic circulations in Fig. 21. In Fig. 21a, u_g increases along the isentropes (in the direction such that cold air is to the left) in the entrance region of the jet, yielding positive forcing and a direct circulation. Indirect circulations in the exit region of the jet in Fig. 21a and the frontal zone in Fig. 21b are associated with decreases in u_g along the isentropes.

The patterns in Fig. 22 from Eliassen (1962) are suitable for interpreting the geostrophic forcing in terms of (3.21a). In Fig. 22a, $\partial v_g/\partial p$ is taken to be zero, negating the first term in (3.21a). The configuration of $\partial u_g/\partial p < 0$ [colder air to the north according to (2.5)] and $\partial v_g/\partial y < 0$ (confluence) implies positive forcing and a direct circulation. This pattern corresponds to a cross section through the entrance region of the jet in Fig. 21a. In Fig. 22b, the confluence effect is eliminated through the assumption that v_g varies only with pressure, which isolates the horizontal shear effect. With $\partial v_g/\partial p > 0$ ($\partial\theta/\partial x < 0$, the opposite of that in Fig. 21b) and cyclonic shear ($\partial u_g/\partial y < 0$) within the frontal zone, the forcing is positive and the circulation is direct. Outside the front, the sense of the lateral shear of u_g is anticyclonic and the circulations are indirect.

The frictionless, adiabatic forms of the quasi-geostrophic equations for the vertical shear of the along-front wind component (3.16) and the cross-front potential temperature gradient (3.17) will be used in conjunction with Figs. 21 and 22 to illustrate in detail how differential advection by the geostrophic wind disrupts thermal wind balance. Inspection of the first term in (3.21b) shows that confluence tends to reduce the magnitude of the vertical wind shear (decreased negative values of $\partial u_g/\partial p$), since larger positive values of u_g at upper levels compared with lower levels ($\partial u_g/\partial p < 0$) differentially advect less positive values of u_g ($\partial u_g/\partial x > 0$) at a greater rate at upper levels than at lower levels. From Fig. 21a and the first term in (3.22b) it can be seen that confluence tends to enhance the magnitude of the cross-front potential temperature gradient (increased negative values of $\partial\theta/\partial y$) by compressing isentropes in the y direction. Consequently, the contributions of geostrophic advection to $d(\partial m/\partial p)/dt$ and $d(\gamma\partial\theta/\partial y)/dt$ are respectively positive and negative. This tendency toward imbalance in the thermal wind is counteracted by a direct circulation ($\partial v_{ag}/\partial p < 0$, $\partial\omega/\partial y > 0$; Fig. 20a), which simultaneously increases the magnitude of the vertical wind shear by contributing positively to u_g at upper levels and negatively at lower levels (3.16), and decreases the magnitude of the cross-front potential temperature gradient by adiabatically warming the cooler air to the north of the front and cooling the warmer air to the south of the front (3.17).

In the case of the horizontal shear effect illustrated in Fig. 22b, reference to the second term in (3.21b) shows that the vertical shear in v_g ($\partial v_g/\partial p > 0$) tends to tip the u_g isotachs into the vertical where the horizontal shear is cyclonic ($\partial u_g/\partial y < 0$), diminishing the magnitude of the vertical wind shear. Examination of

sen equation tends to be relatively small at the LMW relative to mid- and upper-tropospheric values, since horizontal potential temperature gradients are typically indistinct at the LMW. Nevertheless, the upper horizontal branch of the transverse ageostrophic circulation, which is effectively bounded by the large increase in static stability at the tropopause, is usually maximized at the LMW, consistent with the above expectations from the momentum and vorticity equations. Consequently, evaluating the Sawyer-Eliassen forcing at the LMW *alone* can give the misleading impression that there is little or no forcing of transverse ageostrophic flow associated with upper-level jet-front systems.

the second term in (3.22b) reveals that cyclonic shear in the presence of along-front decreases in potential temperature ($\partial\theta/\partial x < 0$) tends to augment the magnitude of the cross-front potential temperature gradient, since larger positive values of u_g south of the front relative to north of the front differentially advect higher values of potential temperature at a greater rate south of the front relative to north of the front. A direct circulation in the same sense as in the confluence case is required to preserve thermal wind equilibrium.

The above interpretations of (3.12) and (3.19) bring out the importance of accounting for the contributions of differential geostrophic advection of both the wind and thermal fields when considering the forcing for the transverse ageostrophic circulation. Qualitative interpretations often emphasize the effects of confluence and horizontal shear on the cross-front potential temperature gradient (3.22b), while neglecting their corresponding effects on the vertical wind shear (3.21b), which are more difficult to visualize. The given interpretation is believed to be appealing because it places the secondary circulation in the physically familiar context of an adjustment to a continuously imposed imbalance, which may be viewed as a negative feedback.

Figure 23 displays various configurations of the potential temperature field relative to a straight upper-tropospheric jet maximum, which is revealed by the u_g field. The sign of the geostrophic forcing and sense of the transverse ageostrophic circulation can be determined from (3.22a) or its companion formulation in natural coordinates. Figures 23a and 23b exhibit patterns of potential temperature that respectively isolate the effects of confluence ($\partial\theta/\partial x = 0$ as in Fig. 21a) and horizontal shear ($\partial\theta/\partial y = 0$). Figures 23c and 23d depict straight isentropes rotated at an angle from the jet axis, respectively resulting in cold and warm advection in the along-front direction. These examples show the effect of combining the confluence and horizontal shear mechanisms. The influence of confluence and diffluence in forcing direct and indirect transverse circulations in the entrance and exit regions is apparent. The superimposed effect of horizontal shear is to shift the direct and indirect circulations laterally toward the cyclonic or anticyclonic shear sides of the jet axis, depending on the orientation of the isentropes relative to the jet and the resulting sign of the along-front thermal advection. For example, in the confluent entrance region of the cold advection case (Fig. 23c), the direct circulation is shifted toward the anticyclonic shear side of the jet, so that the region of maximum midtropospheric subsidence is located beneath the jet axis rather than the cyclonic shear side, as in the case of confluence alone (Fig. 23a). Figures 23e and 23f permit the sense of the along-front thermal advection to change sign at the jet maximum by placing the jet in a thermal ridge and trough, respectively. In the case of the thermal ridge (Fig. 23e), the entrance and exit regions are respectively characterized by cold and warm advection. The transverse circulations are shifted to the anticyclonic shear side of the jet, as in the entrance and exit regions of Figs. 23c and 23d.

The discussion of Fig. 23 illustrates the importance of considering the modifying influence of along-front thermal variations on the four-quadrant distribution of midtropospheric vertical motion in straight jets (Figs. 21a and 23a), which is based on deductions from the momentum or vorticity equations. This idealized pattern of vertical motion has been shown to hold only for the special case in which the isentropes are parallel to the jet axis. A weakness of qualitatively inferring the vertical motion pattern from the cross-front ageostrophic wind component due to parcel accelerations or from the sign of the divergence due to vorticity changes along a parcel trajectory is that the effect of along-front thermal variations is not taken into account.

The above analyses and interpretations of the Sawyer-Eliassen equation can be extended in a number of directions. The influence of frictional and diabatic forcing associated with CAT has been analyzed by Shapiro (1981); a similar analysis of nonconservative forcing due to deep convection appears in Shapiro (1983). It is possible to transform the Sawyer-Eliassen equation into alternative coordinate systems. Replacing y with m in (3.12) (Eliassen, 1962) reduces the left side to a form similar to the quasi-geostrophic version (3.19). The baroclinicity term is absorbed into the transformation from y to m and physically reappears in the tilted m coordinate lines. Absolute momentum is a stretched coordinate in the sense that contours of constant m are concentrated in regions of large absolute vorticity, affording enhanced horizontal resolution in frontal regions (Fig. 8). The transformation from (y, p) to (m, p) is the two-dimensional counterpart to that leading to the three-dimensional semigeostrophic equations developed by Hoskins (1975). It is also possible to transform the vertical coordinate from pressure to potential temperature; the Sawyer-Eliassen equation expressed in (y, θ) coordinates is given by Hoskins and Draghici (1977). Although an obvious extension would be to combine the horizontal and vertical stretching properties of m and θ, a version of the Sawyer-Eliassen equation in (m, θ) coordinates has not to our knowledge appeared in the literature.

Hoskins and Draghici (1977) and Hoskins et al. (1978) generalized the two-dimensional theory leading to the Sawyer-Eliassen equation to apply to three dimensions, an approach that accounts for contributions to the horizontal divergence by the along-front component of the ageostrophic flow. This approach is based on the geostrophic momentum approximation, which is justifiable if the time scale of momentum change following a parcel is much greater than f^{-1} (Hoskins, 1975). For adiabatic, frictionless flows, this condition should be satisfied if (i) the temporal rate of change of

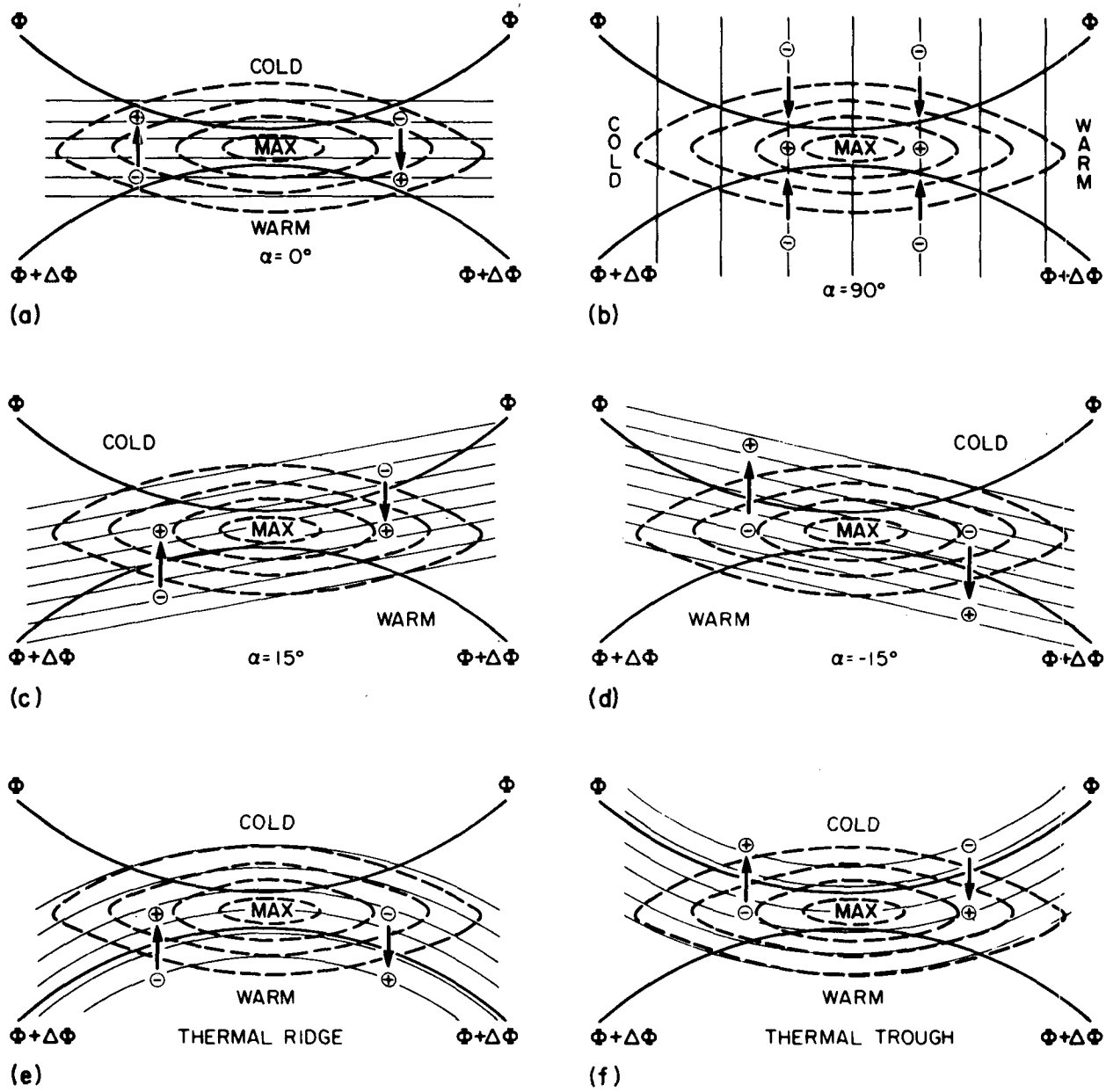

FIG. 23. Schematic illustration on a constant pressure surface of various idealized configurations of potential temperature and along-front geostrophic wind for a straight upper-tropospheric jet maximum. Thick solid lines, geopotential height contours; thick dashed lines, isotachs of the along-front wind component; thin solid lines, isentropes or isotherms; thick solid arrows, sense of cross-front ageostrophic wind component at level of maximum wind; plus and minus signs, sense of midtropospheric pressure-coordinate vertical velocity, ω. (a) Pure confluence and diffluence in the absence of along-jet thermal advection ($\partial\theta/\partial x = 0$); (b) pure horizontal shear with $\partial\theta/\partial x > 0$ in the absence of the effect of confluence and diffluence ($\partial\theta/\partial y = 0$). (c)–(f) Mixed cases of confluence/diffluence and horizontal shear: (c) along-jet cold advection, (d) along-jet warm advection, (e) jet in a thermal ridge, (f) jet in a thermal trough. From Shapiro (1983).

horizontal wind speed along a parcel trajectory is much less than the Coriolis acceleration ($|dV/dt| \ll fV$) and (ii) the radius of parcel trajectory curvature, R_t, is not too small ($V/f|R_t| \ll 1$). The ageostrophic streamfunction (3.6) becomes a vector, ψ, defined such that $u_{ag} = -\partial\psi_x/\partial p$, $v_{ag} = -\partial\psi_y/\partial p$ and $\omega = \nabla_p \cdot \psi$, which satisfies the three-dimensional continuity equation in pressure coordinates. A coupled system of second-order elliptic partial differential equations for the ageostrophic circulations in the (x, p) (ψ_x) and (y, p) (ψ_y) planes replaces (3.12) or its quasi-geostrophic counterpart (3.19). This system of equations can be combined into a single diagnostic equation for the vertical motion, ω, with the dynamical forcing expressed in a revealing way that links vertical circulations directly to frontogenesis. The quasi-geostrophic version of the

diagnostic ω equation will be reproduced because of its relatively simpler mathematical form.

The form of the quasi-geostrophic ω equation that results from combining the diagnostic equations for the ageostrophic circulations in the (x, p) and (y, p) planes is

$$\left(-\gamma \frac{d\Theta}{dp}\right)\nabla_p^2\omega + f\frac{\partial^2\omega}{\partial p^2} = -2\gamma(\nabla_p \cdot \mathbf{Q}) - \mathbf{k}\cdot\left(\nabla_p \times \frac{\partial \mathbf{F}}{\partial p}\right) - \gamma\nabla_p^2\dot{\theta}. \quad (3.23)$$

The terms on the right of (3.23) respectively quantify the dynamical, frictional and diabatic forcing of the vertical motion. The dynamical forcing is proportional to the horizontal divergence of the so-called "Q vector," consisting of the temporal rate of change following the geostrophic motion of the horizontal potential temperature gradient; i.e.,

$$\mathbf{Q} = \frac{d}{dt}\nabla_p\theta = -J_{xy}(v_g, \theta)\mathbf{i} + J_{xy}(u_g, \theta)\mathbf{j} \quad (3.24)$$

and d/dt is defined in (3.14). The components of $\mathbf{Q}$ in the x and y directions respectively contribute to the forcing of the ageostrophic circulations in the (x, p) and (y, p) planes. Hoskins et al. (1978) and Hoskins and Pedder (1980) showed that the dynamical forcing of (3.23) comprising the Q vector is equivalent to the conventional form involving the vertical shear of the vorticity advection and Laplacian of the thermal advection (Holton, 1979, pp. 136–140):

$$-2\gamma(\nabla_p \cdot \mathbf{Q}) = \frac{\partial}{\partial p}(\mathbf{V}_g \cdot \nabla_p\zeta_g) + \gamma\nabla_p^2(\mathbf{V}_g \cdot \nabla_p\theta). \quad (3.25)$$

The expression of the dynamical forcing for the vertical circulation in terms of frontogenetical processes associated with the geostrophic wind field leads to the significant interpretation that the forcing of vertical motions within midlatitude baroclinic flows is most concentrated and pronounced in frontal regions. This perspective emphasizes the important role of fronts in the dynamics of midlatitude baroclinic waves and cyclones.

4. Dynamical models of upper-level frontogenesis

This section considers time-dependent modeling studies of upper-level frontogenesis in two and three dimensions with the intent of isolating and elucidating significant physical mechanisms and processes rather than focusing on mathematical aspects, which will be left to individual references. Results of two- and three-dimensional model simulations will be used to confirm and illustrate the schematic representations of ageostrophic circulations associated with upper-level jet-front systems proposed in Fig. 23, which, in turn, can be related to the conceptual model of the progression of a jet-front system through an evolving baroclinic wave presented in Fig. 19. In two dimensions, the interpretations are simplified considerably, since ageostrophic circulations are confined to the cross-front plane and the Sawyer-Eliassen equation developed in Section 3b is applicable. In three dimensions, the interpretations are more complicated because of the possible contribution of the along-front component of the ageostrophic flow to the horizontal divergence and vertical circulations. Considerations of the along-front component of the ageostrophic flow will be based on gradient wind concepts.

a. Two-dimensional processes

The first time-dependent studies of upper-level frontogenesis were performed with the adiabatic, frictionless semigeostrophic equations in two dimensions, and are physically described in Hoskins (1971, 1972) and mathematically formulated in Hoskins and Bretherton (1972). The initial conditions consist of a baroclinic troposphere separated from a barotropic stratosphere by a sloping tropopause, and the troposphere and stratosphere are characterized by relatively small and large static stabilities. The cross-front variation of potential temperature is specified in terms of an arctangent function, and the frontogenesis is driven by confluence in the nondivergent basic-state wind field in which $v = -\alpha y$, $u = \alpha x$ and α is a constant ($=1 \times 10^{-5}$ s^{-1}). In this specification, which describes a hyperbolic deformation field, the isentropes are oriented parallel to the axis of dilatation for the basic-state wind field (the x axis), a configuration which is kinematically optimal for frontogenesis (Petterssen, 1956, pp. 200–205).

Figure 24 illustrates the structure of the frontal zone after considerable development has taken place. A jet has formed along the tropopause, which has folded into the midtroposphere and has extended downward nearly to 450 mb. The frontal structure at upper levels is quite realistic in comparison with the wind (Fig. 5a) and potential temperature (Fig. 5b) patterns analyzed by Reed and Danielsen (1959). Features realistically reproduced by the model include the jet core along the tropopause, and the barotropic structure of the cold air and baroclinic structure of the warm air separated by the frontal zone in the middle and upper troposphere. The main shortcoming of the model is that the folded tropopause does not extend to the 600–700 mb levels as documented observationally for well-developed cases (e.g., Reed, 1955). Related to this deficiency is that the cyclonic shear and cross-front potential temperature gradient defining the frontal zone are maximized near the base of the tongue of stratospheric air, and do not extend into the midtroposphere. In fact, these quantities are most diffuse at this level. A frontal zone also develops at the surface in response to the initial specification of the cross-front variation of potential temper-

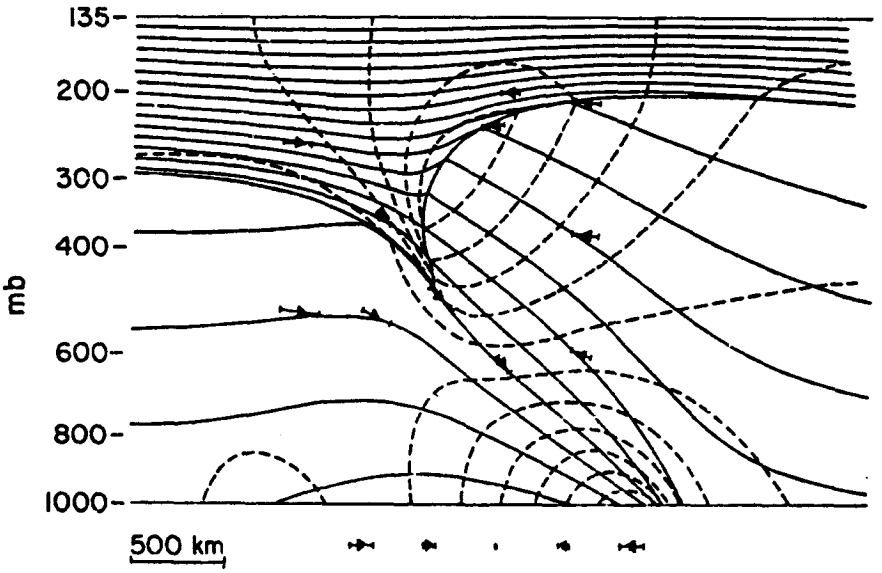

FIG. 24. Analytically derived cross section indicating tropopause folding and frontogenesis at the tropopause and surface due to the effect of confluence in a two-dimensional semigeostrophic model. Solid lines, isentropes (contour interval 7.8 K); dashed lines, isotachs of along-front wind component (contour interval 10.5 m s^{-1}). The tropopause is indicated by a solid line separating regions of high and low potential vorticity. Vector arrows within the figure reveal short-term parcel trajectories; those beneath the lower surface depict the basic-state geostrophic deformation field. The ordinate in this figure and in Figs. 25–28 is linear in the so-called pseudoheight, z, introduced by Hoskins and Bretherton (1972), which is proportional to p^{R/c_p}. From Hoskins (1972).

ature, which is invariant with height in the troposphere. The development of the unrealistically strong jet at the surface can proceed because of the free-slip lower boundary condition. The frontogenesis at upper levels is affected little by that at the surface (Buzzi et al., 1981).

Keyser and Pecnick (1985a) generalized the above two-dimensional problem by including the effects of the along-front variation of potential temperature in a primitive equation model formulation, allowing for the simultaneous treatment of the confluence and horizontal shear mechanisms referred to in Figs. 21 and 23. Figure 25 displays cross sections of the initial conditions for potential temperature and cross-front geostrophic wind, v_g, for the pure confluence case (Fig. 25a) discussed above and for cases in which the along-front variation of potential temperature is respectively positive (upper-level cold advection, Fig. 25b) and negative (upper-level warm advection, Fig. 25c). Accordingly, the configurations in Figs. 25a–25c correspond to infinitely long jet entrance regions (an artifact of the two-dimensional nature of the model formulation) for the potential temperature patterns respectively shown in Figs. 23a, 23c and 23d. The 48 h evolution of the along-front wind component and potential temperature in Fig. 26a confirms the results of the semigeostrophic model appearing in Fig. 24 and provides a benchmark for considering the results of the "cold advection" and "warm advection" cases in Figs. 26b and 26c. The presence of upper-level cold advection results in a well-defined zone of cyclonic shear and cross-front potential temperature gradient apparent down to the 600 mb level. The upper-level and surface fronts are clearly distinct, structurally separate features. The presence of upper-level warm advection also leads to the generation of frontal properties in the upper and middle troposphere, but the upper-level and surface frontal zones are "connected" in the sense that a single envelope of isentropes defines both fronts, similar to the pure confluence case.

The temporal history of the transverse circulations for the above three cases is revealed in the back trajectories displayed in Fig. 27 for parcels originating at 0 h immediately above the initial tropopause and terminating at 48 h within the respective frontal zones. The effect of confluence is apparent as parcels on the cold and warm sides of the frontal zones migrate toward confluent asymptotes within the frontal zones. The trajectory patterns for the pure confluence (Fig. 27a) and warm advection (Fig. 27c) cases are qualitatively similar, with the frontal zones separating descending cold air from ascending warm air. In contrast, in the cold advection case (Fig. 27b), the frontal zone comprises sinking air and the strongest descent appears on its warm side. Parcels originating just above the tropopause and terminating within the frontal zone approach the 700 mb level. The dramatic vertical excur-

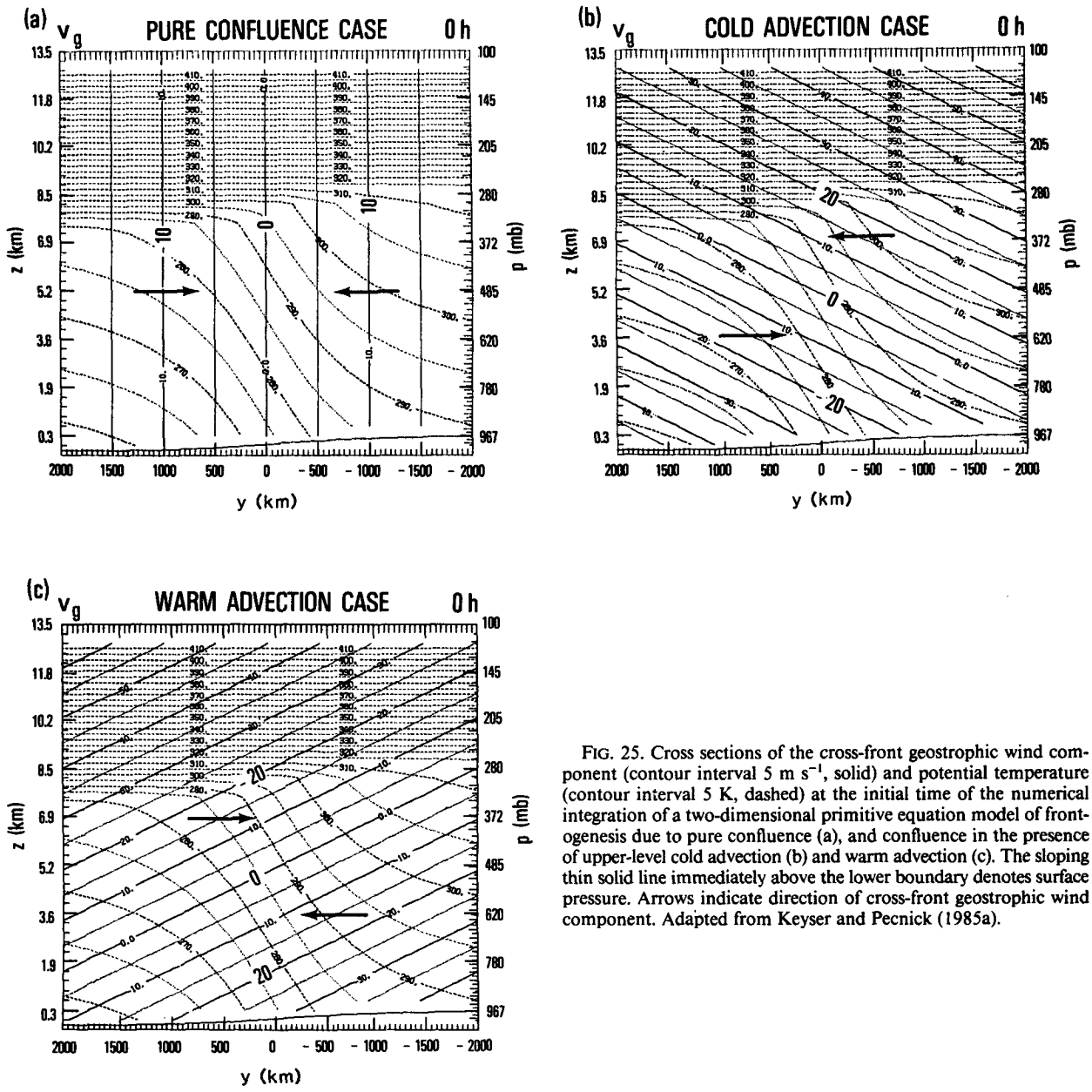

FIG. 25. Cross sections of the cross-front geostrophic wind component (contour interval 5 m s^{-1}, solid) and potential temperature (contour interval 5 K, dashed) at the initial time of the numerical integration of a two-dimensional primitive equation model of frontogenesis due to pure confluence (a), and confluence in the presence of upper-level cold advection (b) and warm advection (c). The sloping thin solid line immediately above the lower boundary denotes surface pressure. Arrows indicate direction of cross-front geostrophic wind component. Adapted from Keyser and Pecnick (1985a).

sions of parcels in the cold advection case are indicative of realistic tropopause folding and reflect the importance of vertical motions in the upper-level frontogenesis process.

The instantaneous transverse ageostrophic circulations at 24 h indicate thermodynamically direct patterns for the pure confluence (Fig. 28a) and warm advection (Fig. 28c) cases, with sinking and rising motion situated respectively to the cold and warm sides of the developing frontal zones. A thermodynamically direct circulation also occurs for the cold advection case (Fig. 28b), but its center is shifted laterally toward the warm air to such an extent that subsidence is maximized within and to the warm side of the developing frontal zone at upper levels. A consequence of this lateral shift in the ageostrophic circulation is a change in sign of the cross-stream gradient of vertical motion within the frontal zone from the thermally direct sense ($\partial\omega/\partial y > 0$) in the pure confluence and warm advection cases to thermally indirect ($\partial\omega/\partial y < 0$) in the cold advection case. Nevertheless, the overall circulation pattern in the cold advection case is in the direct sense, as required for the respective generation of westerly and easterly momentum at upper and lower levels (Fig. 26b).

The shift in the transverse ageostrophic circulation in the cold advection case relative to the pure conflu-

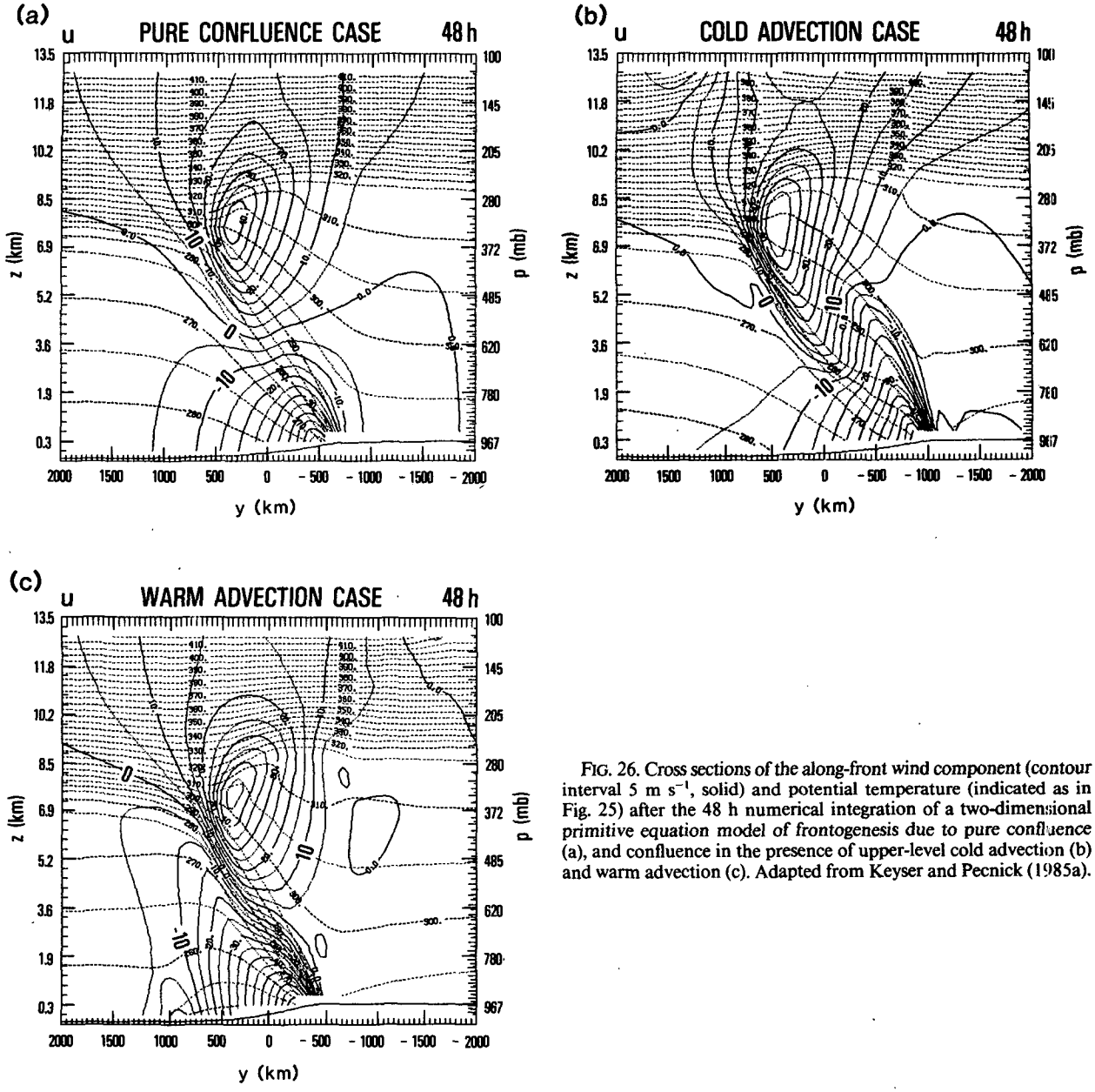

FIG. 26. Cross sections of the along-front wind component (contour interval 5 m s^{-1}, solid) and potential temperature (indicated as in Fig. 25) after the 48 h numerical integration of a two-dimensional primitive equation model of frontogenesis due to pure confluence (a), and confluence in the presence of upper-level cold advection (b) and warm advection (c). Adapted from Keyser and Pecnick (1985a).

ence case is compatible with the qualitative predictions from the two-dimensional Sawyer-Eliassen equation (3.12) applied to the entrance region of a straight jet maximum. In particular, in the cold advection case (Fig. 28b), midtropospheric subsidence is maximized beneath the jet core, as indicated in Fig. 23c, compared with the pure confluence case (Fig. 28a), where midtropospheric subsidence is maximized to the cyclonic shear side of the jet axis, as indicated in Fig. 23a. In the warm advection case, the predicted shift of the ageostrophic circulation toward the cyclonic shear side of the jet core (Fig. 23d) is suggested in the model circulation pattern in Fig. 28c. There is an indication of mid- and upper-tropospheric ascent beneath the jet core in the warm advection case, which is absent from the pure confluence case.

An analysis of the prognostic equations for vorticity (3.7) and cross-front potential temperature gradient (3.9) partitioned between horizontal and vertical motions reveals fundamental dynamical differences in upper-level frontogenesis for the pure confluence and warm advection cases compared with the cold advection case. Under adiabatic, frictionless, Boussinesq conditions, the above-mentioned equations reduce to

$$\frac{d}{dt}\left(\frac{\partial m}{\partial y}\right) = -\frac{\partial m}{\partial y}\frac{\partial v_{ag}}{\partial y} - \frac{\partial m}{\partial p}\frac{\partial \omega}{\partial y}, \qquad (4.1)$$

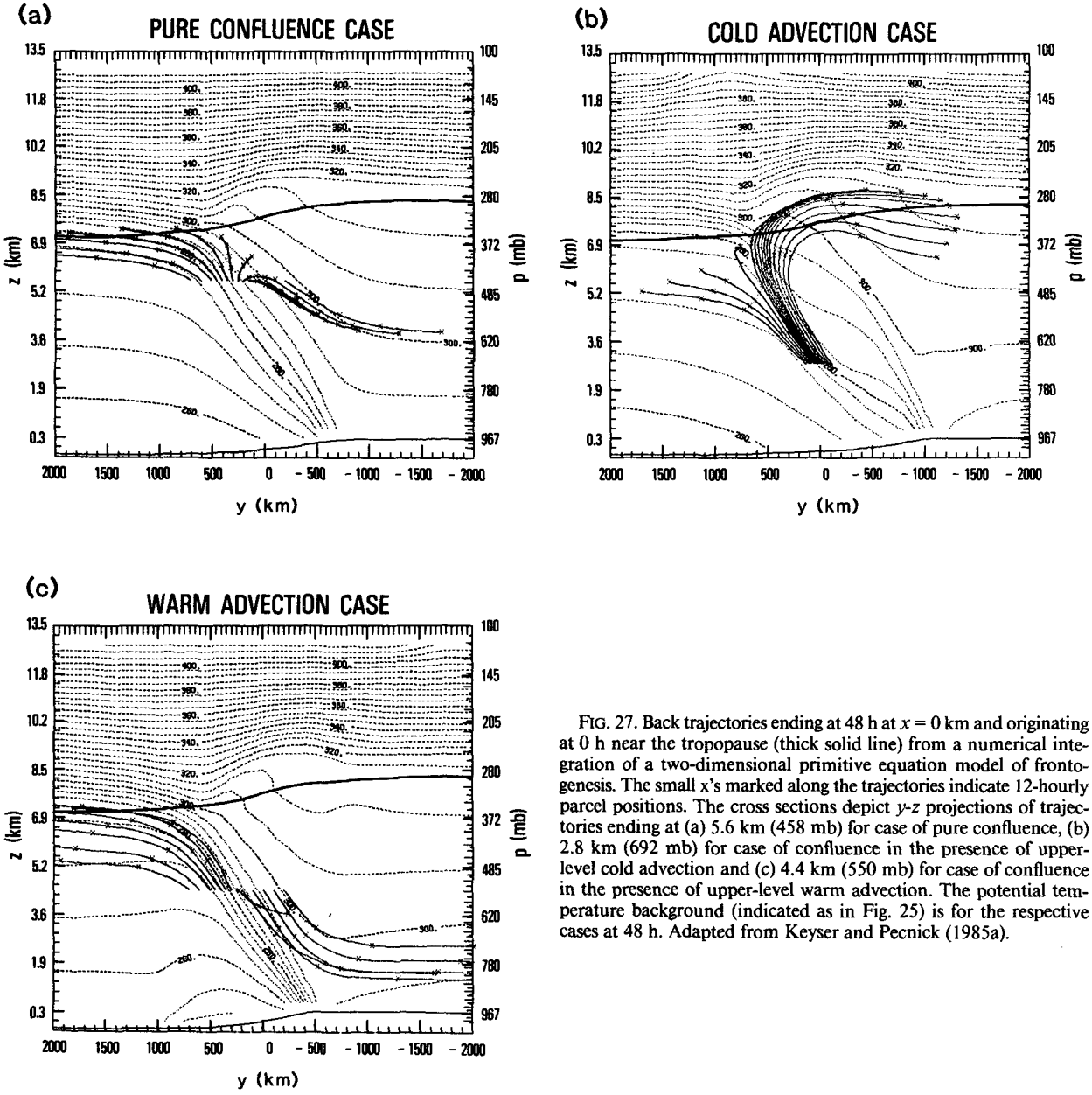

FIG. 27. Back trajectories ending at 48 h at $x = 0$ km and originating at 0 h near the tropopause (thick solid line) from a numerical integration of a two-dimensional primitive equation model of frontogenesis. The small x's marked along the trajectories indicate 12-hourly parcel positions. The cross sections depict y-z projections of trajectories ending at (a) 5.6 km (458 mb) for case of pure confluence, (b) 2.8 km (692 mb) for case of confluence in the presence of upper-level cold advection and (c) 4.4 km (550 mb) for case of confluence in the presence of upper-level warm advection. The potential temperature background (indicated as in Fig. 25) is for the respective cases at 48 h. Adapted from Keyser and Pecnick (1985a).

$$\frac{d}{dt}\left(\gamma\frac{\partial\theta}{\partial y}\right) = \left[-\gamma\left(\frac{\partial v_g}{\partial y}\frac{\partial\theta}{\partial y} + \frac{\partial u_g}{\partial y}\frac{\partial\theta}{\partial x}\right) - \gamma\frac{\partial v_{ag}}{\partial y}\frac{\partial\theta}{\partial y}\right] - \gamma\frac{\partial\theta}{\partial p}\frac{\partial\omega}{\partial y}, \quad (4.2)$$

where the first term in (4.1) and the bracketed term in (4.2) consist of horizontal frontogenetical effects, and (3.22b) has been used to replace the $J_{yp}(u_g, v_g)$ term in (3.9).

In the pure confluence and warm advection cases, the terms in (4.1) and (4.2) involving horizontal motions are frontogenetical in the mid- and upper-tropospheric portions of the frontal zone and dominate the tilting terms, which are frontolytical because of the direct sense of the cross-frontal gradient of vertical motion ($\partial\omega/\partial y > 0$) in the presence of increasing westerly winds with height ($\partial m/\partial p < 0$) and a statically stable stratification ($\partial\theta/\partial p < 0$). The situation is essentially reversed in the cold advection case. In this case, horizontal motions are frontolytical and are dominated by the tilting terms, which are frontogenetical because of the "locally indirect" sense of the cross-frontal gradient of subsidence ($\partial\omega/\partial y < 0$). The dominance of the tilting terms in the cold advection case compared with the

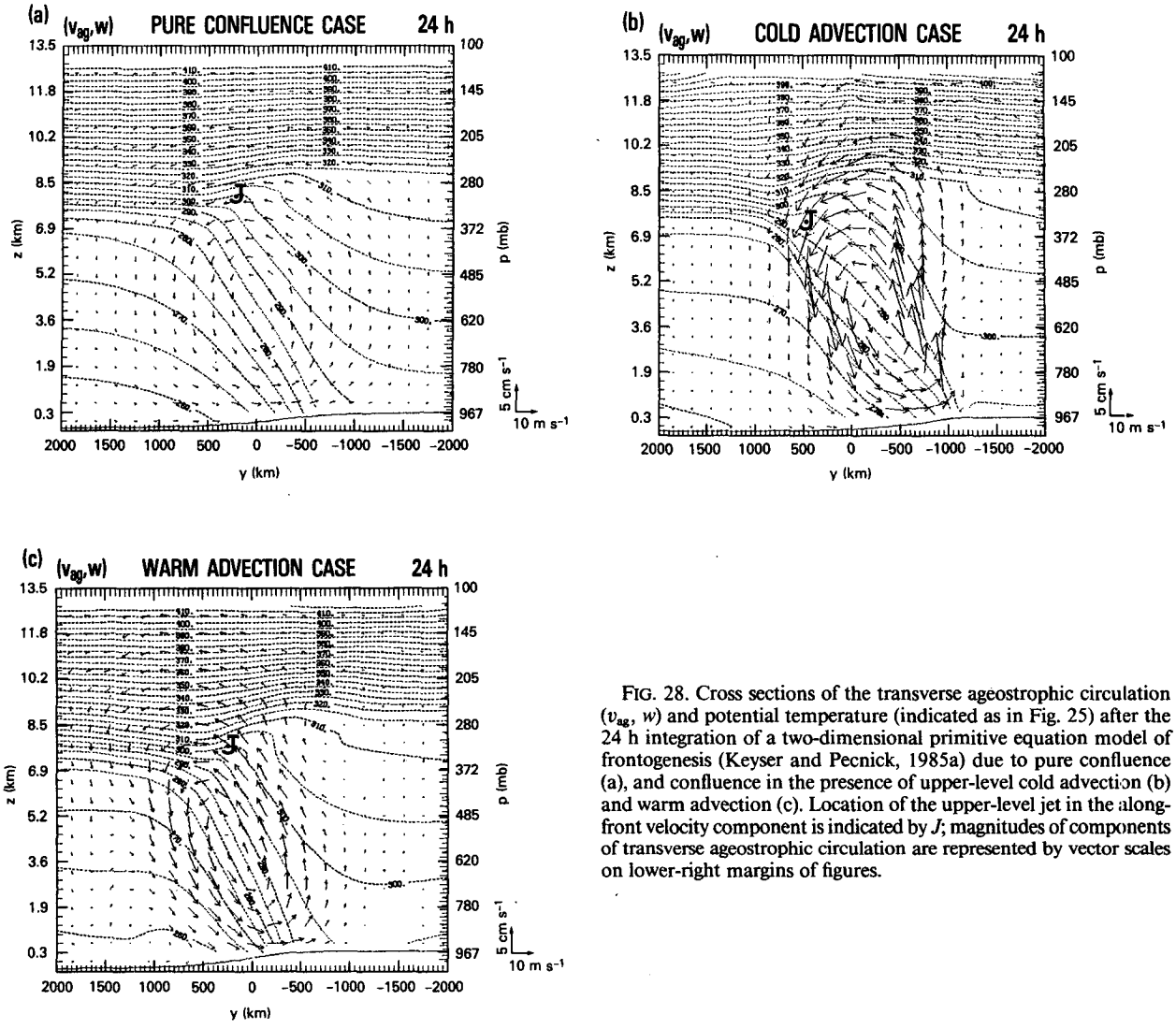

FIG. 28. Cross sections of the transverse ageostrophic circulation (v_{ag}, w) and potential temperature (indicated as in Fig. 25) after the 24 h integration of a two-dimensional primitive equation model of frontogenesis (Keyser and Pecnick, 1985a) due to pure confluence (a), and confluence in the presence of upper-level cold advection (b) and warm advection (c). Location of the upper-level jet in the along-front velocity component is indicated by J; magnitudes of components of transverse ageostrophic circulation are represented by vector scales on lower-right margins of figures.

pure confluence and warm advection cases is related to the magnitude of the subsidence in the former, which approaches a value of 10 cm s^{-1}, as also noted in several observational case studies (Reed and Sanders, 1953; Staley, 1960; Shapiro, 1970). The strong subsidence in the cold advection case is frontogenetical not only in the sense that it generates frontal properties along parcel trajectories, but also in that it transports these properties downward as they are generated.

The Sawyer-Eliassen equation (3.12) can be used to identify interactions between the transverse ageostrophic circulation and its geostrophic forcing. Consideration of the geostrophic forcing in the form of (3.22b) reveals that feedbacks in a two-dimensional model formulation are restricted to modifications to the cross-front potential temperature gradient, $\partial\theta/\partial y$, and the relative vorticity, $-\partial u_g/\partial y$, since $\partial v_g/\partial y$ and $\partial\theta/\partial x$ are specified externally. Thus, (4.2) and (4.1) can be used to determine how the ageostrophic response respectively affects the confluence and horizontal shear forcing, which, in turn, can lead to changes in the ageostrophic response through the Sawyer-Eliassen equation. As an example, in the cold advection case the differential subsidence within the upper-level frontal zone reinforces the horizontal shear forcing term in (3.22b) by increasing the cyclonic vorticity through (4.1). As suggested in the interpretation of the ageostrophic circulation pattern in Fig. 28b and demonstrated in an analysis of the Sawyer-Eliassen equation (3.12) for the cold advection case by Keyser and Pecnick (1985b), the cyclonic horizontal shear is responsible for shifting the ageostrophic circulation toward the warm air, so that the cross-frontal gradient of subsidence is frontogenetical with respect to the vorticity field. The resulting increases in cyclonic vorticity lead to increases in the horizontal shear forcing and the frontogenetical subsidence, establishing a positive feedback loop.

The results of the preceding analysis of two-dimensional frontal models can be applied to interpret dynamically the schematic representation of the progression of an upper-level jet-front system through a baroclinic wave presented in Fig. 19 (Section 2d). Several limitations of the two-dimensional frontal models should be kept in mind. First, their formulation describes an infinitely long confluent entrance region of a jet, rather than a finite-length jet maximum. Second, the sign of the along-front thermal variation cannot change with time during the frontal evolution, as suggested from the sequence of events in Fig. 19. Despite these restrictions, the pure confluence, cold advection and warm advection cases may correspond respectively to the stages illustrated in Figs. 19a, 19b and 19d, for which the jet-front systems are reasonably straight. The modeled transverse ageostrophic circulations for the three cases (Figs. 28a, 28b and 28c) conform fairly well to those in the jet entrance regions diagnosed qualitatively from the two-dimensional Sawyer-Eliassen equation (Figs. 23a, 23c and 23d), which correspond to the respective stages under consideration in Fig. 19. Furthermore, the change in dominance of vertical motions over horizontal motions in contributing to upper-level frontogenesis in the northwesterly flow inflection (Fig. 19b) to horizontal motions over vertical motions in the southwesterly flow inflection (Fig. 19d), documented observationally in Section 2d, is consistent with the preceding two-dimensional dynamical descriptions for the cold and warm advection cases.

b. Three-dimensional processes

Conspicuously absent from the above interpretation of the stages of the progression of an upper-level jet-front system through a baroclinic wave in terms of two-dimensional considerations is that of the jet-front system situated at the base of the long-wave trough (Fig. 19c). The thermal advection patterns for the configuration in Fig. 19c correspond to the case of a jet in a thermal ridge shown in Fig. 23e, with the major exception that the jet in Fig. 19c is cyclonically curved. The purpose of this subsection is to discuss three-dimensional modifications to the two-dimensional vertical circulation patterns in Fig. 23e introduced by significant curvature in the flow. For this discussion, curved flows may be defined as those in which the curvature component of the relative vorticity is greater than or comparable with the shear component, which may be contrasted to straight flows where the curvature component is much less than the shear component. The discussion begins with Fig. 29, which respectively illustrates idealized cases of pure cross-contour and along-contour ageostrophic flow considered in the absence of frictional and diabatic processes. The designations cross- and along-contour will be used as the three-dimensional counterparts of the two-dimensional terms cross- and along-front. Upper-level fronts

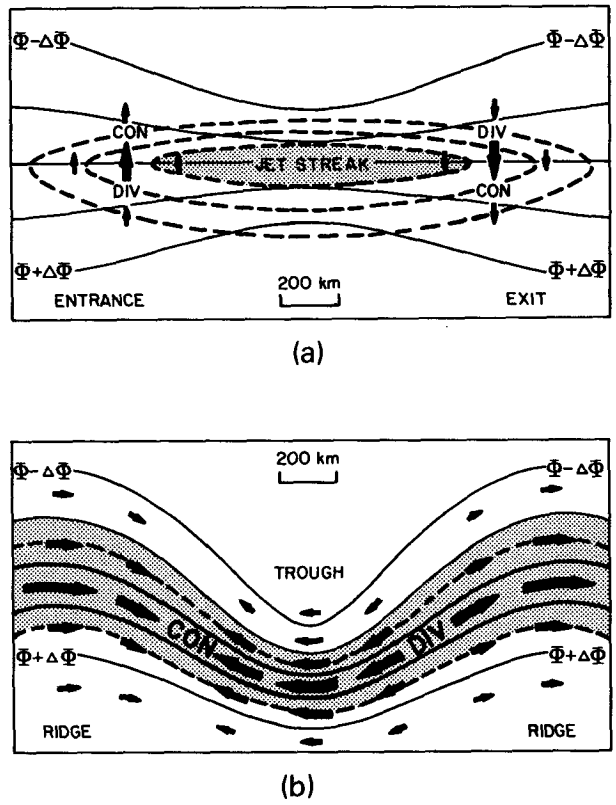

FIG. 29. Schematic representation of the ageostrophic motions (heavy arrows) and associated patterns of convergence (CON) and divergence (DIV) in the vicinity of (a) a straight jet streak in the absence of along-contour thermal advection and (b) a uniform jet stream within a stationary synoptic-scale wave. Both representations are assumed to apply at or near the level of maximum wind, where the horizontal wind distribution is most distinct and the flow is approximately horizontal. Solid lines indicate geopotential height of a constant pressure surface; dashed lines are isotachs (maximum wind speed shaded). Adapted from Shapiro and Kennedy (1981).

and jet features typically are oriented approximately parallel to the geopotential height contours.

The case of pure cross-contour ageostrophic flow shown in Fig. 29a consists of a straight jet streak in the absence of along-contour thermal variations, treated two-dimensionally in the descriptions of Figs. 21a and 23a. In terms of the frictionless u momentum equation subject to the geostrophic momentum approximation ($du_g/dt = fv_{ag}$), cross-contour ageostrophic flow is associated with accelerations in u_g, as parcels tend to migrate through the jet approximately parallel to the geopotential streamlines. The case of pure along-contour ageostrophic flow shown in Fig. 29b consists of a wave pattern in which the wind speed is uniform along the height contours (height contours correspond to isotachs). The wave is assumed to be stationary and steady-state, and horizontal flow is assumed at the level of the wave, so that streamlines and parcel trajectories coincide. With these restrictions, wind-speed accelerations following parcels vanish, eliminating cross-contour

ageostrophic flow. In this special case, parcel accelerations are confined to the cross-contour direction and are required to change the direction of parcels as they migrate through the wave. Under these conditions, the assumptions leading to the gradient wind are satisfied exactly, so that it may be used to quantify the contribution of centripetal accelerations induced by flow curvature to along-contour ageostrophic motions and the related patterns of convergence and divergence.

The gradient wind, $\mathbf{V}_{gr}$, is given by (e.g., Dutton, 1976, pp. 311–315)

$$\mathbf{V}_{gr} = \left(1 + \frac{KV_{gr}}{f}\right)^{-1} \mathbf{V}_g, \tag{4.3}$$

where K is the curvature parameter, defined as the inverse of the radius of parcel trajectory curvature ($K \equiv 1/R_t$). Equation (4.3) confirms that the gradient wind is oriented parallel to the height contours. Consequently, its ageostrophic part,

$$\mathbf{V}_{gr} - \mathbf{V}_g = -\left(\frac{KV_{gr}}{f}\right)\mathbf{V}_{gr}, \tag{4.4}$$

is in the along-contour direction and is proportional to the square of the wind speed and the magnitude of the trajectory curvature. As illustrated in Fig. 29b, the along-contour ageostrophic wind is directed against the gradient wind in the trough ($K > 0$, subgeostrophic flow) and along the gradient wind in the ridge ($K < 0$, supergeostrophic flow). The along-contour ageostrophic flow is zero at the inflections in the wave pattern, where the curvature vanishes. As a consequence of the specification of uniform wind speed along the flow, the required variations of geostrophic wind speed along the flow result in confluence and diffluence of the height contours upstream and downstream of the trough axis, respectively. This pattern of confluence and diffluence, associated with along-flow variations in curvature, should be distinguished from that in the straight-jet case (Fig. 29a), which is associated with along-flow variations in wind speed.

The horizontal divergence of the gradient wind (4.3) for the special case of uniform along-contour wind speed in Fig. 29b is

$$\nabla_p \cdot \mathbf{V}_{gr} = -\left(1 + \frac{KV_{gr}}{f}\right)^{-1}\left[\frac{\beta}{f} v_{gr} + \frac{V_{gr}}{f}(\mathbf{V}_{gr} \cdot \nabla_p K)\right]. \tag{4.5}$$

The above expression contains two contributions, which are respectively suppressed and amplified in the presence of cyclonic and anticyclonic trajectory curvature. The contributions comprise (i) the β-effect, which produces divergence and convergence in the northwesterly ($v_{gr} < 0$) and southwesterly ($v_{gr} > 0$) flows upstream and downstream of the trough axis, and (ii) the advection of curvature weighted by the gradient wind speed. For the example in Fig. 29b, the curvature effect results in maximum convergence and divergence at the flow inflections upstream and downstream of the trough axis along the contour channel containing the highest wind speed (the jet stream). The β-effect opposes, but is subordinate to, the curvature effect except for very long (planetary) waves. It should be emphasized that the horizontal divergence and convergence in the wave pattern in Fig. 29b are associated primarily with along-flow variations in curvature. Furthermore, the ageostrophic wind field (4.4) may have a significant nondivergent component, which does not contribute to the vertical circulation. As an extreme example, a symmetric circular vortex, characterized by constant curvature on an f-plane, is nondivergent according to (4.5) but contains significant ageostrophic flow according to (4.4).

The above analysis of curvature effects based on the concept of gradient flow has been extended by Newton and Trevisan (1984a) to include propagating waves in which the wind speed is uniform along streamlines of the geostrophic flow relative to the motion of the wave. On the basis of earlier work by Palmén and Nagler (1949), they kinematically infer vertical circulations and associated frontogenesis for parcels migrating through such waves, which they refer to as "gradient waves." The outcome of their analysis is that for purposes of qualitative interpretation, it is possible to view three-dimensional ageostrophic circulations as a combination of cross-contour (tranverse) ageostrophic flow associated with along-contour variations in wind speed and along-contour ageostrophic flow associated with along-contour variations in curvature. Stated alternatively, for a cyclonically curved jet maximum (in the absence of along-contour thermal variations) situated in the base of a trough, the ageostrophic flow and convergence/divergence patterns in Figs. 29a and 29b may be linearly superposed, with the implicit assumption that the two patterns are independent of each other in a dynamical sense. In a conceptual sense, this approach is based on a partitioning of the three-dimensional ageostrophic circulation that is linked to identifiable structural features within baroclinic flows. Specifically, the cross-contour component of the ageostrophic circulation is associated primarily with the upper-level jet-front system and the along-contour component is associated primarily with the baroclinic wave in which the jet-front system is embedded. This approach would appear to permit the two-dimensional interpretations based on the Sawyer-Eliassen equation to carry over to describe the vertical circulations associated with cross-contour ageostrophic flow in the three-dimensional case, while using reasoning based on the gradient wind to describe the vertical circulations associated with along-contour ageostrophic flow.

It needs to be emphasized that the above viewpoint is considered appropriate only for qualitatively interpreting and understanding three-dimensional ageostrophic flow patterns in upper-level jet-front systems.

Nevertheless, we choose to proceed with this hybrid approach of synthesizing deductions based on the Sawyer-Eliassen equation and the gradient wind in view of the paucity of examples in the literature of the quantitative diagnosis of three-dimensional ageostrophic circulations associated with upper-level jet-front systems. Such diagnoses appear to require an approach such as the three-dimensional generalization of the Sawyer-Eliassen equation introduced by Hoskins and Draghici (1977), alluded to near the conclusion of Section 3b. This diagnostic method yields ageostrophic vertical circulations in orthogonal planes, i.e., a vector streamfunction, which can be partitioned into cross- and along-contour components. Although we are unaware of such an interpretation, it may be possible in principle to relate the forcing of the along-contour component of the vector streamfunction to dynamical processes linked to flow curvature. An alternative quantitative approach would be to solve a diagnostic equation for the vertical velocity, such as that formulated in terms of quasi-geostrophic theory (3.23) or semigeostrophic theory (Hoskins and Draghici, 1977), but with the vertical velocity expressed in terms of a velocity potential (Eliassen, 1984). Solution of such a diagnostic equation would allow inference of the extent to which the irrotational part of the horizontal ageostrophic flow is oriented in the cross- versus the along-contour direction, as well as determination of the vertical velocity field.

In view of the preceding arguments based on the gradient wind, the vertical circulations associated with the cyclonically curved jet-front system located in the base of the long-wave trough illustrated schematically in Fig. 19c may be inferred qualitatively. The orientation of the isotherms at the base of the trough results in a pattern of along-contour thermal advection similar to that depicted in Fig. 23e. Therefore, the cross-contour (transverse) ageostrophic circulations can be anticipated to be respectively direct and indirect in the jet entrance and exit regions, but shifted laterally toward the anticyclonic shear side of the jet. The influence of curvature should be to force a dipole pattern consisting of midtropospheric subsidence and ascent below the jet axis in the entrance and exit regions, which are situated respectively within the northwesterly and southwesterly flow inflections in Fig. 19c. As a result, the anticipated effect of curvature is to reinforce the downward branch of the direct transverse ageostrophic circulation in the entrance region and the upward branch of the indirect transverse ageostrophic circulation in the exit region along the jet axis. The corresponding vertical branches of the transverse ageostrophic circulations situated below the anticyclonic shear side of the jet axis are weakened by the curvature-induced ageostrophic circulations. The favorable superposition of the upward branches of the cross- and along-contour ageostrophic circulations that occurs beneath the axis of a cyclonically curved jet when its exit region coincides with the inflection in the height contours downstream of a trough axis explains why the flow configuration in Fig. 19c is predisposed to low-level cyclogenesis beneath the jet exit region.

The above expectations on the nature of the vertical circulations associated with a cyclonically curved jet-front system in the base of a trough are confirmed by the results of numerical simulations of baroclinic wave amplification using β-plane primitive equation channel models under adiabatic, frictionless conditions. The initial conditions for these models typically consist of a small-amplitude disturbance (in the cases to be shown, an anticyclone–cyclone couplet extending through the depth of the troposphere) superimposed upon a longitudinally uniform jet possessing lateral and vertical shear and in thermal wind balance with the meridional potential temperature gradient. As the wave disturbance amplifies, a midtropospheric frontal zone forms in the base of the trough, as shown from the results of Buzzi et al. (1977)[12] in Fig. 30a. The temperature field at the base of the trough assumes the characteristic thermal ridge configuration shown in Fig. 19c, and the upper-level jet (not shown) is cyclonically curved approximately along the height contours. The cross sections for the vertical velocity field for the jet entrance (Fig. 30b) and exit (Fig. 30c) regions respectively reveal direct and indirect circulation patterns. The circulations are shifted toward the warm (anticyclonic shear) side of the frontal zone, and the stronger vertical motions are found within the frontal zone, which is situated beneath the jet axis. This asymmetrical character of the vertical motion patterns is suggestive of the influence of an along-contour ageostrophic circulation associated with curvature variations in augmenting the "two-dimensional" transverse ageostrophic circulations in the jet entrance and exit regions.

Diagnostic calculations of frontogenesis with respect to the horizontal potential temperature gradient for this numerical simulation reveal the dominance of vertical over horizontal motions for parcels migrating around the base of the trough through the frontal zone. The orientation of the subsidence pattern relative to the frontal zone in the entrance region of the upper-level jet–front system indicates a frontogenetical role for tilting (1.1) on the horizontal potential temperature gradient, arising from the locally indirect sense of the cross-contour variation of subsidence within the frontal zone (Fig. 30b). Similarly, tilting is frontolytical in the exit region, where the orientation of maximum ascent near the jet axis results in a locally direct sense of the

[12] The numerical model used by Buzzi et al. was formulated in terms of isentropic coordinates in the vertical direction by Eliassen and Raustein (1968, 1970). The ability of isentropic coordinates to represent the structure of upper-level frontal systems was demonstrated in a subsequent application of this type of model by Shapiro (1975).

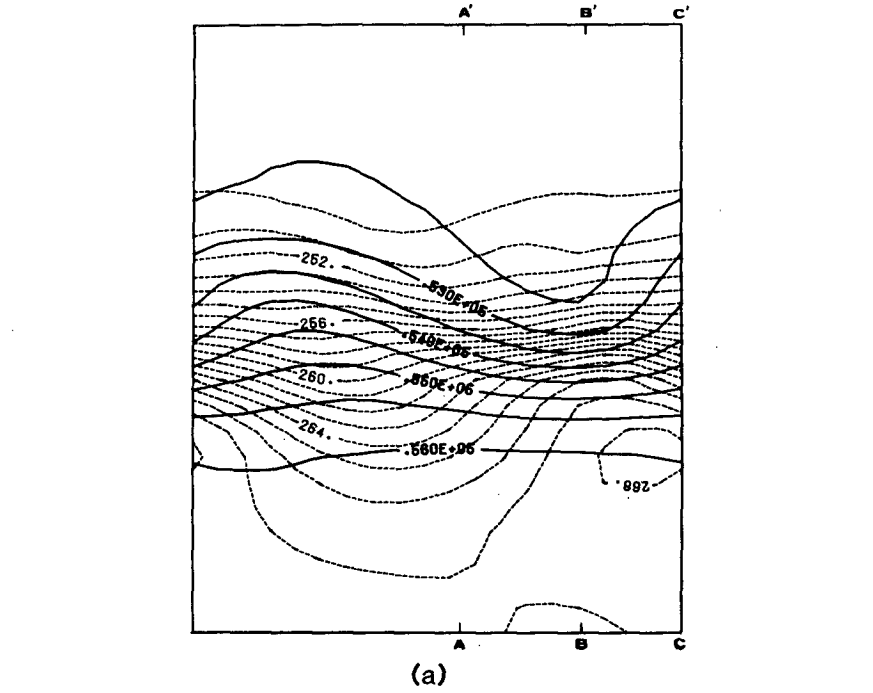

FIG. 30. Analyses illustrating the results of a 48 h numerical simulation of a baroclinically unstable wave in a β-plane primitive equation channel model using potential temperature as the vertical coordinate: (a) 500 mb geopotential ($m^2\ s^{-2}$, solid) and temperature (K, dashed); cross sections of pressure-coordinate vertical velocity ($10^{-1}\ \mu b\ s^{-1}$, dashed) and potential temperature (K, solid) along lines AA' (b) and CC' (c) shown in part (a). From Buzzi et al. (1977).

cross-contour variation of ascent within the frontal zone (Fig. 30c). Both the shift of the transverse ageostrophic circulation toward the warm side of the frontal zone and the dominant frontogenetical role of vertical motions in the entrance region of the jet–front system in the three-dimensional channel model are consistent with the corresponding results from the two-dimensional model of upper-level frontogenesis forced by a combination of cold advection and confluence (Section 4a).

Further documentation of the nature of the vertical circulations associated with an upper-level frontal system situated at the base of a trough of a baroclinic wave is found in the numerical results of Newton and Trevisan (1984b), which are derived from a β-plane channel model very similar to that of Buzzi et al. (1977). The idealized case simulated by Newton and Trevisan consists of the evolution of an upper-level jet stream and its associated frontal structure, which is best defined at the base of the trough. This case should be contrasted with that of Buzzi et al., which contains a jet maximum at the base of the trough (as treated schematically in Figs. 19c and 23e). The case considered by Newton and Trevisan reflects the schematic representation of

a curved jet stream in Fig. 29b, and thus isolates the frontogenetical influence of an along-contour ageostrophic circulation in the absence of transverse ageostrophic circulations in the entrance and exit regions of the frontal zone. Figure 31 illustrates the midtropospheric vertical motion pattern relative to the height field and the orientation of the jet-stream axis simulated by Newton and Trevisan. In agreement with qualitative expectations based on gradient flow (Fig. 29b), subsidence and ascent are maximized near the flow inflections along the jet-stream axis, which corresponds to the warm boundary of the frontal zone (not shown). This orientation of maximum vertical motions relative to the midtropospheric frontal zone is consistent with parcel frontogenesis and frontolysis in the frontal entrance and exit, respectively, as described previously in the discussion of Fig. 30.

Vertical cross sections of the total (geostrophic plus ageostrophic) transverse flow for the inflection in the flow coinciding with the frontal entrance region (Fig. 32) exhibit subsidence along a confluent asymptote corresponding to the jet axis. The confluent asymptote separates a region of widespread descent on the cyclonic shear side of the jet axis from descent in the warm air on the anticyclonic shear side of the jet axis. That this transverse flow pattern is frontogenetical for parcels migrating from the upstream ridge through the inflection to the base of the trough is reflected in the better-developed midtropospheric frontal structure in the isentropes at the trough compared with the ridge (Fig. 32b). The similarity is striking between the transverse flow pattern in Fig. 32 and the trajectory pattern from the two-dimensional model of upper-level frontogenesis due to a combination of cold advection and confluence in Fig. 27b, despite the association of subsidence with an along-contour ageostrophic circulation in the former and a cross-contour ageostrophic circulation in the latter. The similarity between both of the above numerically derived patterns involving the total transverse flow and the idealized schematic of transverse circulations accompanying tropopause folding in Fig. 33 (Danielsen, 1968) suggests the possible general connection between these transverse flow patterns and upper-level frontogenesis.

Identification of frontogenetical feedbacks between the three-dimensional vertical circulations and their forcing is limited to the interpretation of upper-level frontogenesis in a primitive equation β-plane channel model by Mudrick (1974). In this case, a positive feedback is postulated between the subsidence and vorticity patterns for the entrance region of a jet–front system in the northwesterly flow inflection between a ridge and downstream trough (the stage in Fig. 19b). Subsidence beneath the jet axis (Fig. 23c) enhances the cyclonic and anticyclonic shear vorticity on the respective sides of the jet in the midtroposphere through

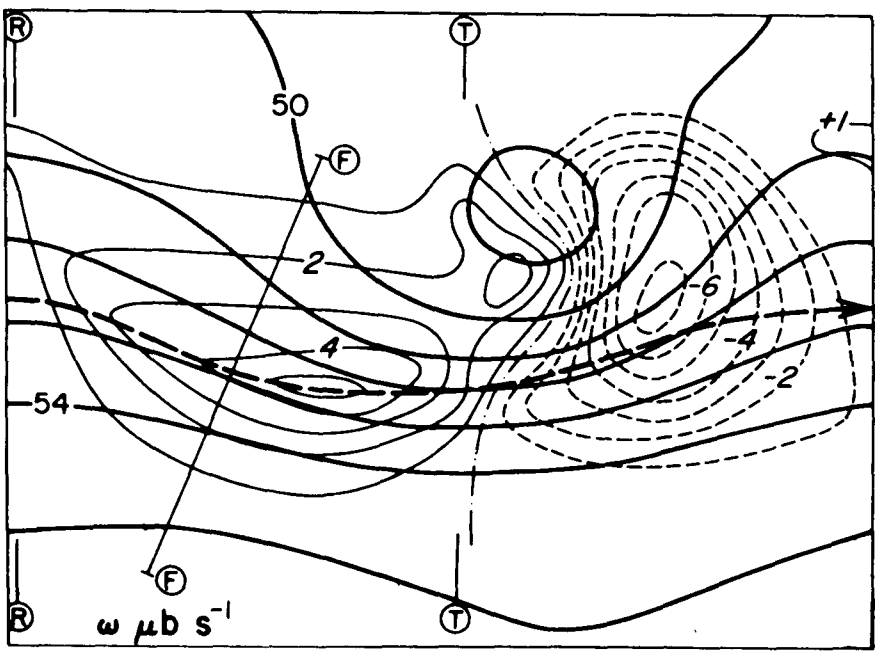

FIG. 31. Analysis at 500 mb illustrating the results of a 72 h numerical simulation of a baroclinically unstable wave in a β-plane primitive equation channel model similar to that referred to in Fig. 30. Thick solid lines are height contours (contour interval 100 m, 50 denotes 5000 m), thin solid and thin dashed lines are pressure-coordinate vertical velocity (contour interval 1 μb s^{-1}), and thick dashed arrow represents axis of intersection of jet stream with the 500 mb level. From Newton and Trevisan (1984b).

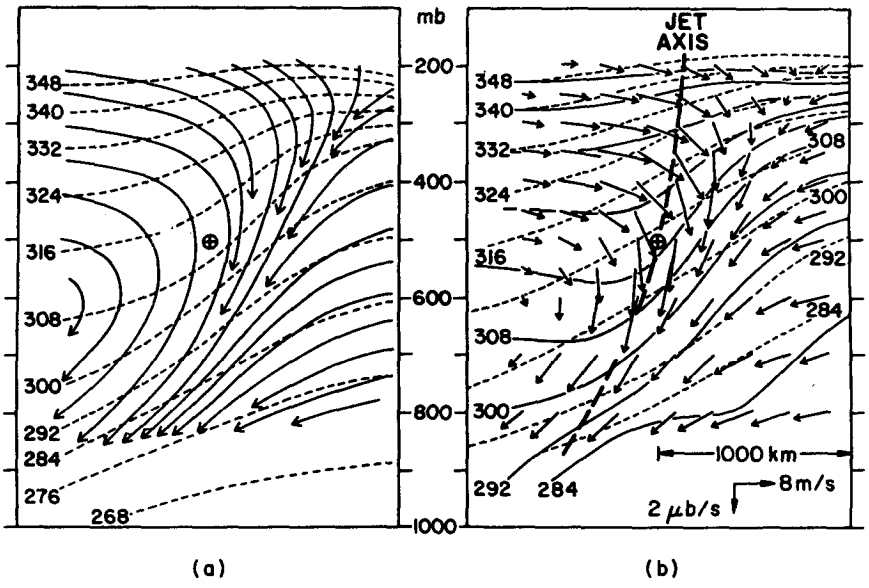

FIG. 32. Total transverse circulation for the northwesterly flow inflection, FF, shown in Fig. 31, indicated by streamlines in (a) and vector arrows in (b). Potential temperature (K) for the inflection, FF, is represented by dashed lines in (a). Potential temperature (K) for the ridge axis, RR, and trough axis, TT, shown in Fig. 31, is represented respectively by dashed and solid lines in (b). The circled plus signs denote the location of the jet at 500 mb within the flow inflection, FF. From Newton and Trevisan (1984b).

tilting (1.2), since the wind speed in the jet increases with height. The tilting thus results in an enhanced cross-contour gradient of vorticity. Mudrick then invokes an argument based on an extension of the quasi-geostrophic ω equation (3.23) to the primitive equations. The "primitive" ω equation consists of a more complicated response (left side) than its quasi-geostrophic counterpart, but its forcing (right side) is the

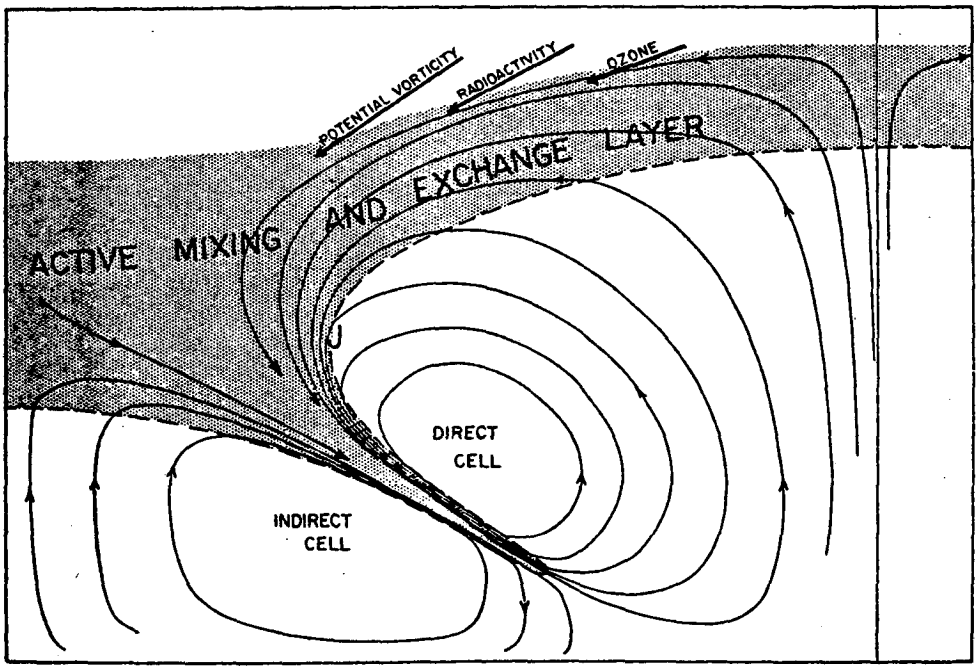

FIG. 33. Schematic illustration of transverse circulations conducive to upper-level frontogenesis and tropopause folding. Note that orientation of figure is reversed from that in Fig. 32. From Danielsen (1968).

same as in the quasi-geostrophic form (3.25) except that the vertical shear of the vorticity advection and Laplacian of the thermal advection involve the total horizontal wind rather than the geostrophic wind. Consequently, the presence of a thermodynamically direct cross-contour ageostrophic circulation in the jet entrance region results in a vertical increase in anticyclonic vorticity advection by the cross-contour component of the ageostrophic wind in the frontal zone. The increase of anticyclonic vorticity advection with height can be expected to be most intense in the vicinity of the jet axis, where the cross-contour gradient of shear vorticity is greatest. The result is midtropospheric subsidence maximized along the jet axis on the warm edge of the frontal zone, which is favorable for frontogenetical tilting and thus closes the positive feedback loop.

Although this subsidence–vorticity argument applies to a three-dimensional flow pattern, it appears to be two-dimensional in the sense that it involves the production of shear vorticity and its advection by the cross-contour component of the ageostrophic circulation. No reference is made to the along-contour component of the ageostrophic circulation, nor its forcing. It is possible that this feedback process is related to that identified in the two-dimensional cold advection case (Section 4a) involving the horizontal shear forcing of the Sawyer-Eliassen equation and subsidence. Nevertheless, the differing forms of the diagnostic equations for the vertical circulation on which the two- and three-dimensional interpretations are based renders their reconciliation problematical.

5. Directions of future research

The preceding sections have presented an overview of current knowledge and perspectives on the structure and dynamics of upper-level frontal zones. The application of synoptic-scale radiosonde observations supplemented by those from research aircraft has led to the synthesis of conceptual models of the structure of upper-level frontal systems. The application of two- and three-dimensional dynamical models has reproduced this structure and elucidated mechanisms and processes involved in upper-level frontogenesis. Nevertheless, a number of unresolved problems and issues can be identified and serve as the subject of discussion for this section. Topics requiring further research include (i) observational documentation of frontal evolution throughout the life cycle of baroclinic waves; (ii) resolution of the relative importance of two- and three-dimensional dynamical processes in upper-level frontogenesis and consideration of the potential importance of dynamical processes excluded by the geostrophic momentum approximation; (iii) investigation of the interaction between upper-level frontogenesis and baroclinic wave amplification and their effect on low-level cyclogenesis, along with the implications for required horizontal and vertical resolution for numerical weather prediction models; (iv) consideration of the relationship between upper-level frontal circulations and low-level circulations, a process sometimes referred to as "coupling"; and (v) investigation of the interaction between mesoscale convective systems and upper-level frontal systems.

A major shortcoming in our understanding of upper-level frontal dynamics is due to the absence of temporally continuous observational documentation of frontal evolution throughout the life cycle of a baroclinic wave. The schematic illustration of this process in Fig. 19 is based on fragmentary and incomplete observational evidence, and thus awaits further confirmation. The primary reasons for the incomplete documentation of frontal evolution are the gaps in the spatial coverage and temporal resolution of operational radiosonde observing networks. These data gaps have limited observationalists to focusing on only portions of the frontal evolution with a few snapshots describing the instantaneous structure. Another "gap" consists of the debatable accuracy of ageostrophic circulations derived from radiosonde data, which is primarily a consequence of uncertainties in the winds, especially at upper levels. These observational uncertainties have hindered progress in documenting three-dimensional vertical circulations within frontal regions. As a result, the application of diagnostic approaches and consideration of dynamical processes involving the ageostrophic part of the flow have been restricted primarily to datasets produced by idealized numerical models in two and three dimensions.

Rapid developments in progress in the field of remote-sensing technology have the potential of filling some of the data gaps in observational descriptions of upper-level jets and fronts. For example, the capability exists of remotely measuring patterns of vertically integrated ozone from satellites, which permits the detection of tropopause folding and the position and perhaps the intensity of upper-level jet streaks (Shapiro et al., 1982; Uccellini et al., 1985). Related advances in ground-based wind-profiling technology based on Doppler radar [see Larsen and Röttger (1982) for a review] offer considerable promise for examining the temporal evolution of the wind field in upper-level frontal regions. Vertical profiles of the horizontal wind field from near the surface to the 100 mb level can be obtained with vertical resolution on the order of several hundred meters and temporal resolution of an hour or less. The accuracy of the one-hourly averaged winds is typically several meters per second, which surpasses that of radiosonde data, especially in the upper troposphere and lower stratosphere.

A recent example of the application of wind profiler measurements to describe upper-level frontal structure is given in Figs. 34–36 (Shapiro et al., 1984a). Figure 34 consists of a subjective analysis of radiosonde observations for the 300 mb level supplemented by several profiler observations over Colorado, depicting a north-

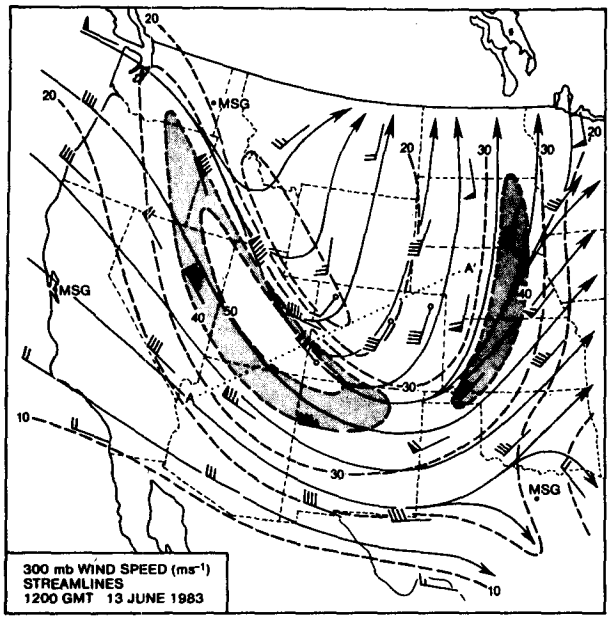

FIG. 34. Wind speed analysis at 300 mb for 1200 GMT 13 June 1983. Profiler wind vectors, open circles; wind speed (m s^{-1}), dashed lines; streamlines, thin solid lines. Winds are plotted according to the standard convention (see caption for Fig. 7a). MSG denotes missing radiosonde wind observations. From Shapiro et al. (1984a).

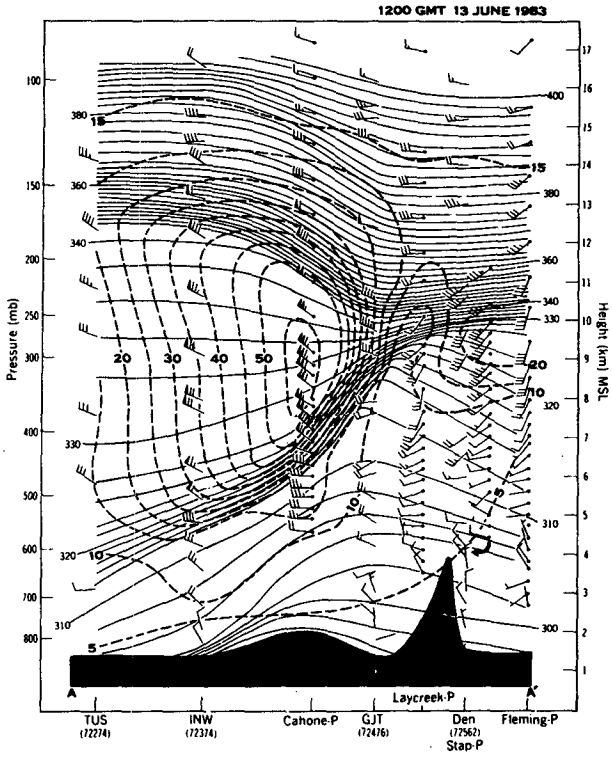

FIG. 35. Cross-section analysis of wind speed (m s^{-1}, dashed lines) and potential temperature (K, solid lines) for 1200 GMT 13 June 1983 along the projection AA′ in Fig. 34. Analysis is a composite of radiosonde and radar wind profiles (designated by letter P on the abscissa). From Shapiro et al. (1984a).

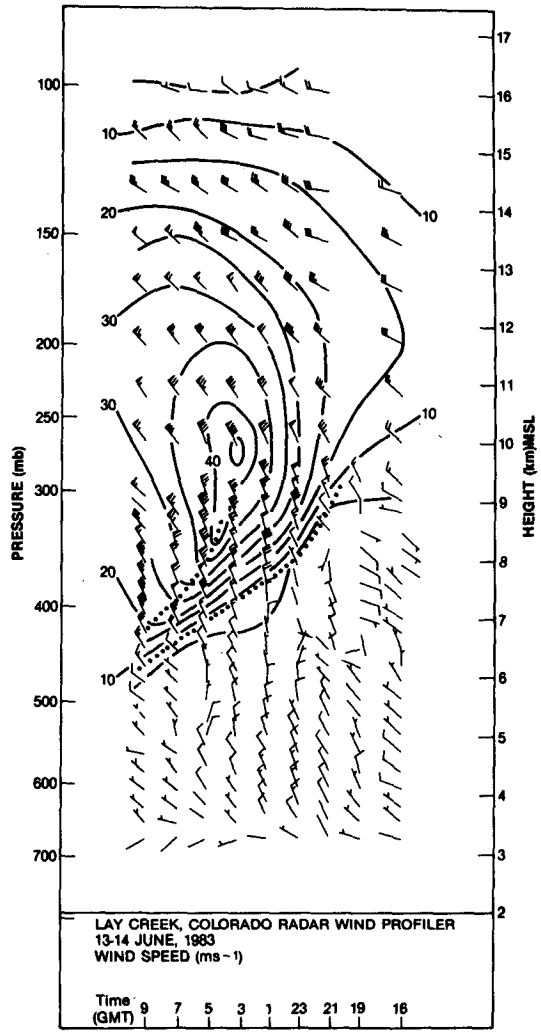

FIG. 36. Time–height cross section of wind speed (m s^{-1}) for 13–14 June 1983 with distances scaled as in Fig. 35. Vector winds are plotted at 2 h intervals at the indicated times; dotted lines indicate frontal boundaries. From Shapiro et al. (1984a).

westerly jet approaching the southwestern corner of Colorado. Figure 35 consists of a southwest–northeast oriented cross section through the jet derived subjectively using a composite of conventional radiosonde winds and temperatures and profiler winds. The structure of the upper-level frontal zone conforms to the expectations from previous analyses based on a combination of radiosonde and aircraft data (e.g., Fig. 7a and 10). The time–height cross section in Fig. 36, drawn from wind profiler data alone, reproduces the structure of the jet in the spatial cross section in Fig. 35 with remarkable fidelity. Frontal research could benefit substantially from the degree of temporal information contained within profiler observations of the wind field. Not only could time–space conversion techniques be applied to extract mesoscale detail from individual wind profiles as in the above example, but the temporal

evolution of upper-level jet systems could be monitored continuously from a profiler network possessing mesoscale horizontal resolution.

Another group of increasingly attractive tools for upper-level frontal research consists of numerical weather prediction models possessing mesoscale spatial resolution (see Anthes, 1983, for a recent review of mesoscale models). If computing technology continues to advance, numerical models with domains sufficiently large to cover the area affected by a synoptic-scale baroclinic wave during its life cycle and with horizontal and vertical resolution capable of explicitly resolving frontal systems could become a reality. Observational case studies could be supplemented with model simulations benefiting from dynamical consistency and the assimilation of data from a variety of sources including satellites, profilers and aircraft as well as conventional radiosondes. On the theoretical side, there is a need to design approaches for modeling the evolution of upper-level fronts in the context of the life cycle of baroclinic waves. The β-plane channel models describing baroclinic wave amplification (Section 4b) produce an upper-level jet-front system that remains at the base of the trough, which fits only one of the stages (Fig. 19c) envisioned during the evolution of baroclinic waves. Theoretical approaches must be devised to simulate the migration of a short-wave feature containing the upper-level jet-front system through a long wave in order to complement numerical simulations of this process anticipated using observational data.

A number of issues related to the evolution of upper-level frontal systems within baroclinic waves require investigation. One question concerns the origin of jet streaks and upper-level fronts, or, alternatively, the initiation of the chain of events represented schematically in Fig. 19. Namias and Clapp (1949) hypothesized that large-scale confluence established between polar and midlatitude airstreams could lead to the initial development and intensification of upper-level frontal systems. To our knowledge, this hypothesis has never been demonstrated, presumably because of the sparsity of radiosonde data in the northern midlatitude regions where the confluence process appears to be preferred (e.g., the Gulf of Alaska and western Canada for upper-level frontal systems affecting North America).

An issue of diagnostic interest identified in Section 4b is determining the relative contributions of the cross-contour (transverse) and along-contour components of the ageostrophic circulation to upper-level frontogenesis as a function of the stage of baroclinic wave evolution. Related questions concern the suitability of the geostrophic momentum approximation in the context of the quasi- and semigeostrophic equations for describing the three-dimensional ageostrophic flow patterns in flow regimes possessing substantial parcel trajectory curvature and where wind speeds are large. Shapiro and Kennedy (1981) and Uccellini et al. (1984) cite observed cases where adopting the geostrophic momentum approximation can lead locally to errors in the magnitude and even the direction of the cross-contour component of the ageostrophic circulation derived by considering accelerations of the along-contour wind component following parcel trajectories. Systematic comparisons between quasi-geostrophic, semigeostrophic and primitive equation formulations, as well as the additional "intermediate models" proposed by McWilliams and Gent (1980), through the integration of prognostic models of idealized baroclinic flows [as in Mudrick (1974)] would be useful for assessing the general validity and accuracy of these approximations. A related but complementary approach consists of utilizing diagnostic formulations based on the above sets of approximations to solve for the three-dimensional ageostrophic circulations from the output of primitive equation model simulations, for which the "true" ageostrophic circulations are known exactly.

A question of considerable practical significance is the extent to which upper-level frontal systems and frontogenetical processes must be resolved in numerical weather prediction models to improve the accuracy of forecasts[13] involving significant midlatitude cyclogenesis and precipitation. A related consideration is the extent to which upper-level jet-front systems must be resolved in initial datasets. These questions are reflected in the closing comments of the synoptic meteorology textbook by Palmén and Newton (1969, p. 585):

> Although some of the principal mechanisms governing cyclogenesis have been exposed, it cannot be said that the process is completely understood. For example, it has been possible to produce replicas of cyclones in numerical prediction experiments without taking into account the existence of fronts (although in some cases these develop in rudimentary form). Since well-developed fronts are characteristic of the real atmosphere and much of the available potential energy and kinetic energy are concentrated in their vicinity, there is still to a certain extent an open question about the fundamental physical relationships between frontogenesis and cyclogenesis.

Although published over 15 years ago, the conflicting viewpoints raised in this passage questioning the extent to which upper-level frontogenesis is a passive consequence or an active causal mechanism for cyclogenesis require reconciliation.

The opposing views concerning the relationship between upper-level frontogenesis and cyclogenesis may be related to differing perspectives on the nature of the cyclogenesis process between the observational and

[13] The concept of "improved forecast accuracy" takes on a precise meaning only when the needs or requirements of a particular user are taken into account, and is, of course, open to considerable interpretation and debate.

theoretical disciplines. The typical sequence of events associated with cyclogenesis identified observationally (e.g., Petterssen, 1955; 1956, pp. 334–338; Palmén and Newton, 1969, pp. 316–324) conforms to the schematic in Fig. 19, with cyclogenesis favored during the stages depicted in Figs. 19b and 19c. In particular, a surface cyclone begins to develop beneath the diffluent (delta) region in the upper-level height contours as a jet-front system propagates from the northwesterly flow inflection toward the base of the trough. The deepening rate then increases as the jet rounds the base of the trough, assuming a cyclonically curved orientation, and migrates toward the southwesterly flow inflection. The implication of this synoptic viewpoint of cyclogenesis is that the upper-level jet-front system plays an active role in the process by organizing and focusing the patterns of upper-level divergence necessary for low-level pressure falls. This viewpoint suggests that in some cases forecasts of the timing, location and intensity of cyclogenesis in numerical weather prediction models may demonstrate a significant degree of sensitivity to the resolution of upper-level jet-front systems.

Most contemporary theoretical perspectives on midlatitude cyclogenesis derive from the original formulations of baroclinic instability theory by Charney (1947) and Eady (1949). These classic theoretical developments, along with the extensive elaborations and generalizations they have inspired, collectively describe the exponential growth to finite amplitude of an infinitesimal wavelike disturbance (referred to as a normal mode) superimposed upon a basic state consisting of a zonal jet possessing vertical (and sometimes lateral) shear and in thermal wind balance with the temperature field. The horizontal scale of the initial disturbance is selected to be that yielding the most rapid growth rate. This theory isolates the dynamical mechanisms and feedbacks involved in the intensification of midlatitude cyclones, referred to as the "self-development" process by Sutcliffe and Forsdyke (1950).

By focusing on the growth process, classic baroclinic instability theory does not treat the complete life cycle of midlatitude cyclones. In particular, the details of the process by which cyclogenesis is initiated are not considered, and are irrelevant in the sense that the structure of the cyclone and its growth rate are determined by the basic state alone, rather than by a combination of factors including the initial conditions (a characteristic of the so-called normal-mode approach). Although realistic reproductions of upper-level and surface fronts are found in the context of baroclinic instability theory, they arise as a consequence of upper-level wave amplification and low-level cyclogenesis, rather than appearing in advance of these processes. The implication of the normal-mode approach to baroclinic instability theory for numerical weather prediction is that the detailed resolution of upper-level jet-front systems does not appear to be required, because the cyclogenesis process depends upon the properties of the large-scale flow pattern, which corresponds to the basic state in the theory.

Reconciliation of the conflicting observational and theoretical viewpoints concerning the active compared with the passive role of upper-level jet-front systems in cyclogenesis appears to require determining the relative influence of the initial conditions compared with the basic state on the baroclinic growth process. Recently, Farrell (1982, 1984) has fit baroclinic instability theory into the mathematical construct of an initial value problem. This approach produces a group of solutions referred to as "nonmodal," required to account for the specification of arbitrarily general initial conditions, in addition to the conventional, but structurally limited, normal-mode solutions. The overall result is that the nonmodal solutions dominate in the early stages of baroclinic growth, while the normal modes are of increasingly greater importance later on in the process. These idealized results may be interpreted as suggestive of an active role for upper-level jet-front systems in the initiation phase in the life cycle of midlatitude cyclones.

As stated in the introduction, this review has focused for organizational necessity on upper-level jet-front systems at the expense of virtually ignoring their low-level counterparts. From the standpoint of Dines' compensation, the divergence patterns forced by jet-front systems at upper levels may be considered to be associated with convergence patterns forced by frontogenetical processes at lower levels. Consequently, although upper-level and lower-level fronts and jets may appear to be structurally separate from each other, under suitable conditions they may be viewed as coupled through their vertical circulations. This interpretation has been applied by Uccellini and Johnson (1979) and Uccellini (1980) to connect upper- and lower-level jets dynamically and relate this coupled jet configuration to the organization of an environment conducive to the initiation and organization of severe convective storms. Shapiro (1983) presents hypothetical schematics of superposed upper-level jets and surface fronts and their associated transverse ageostrophic circulations respectively unfavorable and favorable for the development of severe convective storms. Further observational research is needed to link the establishment of the preconvective environment, as well as the initiation and organization of convective storms, to the three-dimensional ageostrophic circulation patterns forced by coupled upper- and lower-level jets and fronts.

Upper-level jet-front systems may not only contribute to the development of convection, but may in turn be influenced by its presence. Organized convection may contribute to the frictional and diabatic forcing terms in the Sawyer-Eliassen equation (3.12) by vertically transporting momentum and heat, as well as through the direct heating and cooling effects of condensation and evaporation. Shapiro and Kennedy

(1982) suggest that their aircraft measurements of cross-contour ageostrophic flow toward lower heights in the vicinity of the core of a straight jet, for which speed accelerations and curvature effects may be considered negligible, can be accounted for by the nearby presence of a line of deep convection. If frictional effects also can be ignored in the jet core, this cross-contour component of the ageostrophic flow is in the appropriate sense to result in the intensification of the jet. Observational studies (e.g., Ninomiya, 1971; Maddox, 1979; Fritsch and Maddox, 1981; Fuelberg and Browning, 1983; Wetzel et al., 1983; Keyser and Johnson, 1984) and mesoscale numerical model simulations (e.g., Maddox et al., 1981; Anthes et al., 1982) have shown that an organized mesoscale convective system can contribute to the enhancement of a preexisting upper-level jet or even the formation of a new jet through cross-contour ageostrophic circulations associated with the anticyclonic, divergent outflow found at the tropopause level above the convective storm system. The longer-term impact of the convectively generated modifications to upper-level jets over time scales extending beyond the lifetime of the convection has been questioned by Wetzel et al. (1983), who point out that enhancements in jet wind speeds are confined to a relatively shallow layer near the tropopause and do not appear to be in dynamic balance with the thermal field. Additional research is necessary to document further the patterns of the three-dimensional ageostrophic circulations and their forcing involved in the scale interactions between upper-level jet-front systems and mesoscale convective storms.

6. Conclusion

Our knowledge and understanding of the structure and dynamics of upper-level frontal zones and their interactions with larger- and smaller-scale phenomena and processes have advanced considerably since their discovery and initial observational description with the advent of upper-air data over 50 years ago. Observational descriptions have evolved to the point of thoroughly documenting the structure of upper-level jet-front systems at particular stages in their life histories. Dynamical descriptions of the associated vertical circulation patterns have been established through the application of two-dimensional theoretical models and diagnostic approaches, and mechanisms involving feedbacks between the primary (geostrophic) and secondary (ageostrophic) circulations have been identified. The theoretical basis has also been introduced for extending two-dimensional diagnostic concepts to three dimensions.

When surveying the results of research into upper-level frontal systems during the past 50 years, one may be impressed by the significant influence of technological innovations on changes in observational and theoretical thinking. The discovery of upper-level fronts was a consequence of interest in exploring the atmosphere above the Earth's surface and documenting its three-dimensional structure, rather than continuing to rely on the limited methods of indirect aerology, which consisted of inferring the upper-air patterns from surface data, cloud observations and air-mass types. Interest in probing the three-dimensional structure of the troposphere must have been heightened by the operational requirements of the fledgling aviation industry. The application of upper-air data eventually led to questioning of the inferences of the Bergen School concerning the existence of a deep polar front encircling the globe at midlatitudes, separating polar from tropical air. By the late 1940s, the development of baroclinic instability theory and approaches for diagnosing cyclogenesis and vertical motions based on quasi-geostrophic theory revealed a shift away from the focus on surface discontinuities and kinematic treatments to a viewpoint of a three-dimensional, continuous atmosphere describable in terms of dynamical principles. With this change in emphasis, fronts were viewed as zones of transition rather than discontinuities, a description appropriate to upper-level fronts. In retrospect, the ideas of Reed, Sanders, Newton and Danielsen in the 1950s on the formation of upper-level fronts through dynamically induced subsidence, rather than through the confluence of polar and tropical air masses as in the case of surface fronts, represented a culmination of the shift in emphasis toward contemporary thinking in synoptic meteorology. The subsequent research involving aircraft measurements has extended and refined modern views on the structure and evolution of upper-level fronts, rather than resulting in major, revolutionary changes.

It may be argued that the implementation of electronic computers and the rapid development of numerical weather prediction as an established meteorological discipline during the 1950s may have lessened interest and slowed frontal research. The early baroclinic models primarily were intended to treat the long-wave patterns on a hemispheric scale, so that upper-level and surface fronts were subgrid-scale phenomena. Encouragingly realistic and accurate predictions could be interpreted to suggest that fronts are of lesser importance in the dynamics of midlatitude baroclinic waves and cyclones than might have been anticipated. The emerging viewpoint was that baroclinic development is a large-scale process of which fronts are a passive consequence, consonant with the results of normal-mode approaches to baroclinic instability theory. Eventual limited improvements in the skill of numerical forecasts, coupled with substantial practical interest in quantitative precipitation forecasting, subsequently led to a focus on developing parameterizations of planetary boundary layer and convective precipitation processes. The development of finer-resolution, mesoscale models suitable for applications involving real data during the 1970s appears to have

been governed by the widespread opinion that major gains in forecast accuracy were to be made through refined treatments of boundary layer and convective processes. This approach reflects the view that baroclinic processes are synoptic-scale and more than adequately resolved in mesoscale models. Consequently, there was relatively little motivation to focus attention and effort systematically on resolving frontal-scale processes in mesoscale models, which consists of emphasizing vertical resolution in objective analysis-initialization schemes and model grid systems.

It is tempting to speculate that a practical context is emerging for renewed interest in upper-level and surface fronts. Mesoscale numerical weather prediction may be progressing to the point of diminishing returns with respect to increases in the accuracy of quantitative precipitation forecasts. It may be that the parameterization of precipitation processes has advanced to the stage where further improvements in precipitation forecasts require explicit resolution of the vertical circulation patterns responsible for initiating and organizing mesoscale convective systems. If such a conjecture is correct, the resolution of fronts becomes important, since they are the primary seat for the forcing of mesoscale vertical circulations. Computing technology now exists to resolve fronts in both mesoscale models and their initial conditions. Novel observing technologies involving the remote sensing of winds from the ground, and temperature, moisture and ozone from space offer promise in filling gaps in the temporal separation, spatial coverage and accuracy of data from conventional radiosonde networks. The likely necessity of explicitly resolving frontal systems in mesoscale models, coupled with the above advances in computing and observing technology, has the potential of renewing interest and stimulating progress in frontal research. Such progress in frontal research should yield not only refinements in mesoscale model forecast skill, but also improved conceptual models of the life cycle of midlatitude cyclones in the spirit of the polar-front cyclone model of the Bergen School in Norway, which undoubtedly served as a tremendous impetus earlier in this century for the intellectual and practical achievements documented in this review.

Acknowledgments. The authors have benefited considerably from the advice, comments and reviews of Drs. R. A. Anthes, L. F. Bosart, K. A. Emanuel, B. F. Farrell, J. M. Fritsch, B. J. Hoskins, R. A. Maddox, C. W. Newton, R. A. Petersen, R. J. Reed, J. Simpson and L. W. Uccellini. The contribution of the first author to this paper was funded in part by the NASA Mesoscale Atmospheric Processes Research Program and by the Air Force Office of Scientific Research through Contract AFOSR-ISSA-85-00008. Ms. Mildred Birchfield expeditiously and accurately typed the numerous versions of the manuscript, and Mr. Lafayette Long assisted in preparing the figures.

APPENDIX

List of Symbols and Acronyms

ag	subscript denoting ageostrophic
c_p	specific heat for dry air at constant pressure
c_v	specific heat for dry air at constant volume
CAT	clear-air turbulence
$d(\ )/dt$	temporal derivative following a parcel trajectory
f	Coriolis parameter
$\mathbf{F}$	friction term in vector equation of motion
F_x	component of friction term in x direction
g	gravity; subscript denoting geostrophic
gr	subscript denoting gradient
$\mathbf{i}$	unit vector in x direction
$\mathbf{j}$	unit vector in y direction
$J_{xy}(\xi_1, \xi_2)$	Jacobian operator in (x, y) plane defined as $(\partial\xi_1/\partial x)(\partial\xi_2/\partial y) - (\partial\xi_1/\partial y)(\partial\xi_2/\partial x)$
$J_{yp}(\xi_1, \xi_2)$	Jacobian operator in (y, p) plane defined as $(\partial\xi_1/\partial y_p)(\partial\xi_2/\partial p) - (\partial\xi_1/\partial p)(\partial\xi_2/\partial y_p)$
$\mathbf{k}$	unit vector in vertical direction
K	inverse of radius of parcel trajectory curvature
ln( )	natural logarithm
LMW	level of maximum wind
m	absolute momentum parameter [defined by (2.2)]
n	horizontal coordinate oriented normal to isentropes (positive toward colder air)
p	pressure
p_0	reference pressure
P	general expression for potential vorticity in isentropic coordinates (2.1)
P_2	two-dimensional (y, p) form for potential vorticity [defined by (2.9)]
$\mathbf{Q}$	vector quantity constituting dynamical forcing of quasi-geostrophic ω equation [defined by (3.24)]
R	ideal gas constant for dry air
R_t	radius of parcel trajectory curvature
Ri	Richardson number [defined by (2.14)]
s	horizontal coordinate oriented along isentropes 90° to the right of n
t	time
u	component of wind velocity in x direction
v	component of wind velocity in y direction
v_n	component of wind velocity in n direction
V	horizontal wind speed
$\mathbf{V}$	horizontal wind velocity
$\mathbf{V}_{ag}$	ageostrophic horizontal wind velocity defined as $u_{ag}\mathbf{i} + v_{ag}\mathbf{j}$
$\mathbf{V}_{ag2}$	ageostrophic vector wind in the (y, p) plane defined in (3.6) as $v_{ag}\mathbf{j} - \omega\mathbf{k}$
w	vertical velocity in z coordinate system $[=dz/dt]$
$\overline{w'\theta'}$	vertical eddy flux of potential temperature
x	horizontal coordinate increasing eastward; along-front coordinate; subscript de-

noting component of a vector in **i** direction

y horizontal coordinate increasing northward; cross-front coordinate (positive toward colder air); subscript denoting component of a vector in **j** direction

z height coordinate; in Section 4a and Figs. 24–28, pressure-dependent pseudo-height introduced by Hoskins and Bretherton (1972)

α confluence parameter introduced in Section 4a, equal to one half of the magnitude of the horizontal deformation.

β latitudinal variation of the Coriolis parameter

γ function of pressure (2.8) appearing in thermal wind (2.5) and hydrostatic (2.7) relations

$\delta(\ )$ operator denoting incremental distance in ( ) direction

ζ relative vorticity evaluated on a constant pressure surface

ζ_θ relative vorticity evaluated on an isentropic surface

ζ_{g2} absolute geostrophic vector vorticity in (y, p) plane [defined by (2.4)]

θ potential temperature

$\dot{\theta}$ diabatic heating rate

Θ pressure-dependent reference distribution of potential temperature introduced through quasi-geostrophic thermodynamic equation

μ_θ slope of isentropes constituting a frontal zone $[=\delta p/\delta y_\theta]$ appearing in (2.15)

ξ dummy variable used in defining Jacobian operators

ρ density of dry air

ϕ geopotential of a constant pressure surface

ψ ageostrophic streamfunction in (y, p) plane [defined by (3.6)]

Ψ vector streamfunction for three-dimensional ageostrophic flow defined such that $u_{ag} = -\partial\psi_x/\partial p$, $v_{ag} = -\partial\psi_y/\partial p$, $\omega = \nabla_p \cdot \Psi$

ω vertical velocity in p coordinate system $[=dp/dt]$

∇_p horizontal gradient operator on a constant pressure surface

∇_θ horizontal gradient operator on an isentropic surface

∇_2 gradient operator in (y, p) plane [defined following (2.4)]

REFERENCES

Anthes, R. A., 1983: Regional models of the atmosphere in middle latitudes. *Mon. Wea. Rev.*, **111**, 1306–1335.

——, Y.-H. Kuo, S. G. Benjamin and Y.-F. Li, 1982: The evolution of the mesoscale environment of severe local storms: Preliminary modeling results. *Mon. Wea. Rev.*, **110**, 1187–1213.

Berggren, R., 1952: The distribution of temperature and wind connected with active tropical air in the higher troposphere and some remarks concerning clear air turbulence at high altitude. *Tellus*, **4**, 43–53.

Bjerknes, J., 1919: On the structure of moving cyclones. *Geofys. Publ.*, **1**(1), 1–8.

——, and E. Palmén, 1937: Investigations of selected European cyclones by means of serial ascents. *Geofys. Publ.*, **12**(2), 1–62.

——, and H. Solberg, 1921: Meteorological conditions for the formation of rain. *Geofys. Publ.*, **2**(3), 1–60.

——, and ——, 1922: Life cycle of cyclones and the polar front theory of atmospheric circulation. *Geofys. Publ.*, **3**(1), 1–18.

Bluestein, H. B., 1986: Fronts and jet streaks: A theoretical perspective. *Mesoscale Meteorology and Forecasting*, P. S. Ray, Ed., Amer. Meteor. Soc., Chapt. 9 (submitted).

Bosart, L. F., 1970: Mid-tropospheric frontogenesis. *Quart. J. Roy. Meteor. Soc.*, **96**, 442–471.

Briggs, J., and W. T. Roach, 1963: Aircraft observations near jet streams. *Quart. J. Roy. Meteor. Soc.*, **89**, 225–247.

Browning, K. A., 1971: Radar measurements of air motion near fronts. *Weather*, **26**, 320–240.

——, and C. D. Watkins, 1970: Observations of clear air turbulence by high power radar. *Nature*, **227**, 260–263.

——, T. W. Harrold and J. R. Starr, 1970: Richardson number limited shear zones in the free atmosphere. *Quart. J. Roy. Meteor. Soc.*, **96**, 40–49.

Buzzi, A., T. Nanni and M. Tagliazucca, 1977: Mid-tropospheric frontal zones: Numerical experiments with an isentropic coordinate primitive equation model. *Arch. Meteor. Geophys. Bioklim.*, **A26**, 155–178.

——, A. Trevisan and G. Salustri, 1981: Internal frontogenesis: A two-dimensional model in isentropic, semi-geostrophic coordinates. *Mon. Wea. Rev.*, **109**, 1053–1060.

Cahir, J. J., 1971: Implications of circulations in the vicinity of jet streaks at subsynoptic scales. Ph.D. thesis, The Pennsylvania State University, University Park, PA 16802, 170 pp.

Charney, J. G., 1947: The dynamics of long waves in a baroclinic westerly current. *J. Meteor.*, **4**, 135–163.

Danielsen, E. F., 1964: Project Springfield report. DASA 1517, Defense Atomic Support Agency, Washington, DC 20301, 97 pp. [NTIS AD-607980].

——, 1968: Stratospheric-tropospheric exchange based on radioactivity, ozone and potential vorticity. *J. Atmos. Sci.*, **25**, 502–518.

Dutton, J. A., 1976: *The Ceaseless Wind: An Introduction to the Theory of Atmospheric Motion.* McGraw-Hill, 579 pp.

Eady, E. T., 1949: Long waves and cyclone waves. *Tellus*, **1**, No. 3, 33–52.

Eliassen, A., 1962: On the vertical circulation in frontal zones. *Geofys. Publ.*, **24**(4), 147–160.

——, 1984: Geostrophy. *Quart. J. Roy. Meteor. Soc.*, **110**, 1–12.

——, and E. Kleinschmidt, 1957: Dynamic meteorology. *Handbuch der Physik*, Vol. 48, S. Flügge, Ed., Springer-Verlag, 1–154.

——, and E. Raustein, 1968: A numerical integration experiment with a model atmosphere based on isentropic surfaces. *Meteor. Ann.*, **5**, 45–63.

——, and ——, 1970: A numerical integration experiment with a six-level atmospheric model with isentropic information surface. *Meteor. Ann.*, **5**, 429–449.

Emanuel, K. A., 1979: Inertial instability and mesoscale convective systems. Part I: Linear theory of inertial instability in rotating viscous fluids. *J. Atmos. Sci.*, **36**, 2425–2449.

——, 1985: Frontal circulations in the presence of small moist symmetric stability. *J. Atmos. Sci.*, **42**, 1062–1071.

Faller, A. J., 1956: A demonstration of fronts and frontal waves in atmospheric models. *J. Meteor.*, **13**, 1–4.

Farrell, B. F., 1982: The initial growth of disturbances in a baroclinic flow. *J. Atmos. Sci.*, **39**, 1663–1686.

——, 1984: Modal and non-modal baroclinic waves. *J. Atmos. Sci.*, **41**, 668–673.

Fritsch, J. M., and R. A. Maddox, 1981: Convectively driven mesoscale weather systems aloft. Part I: Observations. *J. Appl. Meteor.*, **20**, 9–19.

Fuelberg, H. E., and P. A. Browning, 1983: Roles of divergent and rotational winds in the kinetic energy balance during intense convective activity. *Mon. Wea. Rev.*, **111**, 2176–2193.

Fultz, D., 1952: On the possibility of experimental models of the polar-front wave. *J. Meteor.*, **9**, 379–384.

Gidel, L. T., and M. A. Shapiro, 1979: The role of clear air turbulence in the production of potential vorticity in the vicinity of upper tropospheric jet stream–frontal systems. *J. Atmos. Sci.*, **36**, 2125–2138.

Haltiner, G. J., and R. T. Williams, 1980: *Numerical Prediction and Dynamic Meteorology*, 2nd ed. Wiley, 477 pp.

Holton, J. R., 1979: *An Introduction to Dynamic Meteorology*, 2nd ed. *Int. Geophys. Ser.*, Vol. 23, Academic Press, 391 pp.

Hoskins, B. J., 1971: Atmospheric frontogenesis models: Some solutions. *Quart. J. Roy. Meteor. Soc.*, **97**, 139–153.

——, 1972: Non-Boussinesq effects and further development in a model of upper tropospheric frontogenesis. *Quart. J. Roy. Meteor. Soc.*, **98**, 532–541.

——, 1974: The role of potential vorticity in symmetric stability and instability. *Quart. J. Roy. Meteor. Soc.*, **100**, 480–482.

——, 1975: The geostrophic momentum approximation and the semi-geostrophic equations. *J. Atmos. Sci.*, **32**, 233–242.

——, 1982: The mathematical theory of frontogenesis. *Annual Reviews in Fluid Mechanics*, Vol. 14, Annual Reviews, 131–151.

——, and F. P. Bretherton, 1972: Atmospheric frontogenesis models: Mathematical formulation and solution. *J. Atmos. Sci.*, **29**, 11–37.

——, and I. Draghici, 1977: The forcing of ageostrophic motion according to the semi-geostrophic equations and in an isentropic coordinate model. *J. Atmos. Sci.*, **34**, 1859–1867.

——, and M. A. Pedder, 1980: The diagnosis of middle latitude synoptic development. *Quart. J. Roy. Meteor. Soc.*, **106**, 707–719.

——, I. Draghici and H. C. Davies, 1978: A new look at the ω-equation. *Quart. J. Roy. Meteor. Soc.*, **104**, 31–38.

——, M. E. McIntyre and A. W. Robertson, 1985: On the use and significance of isentropic potential-vorticity maps. *Quart. J. Roy. Meteor. Soc.*, **111**, (October issue).

Kennedy, P. J., and M. A. Shapiro, 1975: The energy budget in a clear air turbulence zone as observed by aircraft. *Mon. Wea. Rev.*, **103**, 650–654.

Keyser, D., 1986: Atmospheric fronts: An observational perspective. *Mesoscale Meteorology and Forecasting*, P. S. Ray, Ed., Amer. Meteor. Soc., Chapt. 10 (submitted).

——, and M. J. Pecnick, 1985a: A two-dimensional primitive equation model of frontogenesis forced by confluence and horizontal shear. *J. Atmos. Sci.*, **42**, 1259–1282.

——, and ——, 1985b: Diagnosis of ageostrophic circulations in a two-dimensional primitive equation model of frontogenesis. *J. Atmos. Sci.*, **42**, 1283–1305.

Keyser, D. A., and D. R. Johnson, 1984: Effects of diabatic heating on the ageostrophic circulation of an upper tropospheric jet streak. *Mon. Wea. Rev.*, **112**, 1709–1724.

Krishnamurti, T. N., 1968: A study of a developing wave cyclone. *Mon. Wea. Rev.*, **96**, 208–217.

Larsen, M. F., and J. Röttger, 1982: VHF and UHF Doppler radars as tools for synoptic research. *Bull. Amer. Meteor. Soc.*, **63**, 996–1008.

Maddox, R. A., 1979: The evolution of middle and upper tropospheric features during a period of intense convective storms. *Preprints Eleventh Conf. Severe Local Storms*, Kansas City, Amer. Meteor. Soc., 41–48.

——, D. J. Perkey and J. M. Fritsch, 1981: Evolution of upper tropospheric features during the development of a mesoscale convective complex. *J. Atmos. Sci.*, **38**, 1664–1674.

McWilliams, J. C., and P. R. Gent, 1980: Intermediate models of planetary circulations in the atmosphere and ocean. *J. Atmos. Sci.*, **37**, 1657–1678.

Miller, J. E., 1948: On the concept of frontogenesis. *J. Meteor.*, **5**, 169–171.

Mudrick, S. E., 1974: A numerical study of frontogenesis. *J. Atmos. Sci.*, **31**, 869–892.

Namias, J., and P. F. Clapp, 1949: Confluence theory of the high tropospheric jet stream. *J. Meteor.*, **6**, 330–336.

Newton, C. W., 1954: Frontogenesis and frontolysis as a three-dimensional process. *J. Meteor.*, **11**, 449–461.

——, 1958: Variations in frontal structure of upper level troughs. *Geophysica*, **6**, 357–375.

——, and A. Trevisan, 1984a: Clinogenesis and frontogenesis in jet-stream waves. Part I: Analytical relations to wave structure. *J. Atmos. Sci.*, **41**, 2717–2734.

——, and ——, 1984b: Clinogenesis and frontogenesis in jet-stream waves. Part II: Channel model numerical experiments. *J. Atmos. Sci.*, **41**, 2735–2755.

Ninomiya, K., 1971: Mesoscale modification of synoptic situations from thunderstorm development as revealed by ATS III and aerological data. *J. Appl. Meteor.*, **10**, 1103–1121.

Orlanski, I., and B. B. Ross, 1977: The circulation associated with a cold front. Part I: Dry case. *J. Atmos. Sci.*, **34**, 1619–1633.

Palmén, E., 1958: Vertical circulation and release of kinetic energy during the development of hurricane Hazel into an extratropical storm. *Tellus*, **10**, 1–23.

——, and K. M. Nagler, 1949: The formation and structure of a large-scale disturbance in the westerlies. *J. Meteor.*, **6**, 227–242.

——, and C. W. Newton, 1969: *Atmospheric Circulation Systems: Their Structure and Physical Interpretation. Int. Geophys. Ser.*, Vol. 13, Academic Press, 603 pp.

Petersen, R. A., 1986: Detailed three-dimensional isentropic analysis using an objective cross-sectional approach. *Mon. Wea. Rev.*, **114** (in press).

Petterssen, S., 1936: Contribution to the theory of frontogenesis. *Geofys. Publ.*, **11**(6), 1–27.

——, 1955: A general survey of factors influencing development at sea level. *J. Meteor.*, **12**, 36–42.

——, 1956: *Weather Analysis and Forecasting, Vol. I. Motion and Motion Systems*, 2nd ed., McGraw-Hill, 428 pp.

Reed, R. J., 1955: A study of a characteristic type of upper-level frontogenesis. *J. Meteor.*, **12**, 226–237.

——, and F. Sanders, 1953: An investigation of the development of a mid-tropospheric frontal zone and its associated vorticity field. *J. Meteor.*, **10**, 338–349.

——, and E. F. Danielsen, 1959: Fronts in the vicinity of the tropopause. *Arch. Meteor. Geophys. Bioklim.*, **A11**, 1–17.

Reiter, E. R., 1969: *Jet-Stream Meteorology*. The University of Chicago Press, 515 pp.

——, 1975: Stratospheric-tropospheric exchange processes. *Rev. Geophys. Space Phys.*, **13**, 459–474.

Riehl, H., and Collaborators, 1952: *Forecasting in Middle Latitudes. Meteor. Monogr.*, No. 5, Amer. Meteor. Soc., 80 pp.

——, M. A. Alaka, C. L. Jordan and R. J. Renard, 1954: *The Jet Stream. Meteor. Monogr.*, No. 7, Amer. Meteor. Soc., 100 pp.

Roach, W. T., 1970: On the influence of synoptic development on the production of high level turbulence. *Quart. J. Roy. Meteor. Soc.*, **96**, 413–429.

Sanders, F., 1955: An investigation of the structure and dynamics of an intense surface frontal zone. *J. Meteor.*, **12**, 542–552.

Sawyer, J. S., 1956: The vertical circulation at meteorological fronts and its relation to frontogenesis. *Proc. Roy. Soc. London*, **A234**, 346–362.

Shapiro, M. A., 1970: On the applicability of the geostrophic approximation to upper-level frontal-scale motions. *J. Atmos. Sci.*, **27**, 408–420.

——, 1974: A multiple structured frontal zone-jet stream system as revealed by meteorologically instrumented aircraft. *Mon. Wea. Rev.*, **102**, 244–253.

——, 1975: Simulation of upper-level frontogenesis with a 20-level

isentropic coordinate primitive equation model. *Mon. Wea. Rev.*, **103,** 591–604.

——, 1976: The role of turbulent heat flux in the generation of potential vorticity in the vicinity of upper-level jet stream systems. *Mon. Wea. Rev.*, **104,** 892–906.

——, 1978: Further evidence of the mesoscale and turbulent structure of upper level jet stream-frontal zone systems. *Mon. Wea. Rev.*, **106,** 1100–1111.

——, 1980: Turbulent mixing within tropopause folds as a mechanism for the exchange of chemical constituents between the stratosphere and troposphere. *J. Atmos. Sci.*, **37,** 994–1004.

——, 1981: Frontogenesis and geostrophically forced secondary circulations in the vicinity of jet stream-frontal zone systems. *J. Atmos. Sci.*, **38,** 954–973.

——, 1983: Mesoscale weather systems of the central United States. *The National STORM Program: Scientific and Technological Bases and Major Objectives,* R. A. Anthes, Ed., University Corporation for Atmospheric Research, P.O. Box 3000, Boulder, CO 80307, 3.1–3.77.

——, 1985: Dropwindsonde observations of an Icelandic low and a Greenland mountain-lee wave. *Mon. Wea. Rev.*, **113,** 680–683.

——, and J. T. Hastings, 1973: Objective cross-section analyses by Hermite polynomial interpolation on isentropic surfaces. *J. Appl. Meteor.*, **12,** 753–762.

——, and P. J. Kennedy, 1981: Research aircraft measurements of jet stream geostrophic and ageostrophic winds. *J. Atmos. Sci.*, **38,** 2642–2652.

——, and ——, 1982: Airborne radar altimeter measurements of geostrophic and ageostrophic winds over irregular topography. *J. Appl. Meteor.*, **21,** 1739–1746.

——, A. J. Krueger and P. J. Kennedy, 1982: Nowcasting the position and intensity of jet streams using a satellite-borne total ozone mapping spectrometer. *Nowcasting,* K. A. Browning, Ed., Academic Press, 137–145.

——, T. Hample and D. W. van de Kamp, 1984a: Radar wind profiler observations of fronts and jet streams. *Mon. Wea. Rev.*, **112,** 1263–1266.

——, R. C. Schnell, F. P. Parungo, S. J. Oltmans and B. A. Bodhaine, 1984b: El Chichón volcanic debris in an arctic tropopause fold. *Geophys. Res. Lett.*, **11,** 421–424.

Staley, D. O., 1960: Evaluation of potential-vorticity changes near the tropopause and the related vertical motions, vertical advection of vorticity, and transfer of radioactive debris from stratosphere to troposphere. *J. Meteor.*, **17,** 591–620.

Sutcliffe, R. C., and A. G. Forsdyke, 1950: The theory and use of upper air thickness patterns in forecasting. *Quart. J. Roy. Meteor. Soc.*, **76,** 189–217.

Uccellini, L. W., 1980: On the role of upper tropospheric jet streaks and leeside cyclogenesis in the development of low-level jets in the Great Plains. *Mon. Wea. Rev.*, **108,** 1689–1696.

——, and D. R. Johnson, 1979: The coupling of upper and lower tropospheric jet streaks and implications for the development of severe convective storms. *Mon. Wea. Rev.*, **107,** 682–703.

——, P. J. Kocin, R. A. Petersen, C. H. Wash and K. F. Brill, 1984: The Presidents' Day cyclone of 18–19 February 1979: Synoptic overview and analysis of the subtropical jet streak influencing the precyclogenetic period. *Mon. Wea. Rev.*, **112,** 31–55.

——, D. Keyser, K. F. Brill and C. H. Wash, 1985: The Presidents' Day cyclone of 18–19 February 1979: Influence of upstream trough amplification and associated tropopause folding on rapid cyclogenesis. *Mon. Wea. Rev.*, **113,** 962–988.

Welander, P., 1955: Studies on the general development of motion in a two-dimensional, ideal fluid. *Tellus,* **7,** 141–156.

Wetzel, P. J., W. R. Cotton and R. L. McAnelly, 1983: A long-lived mesoscale convective complex. Part II: Evolution and structure of the mature complex. *Mon. Wea. Rev.*, **111,** 1919–1937.